WATER ADSORPTION ON AGGREGATES OF SPHERICAL AEROSOL NANO PARTICLES

A Dissertation

by

CHU NIE

Submitted to the Office of Graduate Studies of
Texas A&M University
in partial fulfillment of the requirements for the degree of

DOCTOR OF PHILOSOPHY

August 2005

Major Subject: Nuclear Engineering

WATER ADSORPTION ON AGGREGATES OF SPHERICAL AEROSOL NANO PARTICLES

A Dissertation

by

CHU NIE

Submitted to the Office of Graduate Studies of
Texas A&M University
in partial fulfillment of the requirements for the degree of

DOCTOR OF PHILOSOPHY

Approved by

Chair of Committee,	William H. Marlow
Committee Members,	George Kattawar
	Robert Lucchese
	Yassin Hassan
Head of Department,	William E. Burchill

August 2005

Major Subject: Nuclear Engineering

ABSTRACT

Water Adsorption on Aggregates of Spherical Aerosol Nano Particles. (August 2005)

Chu Nie, B.S., Nanjing University

Chair of Advisory Committee: Dr. William H. Marlow

A three dimensional integral equation is developed in order to compute water adsorption onto aggregates of spherical aerosol nano particles. The integral equation is derived from molecular density functional theory, with a weighted density approximation and a direct correlation function interpolation rule. Only required inputs are the direct correlation functions of the uniform fluid or gas at both high-density and low-density limits. The equation has been tested on argon adsorption onto a graphite planer substrate; the result corresponds well with previous simulation work.

Adsorption of both noble gas and water onto a single spherical nano particle and aggregates of spherical nano particles has been computed with the developed equation. For the adsorption of a single spherical substrate, layer structure has been found, the adsorption shows a transition property when substrate size increases and when the substrate size is over 100Å the adsorption is nearly the same as that of a planer substrate.

For adsorption of aggregates of spherical nano particles, not only much strong adsorption appears but also adsorption property changes with different configurations of spherical nano particles.

ACKNOWLEDGMENTS

I would like to express my thanks to my dissertation committee chair, Dr. W.H.Marlow, for his guidance and his attention to details. I am also grateful to my committee members, Dr. Yassin Hassan, Dr. George Kattawar and Dr. Robert Lucchese for providing additional insight throughout this process. I would also like to thank Mr. Peter Yunker for his variety of advice and discussion on this dissertation. Most of all, I would like to thank my parents for their unconditional and continuous support, trust, encouragement and love through the years.

TABLE OF CONTENTS

CHAPTER Page

LIST OF FIGURES

FIGURE Page

FIGURE Page

CHAPTER I

INTRODUCTION

An important but poorly understood fraction of the atmospheric aerosol is solid, nanometer range particles including those produced in combustion of fossil fuels and in many industrial processes. Indeed, detailed electron microscopic examinations have revealed that they are usually aggregates comprised of adhering, spherical nanoparticles. While issues of water uptake by these aggregate particles are central to understanding their roles in air chemistry, visibility degradation, human respiratory system exposure, cloud condensation nucleation, and elsewhere, the technical literature does not provide guidance for addressing these questions as it does for large particles.

The structures of aggregate particles may well be important in urban and regional air chemistry for several reasons. Firstly is the exposure of surfaces that facilitate many chemical reactions. For high fractal dimension particles D~3, because the interior surface of the aggregate is no longer directly exposed to the background gas, this structure can be expected to show lower heterogeneous reactivity than for particles with $D \leq 2$. A second set of important properties of aggregate particles affected by its structure are those of its transport. Since drag and diffusivity largely govern respiratory deposition, particle structure including condensed water therefore will significantly affect regional deposition in the respiratory tract and, consequently, the health effects of urban and regional air pollution. These same transport properties are also critical in atmospheric dry and wet deposition of the aerosol particles and for clean up of process-gas emissions to the atmosphere. Details of respiratory deposition are particularly important for carbonaceous aggregate particles because they are generally associated with the semi-volatile organic compounds and other biologically active molecular species identified with the harmful

---

This dissertation follows the style of *Physical Review E*.

health impact of air pollution. A third important way that the aggregate particle structure can affect urban and regional environment is via visibility and the related question of cloud nucleation. Depending upon the amount the water, the aggregate will contribute to visibility degradation or other background haze. Alternatively, aggregates can serve as cloud condensation nuclei even at relatively low humidity. Consequently, these particles will be important contributors to the depletion of gas phase water from the atmosphere in cities and the surrounding regions and therefore to the complex of issues of meteorology on the urban and regional scale including such questions as non precipitating clouds and the urban heat island. These numerous effects of aggregate particle structure argue for the development of a detailed understanding of the factors affecting them.

In the macroscopic case, the equilibrium vapor pressure of water over a surface is a function of the thermodynamic free energies and entropies of the water in the vapor and condensed, or surface, phases. In the macroscopic or continuum treatment of substrate coverage by condensate, a widely used formalism of equilibrium thermodynamics (Refs. [1, 2]) is to calculate the vapor pressure over a condensate droplet on the substrate surface. Then, condensation is thermodynamically favored when total interfacial energy loss due to growth of the droplet exceeds the heat gain resulting from entropy loss associated with condensation. No accounting is made for thin or thick films and, as in the Kelvin equation (Ref. [3]); the Laplace description of differential pressure across a curved condensate gas surface (Ref. [4]) is used. Provided the substrate particle is much larger than the condensate molecule, and other dimensions and conditions are suitable for use of experimentally determined, static contact angles, this approach can be useful for particles of radii on the order of or larger than 50 nm.

For particulate substrates in the small nanometer range, a number of crucial differences from the macroscopic case can be identified. Substrate coverage by condensate is not adequately described as continuous in the same sense as for a macroscopic substrate where coverage can be averaged over areas that are significantly larger than the 0.5-1 nanometer domains where

condensate clustering and discontinuity occur. This averaging rationalizes the sequence of partial coverage to full coverage to multi-layer coverage of the substrate in the continuum picture but is not meaningful where the substrate itself changes significantly over distances of a small number of nanometers. In the macroscopic picture derived from the equilibrium of a droplet on a surface, as described above, local multi-layers are effectively assumed from the outset. This assumption has been applied to the calculation of the equilibrium vapor pressure over the pendular ring of condensation between two adhering, macroscopic spheres (Ref. [2]). In addition, the interaction of monolayer condensate adsorption with the macroscopic particulate substrate is defined in relation to the macroscopic planar reference state. In contrast, the interaction energy of condensate and substrate for nanometer substrate spheres is dependent upon particle radius (Ref. [5]), an effect that has not yet been adequately explored for either monolayers or for higher coverage. Finally, for adhering, nanometer spheres, and the accessibility to water molecules of the interstitial zone between the spheres is not entirely clear. When the substrate size comes to the nanometer range, the word "density distribution" is a more precise terminology instead of vapor pressure because the macroscopic picture fails.

In the former study (Ref. [6]), Monte Carlo simulations of the interaction energies of a nominal mono layer of water on a plane surface and on 1, 1.5 and 2nm radius spheres for which the substrate material interacted with the water via Van der Waals potential (Ref. [7]) expected of tetradecane. Those calculations showed the effect of substrate particle size on the interaction energy between condensate and substrate and the consequences of the resultant size dependence on the structuring of water on the substrate. But sufficient calculations were not conducted to show in useful detail the transition of water-substrate attraction energy from small sphere to plane. Therefore, no film information was derived to indicate when the macroscopic picture would be adequate, according to interaction energy and associated condensate structure criteria. Moreover, Monte Carlo method is not a determinant method and has limitations in predicting the properties of such interacting system with complicated geometries.

Generally speaking, there may be several factors that affect the water uptake by the substrate particles, such as temperature, size, adsorption type (physical adsorption and chemical adsorption), and surface type of the substrate (water-soluble or not). Since in this work the size effects are emphasized, we set the other conditions to be the simplest ones. The adsorption is physical adsorption and the surface is not water-soluble. The advantage of this approach is to put the physical nature of the model in the primary place. Once we understand the size effects, we can add the other factors into the problem.

To complete the translation of the vapor related problem from the macroscopic to the microscopic picture, an integral equation method will be developed. This method will be used to calculate the density distribution functions around a nanoparticle and nanoparticle aggregates, especially for nanoparticles with radii smaller than 5nm. With the integral equation method, the effects of size on the distribution of water around both a single nano-sphere and nanoparticle aggregates will be computationally described for ultra fine particles representative of those produced by combustion. Then a complete picture of the water uptake by a substrate problem can be obtained from the macroscopic case to the microscopic case.

A summary of the background information related to this research problem will be given in Chapter II. This information will include some of the basics on vapor pressure over the macroscopic particles and the density distribution function around the microscopic particles. Also, the development of the van der Waals energy theory and the integral equation theory for solving the density distribution function will be reviewed in Chapter II. Methodology will be described in Chapter III. Chapter IV will show the results of noble gas adsorption onto the nano sphere aggregates obtained from the integral equation theory. Chapter V will show the result of water adsorption onto the nano sphere aggregates. Chapter VI gives the conclusion.

CHAPTER II

LITERATURE REVIEW

II.1. The Macroscopic Theory

The vapor pressure over a substrate is of importance in many fields. Generally it relates to the homogenous and heterogeneous nucleation of super cooled or supersaturated solutions by foreign particles. The dependence of nucleation efficiency on the size and surface properties of the nucleating particles has been investigated extensively. Previously, people used the spherical potential between the substrate and the gas molecule. However, the non-spherical interaction between the substrate and the water molecules is involved in heterogeneous nucleation. For example, a water cap may forms on a spherical particle due to the existence of some soluble species on the surface of the particle or activated oxidized sites on an imperfect surface and a pendular ring may be found between two spherical particles in contact. For the spherical particles whose radii are over 10nm, the macroscopic treatment is able to provide the information on the equilibrium pressure over a single one or aggregate of them.

II.1.1. The Kelvin Equation

Consider a closed system of fixed volume maintained at a constant temperature. Imagine a liquid phase of arbitrary shape within the volume but not filling it and in equilibrium with its vapor. Gravity is neglected and the liquid is assumed not in contact with anything other than vapor, which means the surface phase is the liquid-vapor interface. Since the system has volume and temperature constant, equilibrium will be indicated by a minimum value of the Helmholtz free energy, F (Ref. [3]).

$$dF = -SdT - PdV + \gamma dA + \sum_i \mu_i dn_i \ . \tag{2.1}$$

Where S is the entropy, and P is the pressure, γ is the surface tension, μ is the chemical potential. Consider the liquid and vapor phase separately,

$$dF^l = -P_l dV^l + \gamma dA + \sum_i \mu^l{}_i dn^l{}_i \tag{2.2}$$

$$dF^g = -P^g dV^g + \sum_i \mu^g{}_i dn^g{}_i \tag{2.3}$$

Since any change in the volume of the gas or liquid must come from the other as well as any change in the number molecules,

$$dV^g = -dV^l \tag{2.4}$$

$$dn^l = -dn^g \tag{2.5}$$

Therefore

$$\sum_i (\mu^l{}_i - \mu^g{}_i) dn^l{}_i = (P^l - P^g) dV^l - \gamma dA \tag{2.6}$$

For one component,

$$\mu^l - \mu^g = (P^l - P^g)\left(\frac{\delta V}{\delta n}\right)^l - \gamma\left(\frac{\delta A}{\delta n}\right) \tag{2.7}$$

Since $d\mu^l = \overline{V}^l dP^l$ where $\overline{V}^l = V^l / n^l$

$$\int_{P^*}^{P^l} \overline{V}^l dP^l = \mu^l(T, P^l) - \mu^l(T, P^*) \tag{2.8}$$

Where P^* denotes the normal vapor pressure.

At equilibrium the relation $\mu^l(T, p^*) = \mu^{*g}(T, p^*)$ holds. Then

$$\mu^g(T, P^g) - \mu^{*g}(T, P^*) = \int_{P^*}^{P^l} \overline{V}^l dP^l - (P^l - P^g)\left(\frac{\delta V}{\delta n}\right)^l + \gamma\left(\frac{\delta A}{\delta n}\right) \tag{2.9}$$

If the interface is characterized by two principle radii of curvature, r_1 and r_2 taken within the liquid phase

$$\frac{\delta A}{\delta V} = \frac{1}{r_1} + \frac{1}{r_2} \tag{2.10}$$

Also at equilibrium, all forces must balance.

$$P^l - P^g = \gamma\left(\frac{1}{r_1} + \frac{1}{r_2}\right) \tag{2.11}$$

Above two equations give the result

$$\gamma\left(\frac{\delta A}{\delta n}\right) = \gamma\left(\frac{\delta A}{\delta V^l}\right)\left(\frac{\delta V^l}{\delta n^l}\right) = \gamma\left(\frac{\delta A}{\delta V^l}\right)\left(\frac{1}{r_1} + \frac{1}{r_2}\right) = \left(\frac{\delta A}{\delta V^l}\right)\left(P^l - P^g\right) \tag{2.12}$$

Now to relate chemical potential to vapor pressure and assume the vapor obeys the ideal gas state equation,

$$\mu^g(P^g) - \mu^{*g}(P^*) = RT\ln(P^g / P^*) = \int_{P^*}^{P^l} \overline{V}^l dP \tag{2.13}$$

Suppose $\overline{V}^l$ is constant over the pressure from P^l to P^*,

$$RT\ln(P^g / P^*) = \overline{V}^l(P^l - P^g + \Delta P) \tag{2.14}$$

Where $\Delta P = P^g - P^* << P^l - P^g$. Thus

$$RT\ln(P^g / P^*) = \overline{V}^l\gamma\left(\frac{1}{r_1} + \frac{1}{r_2}\right) = \frac{M_r\gamma}{\rho_l}\left(\frac{1}{r_1} + \frac{1}{r_2}\right). \tag{2.15}$$

II.1.2. Fletcher's Theory

Assume the nucleating particle is a sphere. As plotted in Fig. 1 in [1], let the vapor phase be represented by subscript 1, the water cap by 2, and the substrate by 3. If we denote volume by V and surface area by S, then the free energy of formation of a water cap of radius r on a substrate of radius R is

$$\Delta G = \Delta G_v V_2 + \sigma_{12} S_{12} + (\sigma_{23} - \sigma_{13}) S_{23} \tag{2.16}$$

Where ΔG_v is the free energy difference per unit volume of phase 2 between matter in state 1, and σ_{ij} is the surface free energy of interface between phases i and j.

To evaluate the critical free energy ΔG^* require

$$\frac{\partial G}{\partial r} = 0 \tag{2.17}$$

Together with

$$r^* = -2\sigma_{12} / \Delta G_v . \tag{2.18}$$

Let $x = R / r^*$

The free energy of formation of a water cap is

$$\Delta G^* = \frac{8\pi {\sigma_{12}}^3}{3(\Delta G_v)^2} f(m,x) \tag{2.19}$$

Where

$$f(m,x) = 1 + \left(\frac{1-mx}{g}\right)^3 + x^3\left[2 - 3\left(\frac{x-m}{g}\right) + \left(\frac{x-m}{g}\right)^3\right] + 3mx^2\left(\frac{x-m}{g} - 1\right) \tag{2.20}$$

And

$$g = (1 + x^2 - 2mx)^{\frac{1}{2}} . \tag{2.21}$$

When $x = 0$ it reduces to the homogeneous nucleation.

We also have

$$\Delta G_v = \frac{8\pi}{3}{\sigma_{12}}^3 \frac{f(m,x)}{kT(60.1 + 4.604\log_{10} R)} . \tag{2.22}$$

If the liquid is assumed uncompressible and the vapor is an ideal gas

$$\Delta G_v = \left(\frac{-kT}{V_l}\right)\log\left(\frac{P}{P_\infty}\right) \tag{2.23}$$

Where V_l is the volume of water molecules in the bulk liquid.

Fletcher [1] obtained curves of nucleation efficiency as a function of particle size by using the above expression. He found that the size effect becomes important in the range $100 - 1000$Å of particle radius but small for particles greater than 1000Å .

II.1.3. Crouzet and Marlow's Theory

The meniscus formed at the point of contact of a sphere with a plane is an intermediate case for the sphere-sphere geometry. Take

$$H = \frac{1}{r_1} + \frac{1}{r_2} = const \tag{2.24}$$

where r_1 and r_2 are the principle radii of curvature of the condensate, measured from within the liquid phase. For an axisymmetric geometry, Eq. (2.24) becomes

$$2H = \frac{d^2 z / dr^2}{[1 + (dz/dr)^2]^{\frac{3}{2}}} + \frac{dz/dr}{r[1 + (dz/dr)^2]^{\frac{1}{2}}} \tag{2.25}$$

Where (r, z) are the cylindrical coordinates as depicted in Fig. 2 in [2]. If

$$x = \frac{r}{R} \text{ , and } z = \frac{z}{R} \tag{2.26}$$

$$u = -\sin\varepsilon \tag{2.27}$$

Where ε is the angle made by the local perpendicular to the profile with z axis.

$$2HR = -\frac{du}{dx} - \frac{u}{x} \tag{2.28}$$

$$x_s = \sin\psi \text{ , } y_s = 1 - \cos\psi \text{ , } u_s = -\sin(\theta_s + \psi) \tag{2.29}$$

$$y_p = 0 \quad u_p = -\sin(\pi - \theta_p) \tag{2.30}$$

After steps of manipulations

$$x = -\frac{u \pm \sqrt{u^2 + c}}{2HR} \tag{2.31}$$

$$y = \frac{1}{2HR}\int_{u_p}^{u}\left[\frac{u}{\sqrt{1-u^2}} \pm \frac{u}{\sqrt{(1-u^2)(u^2+c)}}\right]du \tag{2.32}$$

Where

$$c = 4HR\sin\psi[HR\sin\psi - \sin(\theta_1 + \psi)] \tag{2.33}$$

And finally

$$2HR = \frac{1}{y_s}\int_{u_p}^{u}\left[\frac{u}{\sqrt{1-u^2}} \pm \frac{u}{\sqrt{(1-u^2)(u^2+c)}}\right]du \tag{2.34}$$

For general case of two spheres, the final result looks like this

$$H = \frac{R_2 \sin\psi_2 \sin(\theta_2 + \psi_2) - R_1 \sin\psi_1 \sin(\theta_1 + \psi_1)}{{R_2}^2 \sin^2\psi_2 - {R_1}^2 \sin^2\psi_1} \tag{2.35}$$

Eq. (2.35) cannot be solved directly; Crouzet and Marlow [2] used iteration methods to solve those two equations. The process is initiated by specifying Ψ_1 and calculating the corresponding mean curvature H and filling angle Ψ_2. Since the problem has been solved for a sphere in contact with a plane, the method takes advantage of early results and divides the meniscus profile into two half-profiles, thereby reducing the problem to two sphere-plane problems. Consequently, these two half-profiles are searched in such a fashion that at the end of the iterations, when convergence criteria are met, they join at the plane and form together the complete profile of meniscus between the particles. With the solution of (2.35), the vapor pressure can be connected to the curvature with the Kelvin equation

$$S = \frac{P_H}{P_0} = \exp\left(\frac{M_r \gamma_{\mathrm{lg}}}{\rho_l RT} H\right) \tag{2.36}$$

They found that if the contact angle is greater than 90 degrees, condensation is thermodynamically possible only under conditions of super saturation; two spherical structures are not favorable for condensation growth. Conversely, for contact angles smaller 90 degrees, the divergence to infinite negative values at small filling angles suggests that a small pendular ring could always exist in equilibrium, even at very low sub saturation levels. Then, starting from a small amount of liquid already present in the interstitial region between the two particles and follow its evolution as the vapor pressure slowly increases.

II.1.4. Xie and Marlow's Theory

Xie and Marlow [8] used the tabulated data of activity of water over sulfuric acid solutions and the solution density to determine the contact angle of surface liquid residing on substrate spheres for different configurations. Their method is in this way: by giving the trial contact angle, the trial maximum curvature H can be determined. Then calculated the pendular

volume and determine the pendular ring interface composition by assuming a given fixed number of sulfuric acid molecules in this volume. Assume Young's equation

$$\sigma_{sg} - \sigma_{sl} = \sigma_{\lg} \cos\theta_c \tag{2.37}$$

is always correct in the macroscopic domain, with the sulfuric acid weight percentage of the solution the solution density and surface tension $\sigma_{\lg}$ can be determined by using the interpolation programs for surface tension and density of sulfuric acid. Then a new contact angle can be obtained. The procedure is repeated until all quantities satisfy Young's equation.

Their calculation showed that for the same contact angle, the calculation indicates that the pendular ring formed on two macroscopic spheres is more favorable for condensation than the single spherical cap formed on a sphere, whether the interface liquid is water or sulfuric acid solution. Particularly, their calculations indicate the condensational growth of a sphere with a surface deposit of sulfuric acid is distinctly limited for sub saturation relative humidity. The equilibrium vapor pressure of water over sulfuric acid solution is lower than over pure water for either geometric configuration, if all the other conditions are same. Consequently, the solution effect enhances condensation. They also found that the volumes in both geometric configurations are very different since the pendular ring holds a much greater volume of liquid than the single cap does.

II.2. The Integral Equation Theory

The Ornstein-Zernike equation (OZ equation) (2.38) was first introduced into statistical mechanical theory by Ornstein and Zernike in connection with the theory of fluctuations. In recent years progress has been made in treating uniform liquids and non-uniform liquids.

$$h^{(a,b)}(\vec{q}_1, \vec{q}_2) = c^{(a,b)}(\vec{q}_1, \vec{q}_2) + \sum_{\alpha=a,b} \int \rho^{(\alpha)}(\vec{q}_3) h^{(a,\alpha)}(\vec{q}_1, \vec{q}_3) c^{(b,\alpha)}(\vec{q}_2, \vec{q}_3) d\vec{q}_3 \tag{2.38}$$

Where $h^{(a,b)}(\vec{q}_1, \vec{q}_2)$ is the total correlation function and $c^{(a,b)}(\vec{q}_1, \vec{q}_2)$ is the direct correlation function, a, b denotes the different species of molecules and $\vec{q}_i$ stands for the coordinates of the

molecule i including the orientational coordinates, $\rho^{(\alpha)}$ is the density of different species molecules. The OZ equation must be solved together with an approximation equation called the closure equation. Generally there are three kinds of approximations for the non-uniform case, namely the mean spherical approximation, the convoluted hypernetted approximation and Percus-Yevick (PY) approximation.

$$c^{(2)} = -\beta u \qquad \text{(Mean spherical approximation)} \qquad (2.39)$$

$$c^{(2)} = h^{(2)} - \ln g^{(2)} - \beta u \qquad \text{(Convoluted hypernetted approximation)} \qquad (2.40)$$

$$c^{(2)} = g^{(2)}[1 - \exp(\beta u)] \qquad \text{(PY approximation)} \qquad (2.41)$$

where $c^{(2)}$ is the direct correlation function, $h^{(2)}$ is the total correlation function, $g(2)$ is the radial distribution function, and u is the potential between two molecules.

II.2.1. Solution of the OZ Equation of Some Types

The OZ equation by PY approximation has been exactly solved for hard spheres. In PY approximation, $c^{(2)}$ vanishes outside the hard-sphere diameter, and $g^{(2)}$ vanishes inside this domain. It is to be noted that MS and PY approximation are formally equivalent for this case. Solution of OZ equation involves transformation to bipolar coordinates and Laplace transformation of the resulting equations. The hard-sphere pair correlation function obtained can be written as

$$c^{(2)} = -a_1 \quad r < 0 \qquad (2.42)$$

$$c^{(2)} = -a_1 - 6\eta_a a_2 r - \frac{1}{2}\eta_a z_1 r^3 \quad 0 < r \le 1 \qquad (2.43)$$

$$c^{(2)} = 0 \qquad r > 1 \qquad (2.44)$$

Where

$$a_1 = (1 + 2\eta_a)^2 / (1 - \eta_a)^4 \qquad (2.45)$$

$$a_2 = -(1+\frac{1}{2}\eta_a)^2/(1-\eta_a)^4 \tag{2.46}$$

$$\eta_a = \pi\rho_a\sigma_a{}^3/6 \tag{2.47}$$

where σ_a is the hard sphere diameter.

The pair correlation can be written in the form of a Laplace transformation as

$$L(rg^{(2)}(t)) = \int rg(r)e^{-rt}dr = tL(t)/2\eta_a[S(t)e^t + L(t)] \tag{2.48}$$

With

$$L(t) = 12\eta_a[(1+\frac{1}{2}\eta_a)t + 1 + 2\eta_a] \tag{2.49}$$

And

$$S(t) = (1-\eta_a)^2 t^3 + 6\eta_a(1-\eta_a)t^2 + 18\eta_a{}^2 t - 12\eta_a(1+2\eta_a) \tag{2.50}$$

Inversion of Eq. (2.48) involves integration in the complex plane and the result is not straightforward. Nevertheless a hard-sphere, uniform fluid $g^{(2)}$ can be calculated fairly readily (Ref. [9]).

Wertheim [10] suggested a method to solve the mean spherical model for fluids of hard spheres with permanent electric dipole moments exactly. In his treatment, the intermolecular potential is written like this

$$V(12) = -m^2 r^{-3}[3r^{-2}(\vec{s}_1\cdot\vec{r})(\vec{s}_2\cdot\vec{r}) - (\vec{s}_1\cdot\vec{s}_2)] \tag{2.51}$$

Where m is the dipole moment, $\vec{s}_i$ is a unit vector in the direction of the dipole moment of molecule i, and $\vec{r} = |\vec{r}_1 - \vec{r}_2|$. He selected three basis functions

$$I(12) = 1 \tag{2.52}$$

$$\Delta(12) = \vec{s}_1\cdot\vec{s}_2 \tag{2.53.a}$$

$$D(12) = 3r^{-2}(\vec{s}_1\cdot\vec{r})(\vec{s}_2\cdot\vec{r}) \tag{2.53.b}$$

In fact these base functions are the combinations of the first three components of the generalized spherical harmonics. Then $h(12)$ and $c(12)$ can be expanded on the basis functions,

$$h(12) = h_s(r)I(12) + h_D(r)D(12) + h_\Delta(r)\Delta(12) \tag{2.54}$$

$$c(12) = c_s(r)I(12) + c_D(r)D(12) + c_\Delta(r)\Delta(12) \tag{2.55}$$

Together with some certain boundary conditions, $h(12)$ and $c(12)$ can be analytically expressed.

Blum (Refs. [11-13]) obtained a partial solution for the mean spherical model of neutral spheres with electrostatic interactions. The main idea of his method is to expand $h^{(2)}$ and $c^{(2)}$ function in the form of generalized spherical harmonics.

$$h(\vec{r}_1, \vec{r}_2) = \sum_{mnl,\mu\nu} h_{\mu\nu}{}^{mnl}(R_{12})\Phi_{\mu\nu}{}^{mnl}(\Omega_1, \Omega_2, \hat{R}_{12}) \tag{2.56}$$

$$c(\vec{r}_1, \vec{r}_2) = \sum_{mnl,\mu\nu} c_{\mu\nu}{}^{mnl}(R_{12})\Phi_{\mu\nu}{}^{mnl}(\Omega_1, \Omega_2, \hat{R}_{12}) \tag{2.57}$$

Where $\vec{X}_i = \vec{R}_i, \Omega_i$, $\vec{R}_i$ is the position of molecule i, and $\Omega_i = \alpha_i, \beta_i, \gamma_i$, are Euler angles for the orientation of molecule i. The rotational invariants $\Phi\ (\Omega_1, \Omega_2, \hat{R}_{12})$ are defined by

$$\begin{aligned}\Phi_{\mu\nu}{}^{mnl}(\Omega_1, \Omega_2, \hat{R}_{12}) &= [(2m+1)(2n+1)]^{\frac{1}{2}} \sum_{\mu',\nu',\lambda'} \begin{pmatrix} m, n, l \\ \mu', o', \lambda' \end{pmatrix} \\ &\times D_{\mu\mu'}{}^{m}(\Omega_1) D_{\nu\nu'}{}^{n}(\Omega_2) D_{0\lambda'}{}^{l}(\hat{R}_{12})\end{aligned} \tag{2.58}$$

With the general notation for the Wigner $3-j$ symbols and generalized spherical harmonics.

After the three dimensional Fourier transformation,

$$h(\omega_1, \omega_2, \vec{k}) = c(\omega_1, \omega_2, \vec{k}) + \frac{1}{8\pi^2}\int d\omega_3 c(\omega_1, \omega_3, \vec{k})\rho h(\omega_3, \omega_2, \vec{k}) \tag{2.59}$$

Then a set of algebraic equations are found,

$$\begin{aligned}h_{\mu\nu}{}^{mnl}(k) &= c_{\mu\nu}{}^{mnl}(k) + \sum_{n'l'l''\nu'} (-1)^{m+n+n'} \begin{pmatrix} l'', l', l \\ 0,0,0 \end{pmatrix} \begin{Bmatrix} l', l', l \\ m, n, n' \end{Bmatrix} \\ &\times c_{\mu\nu'}{}^{mn'l''}(k)\rho h_{\nu'\nu}{}^{n'nl''}(k), |\nu'| \le n'\end{aligned} \tag{2.60}$$

After another Fourier transformation, $h_{\mu\nu}{}^{mnl}(r)$ can be obtained.

The solution was given in terms of a linear transformation of the direct correlation function, which was a polynomial in r inside the hardcore diameter. The coefficients of this polynomial were determined from a set of boundary conditions. The method, in principle can solve the problem, but the computational job left is nearly impossible to complete. Only for simple cases, such as linear dipole and quadruples, it is possible to find the complete solution.

Steven et al. [14] followed Blum's way to examine the solution of OZ equations for the correlation functions of a fluid mixture in which the molecular interactions consist of a hard sphere plus a multipole that contained columbic, dipolar as well as quadrupolar terms, but there existed differences in their derivations. They also obtained an analytic solution of a pure tetrahedral quadrupolar hard sphere fluid in the MSA. The significance of the work lies in that a tetrahedral quadrapole tensor can be used to represent the quadrapole tensor of water. And a quadrapole tensor is in the form of

$$\theta_T = \begin{pmatrix} \theta_T & 0 & 0 \\ 0 & -\theta_T & 0 \\ 0 & 0 & 0 \end{pmatrix}. \tag{2.61}$$

Such a quadrapole tensor can be obtained by putting two positive charges and two negative charges of equal magnitude at the vertices of a rectangular tetrahedron.

II.2.2. HNC Approximation

In recent years, the HNC approximation is one of the most successful and widely used integral equation theories for liquids and solutions. Partial differentiation of Eq. (2.40) (Ref. [15])

$$\frac{\partial c(12)}{\partial r} = \frac{\partial h(12)}{\partial r} - \frac{1}{g(12)} \frac{\partial g(12)}{\partial r} - \beta \frac{\partial u(12)}{\partial r} \tag{2.62}$$

Which can be rearranged to give

$$\frac{\partial c(12)}{\partial r} = -h(12) \frac{\partial W(12)}{\partial r} - \beta \frac{\partial u(12)}{\partial r} \tag{2.63}$$

Where

$$W(12) = -\eta(12) + \beta u(12) \tag{2.64}$$

And

$$\eta(12) = h(12) - c(12) \tag{2.65}$$

The HNC closure becomes

$$c(12) = \int_r^\infty h(12)\frac{\partial W(12)}{\partial r}dr - \beta u(12) \tag{2.66}$$

If $W(12)$ and $u(12)$ are expanded in generalized spherical harmonics,

$$\begin{aligned} c(12) = & \sum_{\substack{m_1,n_1,l_1 \\ \mu_1,\nu_1}} \sum_{\substack{m_2,n_2,l_2 \\ \mu_2,\nu_2}} \Phi_{\mu_1\nu_1}{}^{m_1n_1l_1}(\Omega_1,\Omega_2,\hat{r})\Phi_{\mu_2\nu_2}{}^{m_2n_2l_2}(\Omega_1,\Omega_2,\hat{r}) \\ & \times \int_r^\infty h_{\mu_1\nu_1}{}^{m_1n_1l_1}(r)\frac{\partial W_{\mu_1\nu_1}{}^{m_1n_1l_1}(\Omega_1,\Omega_2,\hat{r})}{\partial r}dr - \beta \sum_{\substack{m,n,l \\ \mu,\nu}} u_{\mu\nu}{}^{mnl}(r) \\ & \times \Phi_{\mu\nu}{}^{mnl}(\Omega_1,\Omega_2,\hat{r}) \end{aligned} \tag{2.67}$$

The reference HNC approximation (RHNC) (Ref. [15]) is based upon the separation of the pair potential and correlation functions into reference and perturbation parts. It is convenient to write the closure in terms of variables of the form

$$\Delta X(12) = X(12) - X_R(12) \tag{2.68}$$

And $X(12)$ is a property of the system of interest and $X_R(12)$ refers to a spherically symmetric reference system. Then

$$\Delta c(12) = \Delta h(12) - \ln[g_R(r) + \Delta h(12)] + \ln g_R(r) - \beta \Delta u(12) \tag{2.69}$$

And

$$\begin{aligned} c(12) = & \sum_{\substack{m_1,n_1,l_1 \\ \mu_1,\nu_1}} \sum_{\substack{m_2,n_2,l_2 \\ \mu_2,\nu_2}} P \times \int_r^\infty \Delta h_{\mu_1\nu_1}{}^{m_1n_1l_1}(r)\frac{\partial \Delta W_{\mu_1\nu_1}{}^{m_1n_1l_1}(\Omega_1,\Omega_2,\hat{r})}{\partial r}dr \\ & + \sum_{\substack{m,n,l \\ \mu,\nu}} [\int_r^\infty h_R(r)\frac{\partial \Delta W_{\mu\nu}{}^{mnl}(\Omega_1,\Omega_2,\hat{r})}{\partial r}dr - \int_r^\infty \Delta h_{\mu\nu}{}^{mnl}\frac{\partial}{\partial r}\ln g_R(r)dr \\ & - \beta \Delta u_{\mu\nu}{}^{mnl}(r)]\Phi_{\mu\nu}{}^{mnl}(\Omega_1,\Omega_2,\hat{r}) \end{aligned} \tag{2.70}$$

Where P depends on the indices $m_1, n_1, l_1, \mu_1, \nu_1$ and $m_2, n_2, l_2, \mu_2, \nu_2$

The numerical solution can be obtained by an iterative method. Fries and Patey [15] proposed this general method for the numerical solution of the full hyper netted chain theory for fluids characterized by angle-dependent pair potentials. As an application of this method, they solved the RHNC theory for a dense fluid of dipolar hard spheres. This method allows the HNC and RHNC theories to be usefully applied to a much greater variety of model fluids than was previously possible. The method avoids the multidimensional integration but it is unstable for strongly anisotropic short- range interactions like those that give rise to the molecular shape.

An alternative way (Ref. [16]) is to differentiate Eq. (2.40) with respect to one of the angular coordinates of molecule 1 or 2, holding the distance r_{12} and the other angular coordinates constant. And the final result looks like

$$[(m \pm \mu)(m \mp \mu + 1)]^{\frac{1}{2}} \{c_{\mu\nu}{}^{mnl}(r) + \beta u_{\mu\nu}{}^{mnl}(r)\} =$$

$$\sum_{\substack{m_1, n_i, l_1, \mu_1, \nu_1 \\ m_2, n_2, l_2, \mu_2, \nu_2}} [(m_2 \pm \mu_2)(m_2 \mp \mu_2 + 1)]^{\frac{1}{2}} (2m+1)(2n+1)(2l+1)(-1)^{m+n+l+\mu_2+\nu_2+\mu_1+\nu_1+1} \tag{2.71}$$

$$\times \begin{Bmatrix} m_1 & n_1 & l_1 \\ m_2 & n_2 & l_2 \\ m & n & l \end{Bmatrix} \begin{pmatrix} m_1, m_2, m \\ \mu_1, \mu_2 \pm 1, -\mu \end{pmatrix} \begin{pmatrix} n1, n_2, n \\ \nu_1, \nu_2, -\nu \end{pmatrix} \begin{pmatrix} l_1, l_2, l \\ 0,0,0 \end{pmatrix} h_{\mu_1\nu_1}{}^{m_1, n_1, l_1}(r) W_{\mu_2 \mp 1, \nu_2}{}^{m_2 . n_2, l_2}(r)$$

II.2.3. Lado's Theory

Lado et al. [17] proposed a more general but different approach to solve the OZ equation for fluids of fully anisotropic rigid molecules requiring three Euler angles configurational description and leading to pair functions of five angular variables. And the method is suitable for all potentials. In their treatment the OZ equation is written like

$$\gamma(12) = \frac{\rho}{8\pi^2} \int d3[c(12) + \gamma(12)]c(32) \tag{2.72}$$

Where

$$\gamma(12) = h(12) - c(12) \tag{2.73}$$

And

$$c(12) = \exp[-\beta u(12) + \gamma(12) + B(12)] - 1 - \gamma(12) \tag{2.74}$$

Here $B(12)$ is the so-called bridge function because of the resemblance of its first density diagram to the Wheatstone bridge circuit. The fivefold angular dependence of the pair functions,

$$X(12) = X(r_{12}, \theta_1, \theta_2, \Phi_{12}, \chi_1, \chi_2) \tag{2.75}$$

A spherical harmonic expansion of the correlation functions is like

$$X(12) = \sum_{l_1 l_2 m n_1 n_2} [(2l_1 + 1)(2l_2 + 1)]^{\frac{1}{2}} X_{l_1 l_2 m}{}^{n_1 n_2}(r_{12}) D_{m n_1}{}^{l_1}(\omega_{12})^* D_{\tilde{m} n_2}{}^{l_2}(\omega_2)^* \tag{2.76}$$

Where the orientations $\omega = (\Phi, \theta, \chi)$, the Euler angles, are here referred to the axial line $\vec{r}_{12}$ between molecular centers, $D^l{}_{nm}(\omega)$ is a generalized spherical harmonic, and $\tilde{m} = -m$. Inversion of the expansion gives the coefficients as

$$X_{l_1 l_2 m}{}^{n_1 n_2}(r_{12}) = \frac{[(2l_1 + 1)(2l_2 + 1)]^{\frac{1}{2}}}{64\pi^2} \int d\omega_1 d\omega_2 X(12) D_{m n_1}{}^{l_1}(\omega_1) D_{\tilde{m} n_2}{}^{l_2}(\omega_2) \tag{2.77}$$

The pair distribution function

$$g(12) = \exp[-\beta u(12) + \gamma(12) + B(12)] \tag{2.78}$$

is obtained from $\gamma(12)$.

They outlined the iterative method to get the solution:

(1) With a finite set of coefficients $\gamma_{l_1 l_2 m}{}^{n_1 n_2}$ in hand, iteration for improved set begins with the construction of $\gamma(12)$, $c(12)$ and its coefficients $c_{l_1 l_2 m}{}^{n_1 n_2}$.

(2) The OZ equation is most conveniently solved in Fourier transform representation. The spatial coefficients

$$c(r;, l_1, l_2 l, n_1, n_2) = \sum_m C(l_1, l_2, l; m, \tilde{m}, 0) c_{l_1 l_2 m}{}^{n_1 n_2} \tag{2.79}$$

are obtained by a Clebsch –Gordon (CG) transformation and used to generate the Hankel transforms

$$\tilde{c}(k;,l_1,l_2l,n_1,n_2) = 4\pi i^l \int_0^\pi drr^2 c(r;,l_1,l_2l,n_1,n_2)\, j_l(kr) \tag{2.80}$$

Where $j_l(kr)$ is a spherical Bessel function of order l. An inverse CG transformation then yields the axial transform coefficients

$$\tilde{c}_{l_1l_2m}{}^{n_1n_2}(k) = \sum_l C(l_1,l_2,l;m,\tilde{m},0)\tilde{c}(k;,l_1,l_2l,n_1,n_2) \tag{2.81}$$

Needed for the OZ equation. In the expressions, $C(l_1,l_2,l;m,\tilde{m},m)$ is a Clebsch –Gordon coefficients.

(3) Fourier transformation of the OZ equation and expansion of the transforms as in Eq. (2.71) leads to

$$\gamma_{l_1l_2m}{}^{n_1n_2}(k) = \rho\sum_{l_3,n_3}(-1)^{m+n_3}[\tilde{c}_{l_1l_3m}{}^{n_1n_3}(k) + \tilde{\gamma}_{l_1l_3m}{}^{n_1n_3}(k)]\tilde{c}_{l_3l_2m}{}^{\tilde{n}_3n_2}(k) \tag{2.82}$$

for which the $\gamma_{l_1l_2m}{}^{n_1n_2}$ are extracted by matrix operations. (4) Begin with a CG transformation to space-fixed coefficients,

$$\tilde{\gamma}(k;,l_1,l_2l,n_1,n_2) = \sum_l C(l_1,l_2,l;m,\tilde{m},0)\tilde{\gamma}_{l_1l_2m}{}^{n_1n_2}(k) \tag{2.83}$$

followed by an inverse Hankel transformation

$$\tilde{\gamma}(k;,l_1,l_2l,n_1,n_2) = \frac{1}{2\pi^2 i^l}\int_0^\pi dkk^2\gamma(r;,l_1,l_2l,n_1,n_2)\, j_l(kr) \tag{2.84}$$

Another inverse CG transformation,

$$\tilde{\gamma}_{l_1l_2m}{}^{n_1n_2}(r) = \sum_l C(l_1,l_2,l;m,\tilde{m},0)\gamma(k;,l_1,l_2l,n_1,n_2) \tag{2.85}$$

yields the new axial coefficients of $\gamma(12)$ and completes one iteration. The new and old $\gamma(12)$ are compared until $\gamma(12)$ is adequately self consistent. One drawback of this method is that

multidimensional integrals have to be evaluated. The methods listed in both Ref. [15] and [17] can be extended to explore the structure of the liquid water (Refs. [18] and [19]).

II.2.4. RISM Method

Chandler and Anderson [20] proposed reference interaction site model (RISM) equation in order to extend the OZ equation to the non-spherical solutes and solvents by introducing site-site correlation functions.

The RISM equation is given as follows:

$$h_{uv} = \omega_{uv} * c_{uv} * (\omega_{uv} + \rho_v h_{vv}) \tag{2.86}$$

Where the symbol "*" denotes a convolution. The term h_{uv} is a matrix having elements of the site-site total correlation function $h_{\alpha\gamma}(r)$ between the interaction site α of solute u and the site γ of solvent v. The term c_{uv} is the matrix of the site-site direct correlation function $c_{\alpha\gamma}(r)$. The terms ω_{uu} and ω_{uv} are the matrices of the site-site intramolecular correlation functions of the solute of solute u and the solvent v respectively. The RISM equation can estimate the site-site distribution. However, it cannot evaluate the spatial distribution.

II.2.5. Separation of Spatial and Orientational Coordinates

Liu and Toshiko [21] adopted another method to get the pair distribution function with spatial and orientational dependence. According to them, a perturbation-type decomposition of the solute-solvent interaction potential leads to a separation of $g(\vec{r},\Omega)$ into two parts, a Ω-dependent part and an Ω-independent part. The Ω-independent part can be solved by integral equation theory and the Ω-dependent part can be treated as a Boltzmann factor. They used their theory to calculate system of water around frozen water clusters and yielded good results in agreement with those from Monte Carlo simulations.

II.3. Non-uniform OZ Equation

The method of establishing non-uniform OZ equation for application to adsorption systems was proposed by Percus [22]. The starting point is a mixture in which each component is present with a uniform density. One component in the mixture is taken to a limit where it becomes infinitely dilute and its molecular radius can be considered to be very large in comparison to that of other species. Similar to the uniform OZ equation, closure equations are needed which also have three forms like those of the uniform OZ equation. The non-uniform OZ equations are in the following forms:

$$\tilde{h}_{12}^{(a,a)} = \tilde{c}_{12}^{(a,a)} + \rho_a \int \tilde{h}_{13}^{(a,a)} \tilde{c}_{32}^{(a,a)} d\vec{q}_{3a} \tag{2.87}$$

$$\tilde{h}_{12}^{(w,w)} = \tilde{c}_{12}^{(w,w)} + \rho_a \int \tilde{h}_{13}^{(w,a)} \tilde{c}_{32}^{(a,w)} d\vec{q}_{3a} \tag{2.88}$$

$$\tilde{h}_{12}^{(w,a)} = \tilde{c}_{12}^{(w,a)} + \rho_a \int \tilde{h}_{13}^{(w,a)} \tilde{c}_{32}^{(a,a)} d\vec{q}_{3a} \tag{2.89}$$

$$\tilde{h}_{12}^{(a,w)} = \tilde{c}_{12}^{(a,w)} + \rho_a \int \tilde{h}_{13}^{(a,a)} \tilde{c}_{32}^{(a,w)} d\vec{q}_{3a} \tag{2.90}$$

In which ρ_a is the density of the component a at a large distance from the component w, and a tilde denotes a function in a uniform phase having this density. $h_{12}^{(w,a)}$ expresses the density variation in a due to the presence of w and therefore has the significance of a singlet correlation function $h^{(a)}$, although it originates as a pair-wise property. Under these conditions the pair distribution $\rho^{(w,a)}$ can be interpreted as a singlet distribution function for the adsorbate fluid $\rho^{(a)}$. We may therefore write

$$\rho^{(a)} = \rho_a g^{(a)} = \rho_a (1 + h^{(a)}) \tag{2.91}$$

Beglov and Roux (Ref. [23] and [24]) used the non-uniform OZ equation to describe the average structure of a polar liquid around a complex molecular solute of irregular shape. They assumed that an isolated molecular solute is immersed in a polar liquid of nonpolarizable spherical particles with an embedded point dipole in their center. The aim of their research is to

determine the average distribution function $\langle \rho(\vec{r}_1, \omega_1) \rangle$, in response to the perturbing potential $U(\vec{r}_1, \omega_1)$, with an HNC approximation used for a single solute in the infinite dilution limit. Their equation is written

$$\langle \rho(\vec{r}_1, \omega_1) \rangle = \overline{\rho} \exp[-\beta U(\vec{r}_1, \omega_1) + \int d\vec{r}_2 \frac{d\omega_2}{4\pi} c(\vec{r}_1, \omega_1, \vec{r}_2, \omega_2) \Delta\rho(\vec{r}_2, \omega_2)] \qquad (2.92)$$

where $c(\vec{r}_1, \omega_1, \vec{r}_2, \omega_2)$ is the correlation function of the unperturbed liquid, and $\Delta\rho(\vec{r}_2, \omega_2)$ is the deviation form the bulk density, $\rho(\vec{r}_2, \omega_2) - \overline{\rho}$. Their numerical solution, obtained on a discrete three-dimensional cubic grid in Cartesian coordinates, yields the average solvent density and polarization density at all points around the solute.

Mitsunori and Junta [25] used the similar method as Beglov and Roux did, but the equation form is a bit different. Their equation is in the following form

$$h_{uv}(\vec{r}) = c_{uv}(\vec{r}) + \rho_v \int c_{uv}(\vec{r}') h_{vv}(\vec{r} - \vec{r}') d\vec{r}' \qquad (2.93)$$

where ρ_v is the density of the solvent, $h_{uv}(\vec{r})$ s the solute-solvent total correlation function, $c_{uv}(\vec{r})$ is the solvent-solvent direct correlation function, and $h_{vv}(\vec{r})$ is the solvent-solvent total correlation function. The coordinates $\vec{r}, \vec{r}'$ include the orientational coordinates. They obtained the spatial water distribution around $5\alpha - cholest - 2 - ene(C_{27}H_{46})$ and used computer graphics technique to visualize it.

The above three methods can deal with the adsorption of dense liquid near a hard wall or a complex molecule. But when the background liquid is dilute, or just gas, these methods would fail because in their calculation they assume that the two-body direct correlation function does not change throughout the whole iteration process. This is obviously unphysical when these methods are applied to the dilute gas adsorption calculation.

II.4. Born-Green-Yvon Approach

Fischer and Methfessel [26] proposed a method using the Born-Green-Yvon equation to solve the gas adsorption problem and their method is applicable to the dense liquid near a hard wall or the gas-liquid interface problem. Their starting point is the Born-Green-Yvon equation

$$\nabla_1 \ln(n(\vec{r}_1)) = -\beta \nabla_1 u^s(\vec{r}_1) + \int n(\vec{r}_2) g(\vec{r}_1, \vec{r}_2)[-\beta \nabla_1 u(r_{12})] d\vec{r}_2 \tag{2.94}$$

For spherical particles with external potential u^s and intermolecular potential u, the total potential can be written as

$$U = \sum_i u^s(r_i) + \sum_{i<j} u(r_{ij}) \tag{2.95}$$

They argued that the repulsive force should essentially determine the structure of a uniform fluid while the attractive force merely form a uniform background potential. For non-uniform fluid, it is rather plausible that the pair correlation function will be less important in the mean attractive force exerted on one particle, than in the mean repulsive force because of the long-range nature of the attractive forces. In this sense, they made a few approximations:

First split the intermolecular potential $u(r)$ into a repulsive part $u^0(r)$ and an attractive part $u^1(r)$, which by insertion into Eq (2.93) yields the mean repulsive and the mean attractive force on particle 1. Then, the attractive force is treated in the simplest way by ignoring any correlations. In the mean repulsive force, the pair correlation function is assumed to be that of a reference system of particles interacting through soft repulsive potential $u^0(r)$. Finally, the repulsive interaction is replaced by the hard-sphere interaction and the pair correlation function is related locally to that of a homogeneous hard sphere fluid at the average density $\bar{n}$.

Under above assumptions, after a few steps the Born-Green-Yvon equation turns into

$$\begin{aligned} \nabla_1 \ln(n(\vec{r}_1)) &= -\beta \nabla_1 u^s(\vec{r}_1) - \beta \nabla_1 \int n(\vec{r}_2) u_1(r_{12}) d\vec{r}_2 \\ &+ \int n(\vec{r}_2) g^{HS}{}_{\text{hom}}(d; \bar{n}) \left(\frac{-\vec{r}_{12}}{r_{12}}\right) \delta(r_{12} - d) d\vec{r}_2 \end{aligned} \tag{2.96}$$

$\overline{n}$ is defined as following

$$\overline{n}(\vec{r}_1,\vec{r}_2)=\frac{1}{V}\int n(\vec{r}+\vec{r}_c)d\vec{r} \tag{2.97}$$

Where the average is done over a sphere of diameter d centered at the point of contact $\vec{r}_c=\frac{1}{2}(\vec{r}_1+\vec{r}_2)$. For one dimensional adsorption problem, for example, the adsorption on a plane (2.96) can be simplified to

$$\begin{aligned} n(z_0) &= n_b \exp(-\beta u^s(z_0) \\ &- \int \beta u^1(r_{02})[n(z_2)-n_b]d\vec{r}_2 + 2\pi\int_{z_0}^{\infty} dz_1 \int_{-d}^{d} dz_{12} n(z_2) g^{HS}{}_{\text{hom}}[d,\overline{n}(z_1,z_2)]z_{12}) \end{aligned} \tag{2.98}$$

This equation was solved by iteration at low temperature and density ($T^*=1.002, \rho=0.02$) and was reported to be in close agreement with the simulation data of Rowley et al. [27].

The underlying character of this theory is to represent the structure of the non-uniform fluid by a non-uniform hard-sphere fluid, which is held together by a long-range attractive force. The essential requirement is that the correct structure is established for the non-uniform hard-sphere fluid and is assured by the coarse graining (doing average without adding weighted function) feature, which feeds back the singlet density through the density $\overline{n}$. It is interesting to note that the BGY equation, without this coarse graining feature, does not successfully predict the singlet density profile for a non-uniform fluid of hard spheres.

A similar method is called Loveet-Mou-Buff equation [28]. Their equation looks like

$$\nabla_1 \ln(n(\vec{r}_1)) = -\beta\nabla_1 u^s(\vec{r}_1) + \int c(\vec{r}_1,\vec{r}_2)\nabla_2 n(\vec{r}_2)]d\vec{r}_2 \tag{2.99}$$

This equation can be used to explore the gas-liquid interface properties (Ref. [29] and [30]). One thing to notice is that $c(\vec{r}_1,\vec{r}_2)$ is a relatively shorter ranged function than $g(\vec{r}_1,\vec{r}_2)$, which will bring some convenience to the calculation, but the gradient operator prevents us from applying this kind of method to the three-dimensional system.

II.5. Molecular Density Functional Theory

Saam and Ebner [31] proposed a density functional theory of classical system.

Consider a classical system with fixed chemical potential μ and temperature T in the presence of an external potential v, which couples to the particle number density n. Then there exists a functional $\Omega[n]$ of n such that the minimum value of

$$\Omega = \Omega[n] + \int d^3 r v(\vec{r}) n(\vec{r}) \tag{2.100}$$

with respect to variation of n at constant μ, T, v, and volume V, is the equilibrium grand free energy of the system; n at the minimum is the equilibrium number density. The minimum condition is

$$\left.\frac{\delta\Omega}{\delta n}\right|_{T,\mu,v,V} = \left.\frac{\delta\Omega[n]}{\delta n}\right|_{T,\mu,V} + v = 0 \tag{2.101}$$

In their notation,

$$v_n = -\left.\frac{\delta\Omega[n]}{\delta n}\right|_{T,\mu,V} \tag{2.102}$$

Perform the functional derivation of v_n with respect to n

$$\frac{\delta v_n}{\delta n} = -\frac{1}{\beta}\left[\frac{\delta(\vec{r}-\vec{r}')}{n(\vec{r})} - c(\vec{r},\vec{r}')\right] \tag{2.103}$$

and the functional integrate (2.101) in the space of density functions, which is characterized by a simple parameter α varying from 0 to 1

$$\beta[v_n(r) - v_0(r)] = -\ln\left[\frac{n(\vec{r})}{n_0(\vec{r})}\right] + \int_0^1 d\alpha \int d^3 r' \frac{\partial n(\vec{r}';\alpha)}{\partial\alpha} c(\vec{r},\vec{r}';\alpha) \tag{2.104}$$

If choose

$$n(\vec{r};\alpha) = n_0(\vec{r}) + \alpha[n(\vec{r}) - n_0(\vec{r})] \tag{2.105}$$

assume that

$$n_0(\vec{r}) = n_0 = const \tag{2.106}$$

and

$$v_0(\vec{r}) = 0 \tag{2.107}$$

(2.102) reduces to

$$\beta v_n(r) = -\ln\left[\frac{n(\vec{r})}{n_0}\right] + \int_0^1 d\alpha \int d^3r' c(\vec{r},\vec{r}';\alpha)[n(\vec{r}') - n_0] \tag{2.108}$$

Further integrating (2.99) yields the expression for the grand free energy if following the same path in the space of density functions

$$\begin{aligned}\beta(\Omega - \Omega_0) &= \beta \int d^3r v(\vec{r})[n(\vec{r}) - n_0] + \int d^3r n(\vec{r}) \ln\left(\frac{n(\vec{r})}{n0}\right) \\ &- \int d^3r [n(\vec{r}) - n_0] \\ &- \int_0^1 d\alpha \int_0^{\alpha'} d\alpha' \int d^3r d^3r' c(\vec{r},\vec{r}';\alpha)[n(\vec{r}) - n_0][n(\vec{r}') - n_0]\end{aligned} \tag{2.109}$$

There are many ways to remove the α dependence in the two-body direct correlation function. Like Ebner and Saam [32] assumed that

$$\int_0^1 d\alpha \int_0^{\alpha'} d\alpha' c(\vec{r},\vec{r}';\alpha) = \frac{1}{2} c(\vec{r},\vec{r}';\bar{n}) \tag{2.110}$$

where

$$\bar{n} = \frac{1}{2}[n(\vec{r}) + n(\vec{r}')] \tag{2.111}$$

Instead of solving (2.106) directly, they propose a trial solution of the density file and substitute the trial solution into (2.107) and minimize the grand free energy and get the solution of the density profile. The advantage of this method is that it only requires the direct correlation function in homogeneous fluid as input and this direct correlation function in homogeneous fluid can be evaluated fairly accurately with the uniform OZ equation.

However, according to Lane et al. [33] the density functional theory did not give very good results compared with the computer simulation for the one-dimensional case. A weak point is that it does not appear to contain the correct Henry law limit and must therefore be suspect at low adsorbate coverage.

Other density functional methods [34-37] are a bit different from what Saam and Ebner did. Usually what they did was to separate the Helmholtz free energy into two parts:

$$F[\rho(\vec{r})] = F^{id}[\rho(\vec{r})] + F^{ex}[\rho(\vec{r})] \tag{2.112}$$

And the ideal part can be exactly given as

$$F^{id}[\rho(\vec{r})] = kT\int d\vec{r}\rho(\vec{r})[\ln(\rho(\vec{r})\Lambda^3) - 1] \tag{2.113}$$

The excess free energy $F^{ex}[\rho(\vec{r})]$ is the contribution from the intermolecular interactions and its functional expression remains to be determined. After a functional minimization of the grand potential of an inhomogeneous system, subject to the chemical potential μ and external potential $V_{ext}(\vec{r})$, the density profile can be solved through the Euler-Lagrange equation

$$\rho(\vec{r}) = \rho_b \exp\left(\beta\mu_{ex} - \beta\frac{\delta F^{ex}[\rho(\vec{r})]}{\delta\rho(\vec{r})} - \beta V_{ext}(\vec{r})\right) \tag{2.114}$$

The only thing left is to determine the functional form of $F^{ex}[\rho(\vec{r})]$. Usually $F^{ex}[\rho(\vec{r})]$ is divided into repulsive part and attractive part, and the repulsive part is usually replaced by the hard sphere model, because the functional form of a hard sphere model is very clear now. This method gained some success but for complex intermolecular interaction, it is not so easy to obtain the correct functional form of $F^{ex}[\rho(\vec{r})]$. Therefore it may not work well for the water adsorption problem. So far the hard sphere system, Lennard-Jones system and Yukuwa system are reported to work well with this method.

Another feature in this method is the introduction of the non-local free energy functional through a smoothed (or coarse grained) density distribution $\overline{\rho}(\vec{r})$, which is at each point a non-local functional of $\rho(r)$. Any narrow peak in the real density distribution will be smeared down in the average density distribution, which can be viewed as the mean density around a particle in a volume somewhat related with the range of the interactions.

II.6. Simulation

Fang et al. [6] did canonical ensemble Monte Carlo simulations for water on a planar substrate and on spherical substrates under different temperatures. As they pointed out, extensive work has been done on one-dimensional system, but few people stress the size dependence of the adsorption on nano spherical particles and even the aggregates of those nano spherical particles. The situation can be easily understood, since the simulation in three-dimension is so difficult that the boundary condition cannot be used readily in the adsorption system. If boundary condition is not used, one has to take some special measure to set the particle acting as in the uniform liquid when a particle is far from the substrate.

In their simulation, reflecting plane barrier and a reflecting spherical surface barrier were placed beyond the surface of the planer substrate of the plane substrate and the surface of the spherical substrate, respectively. These barriers created a finite vapor pressure in the systems. However, the most effective way to study the adsorption in such systems is the grand canonical ensemble Monte Carlo simulation or the grand canonical ensemble molecular dynamics simulation and such efforts are very rare. And they reported the water structure were sensitive to substrate size. For example, they indicated that the normalized density distributions narrows as the substrate size increases at the same temperature and the higher the temperature is, the wider the width of density distribution.

II.7. Summary

From Fletcher's work to Marlow's work give a description of the equilibrium of the gas (mainly water vapor) on the aerosol particles with large sizes. While in microscopic range, especially in the nano range, the theory is inadequate and cannot give a good description. Non-uniform OZ equation gives good result when the background is in liquid phase. BGY equation and density functional theory can be applied to one-dimensional adsorption but hard to extend to three-dimensional system. Therefore it is necessary to develop a method to compute the

adsorption in a real three-dimensional system and the detail of this method will be appeared in chapter III, IV and V.

CHAPTER III

METHODOLOGY

III.1. Overview

In this chapter we develop a method that can be used to compute gas adsorption onto a real three-dimensional system including those with nanoscale features. Our integral equation, which resembles a non-uniform OZ equation, is derived from density functional theory. The only required inputs are the direct correlation functions of the uniform fluid at high and low densities. We take argon adsorption onto carbon dioxide and graphite planar substrates as examples to illustrate the method. Finally we compare our results with previous simulation work and find that our results agree with them under the same conditions.

III.2. Introduction

The equations that have been used to compute adsorption phenomenon can be categorized into three classes: the OZ equation, the density functional theory, and the BGY equation. The exact non-uniform OZ equation cannot be solved since it contains the unknown non-uniform correlation functions and the singlet functions. The following type of approximate equation

$$h^{(1)}(r) = c^{(1)}(r) + \rho_b \int h^{(1)}(\vec{r}')c^{(2)}(|\vec{r} - \vec{r}'|)d\vec{r}' \tag{3.1}$$

$$h^{(1)}(r) = c^{(1)}(r) + \rho_b \int c^{(1)}(\vec{r}')h^{(2)}(|\vec{r} - \vec{r}'|)d\vec{r}' \tag{3.2}$$

where $h^{(1)}(r)$ the wall-particle total correlation function, $c^{(1)}(r)$ is the wall-particle direct correlation function, and $c^{(2)}(|\vec{r} - \vec{r}'|)$ is the particle-particle direct correlation function, can be solved by introducing a relationship between $c^{(1)}$ and $h^{(1)}$, provided that $h^{(2)}$ or $c^{(2)}$ are known. In fact, $h^{(2)}$ or $c^{(2)}$ can be obtained from uniform OZ equation. The PY and HNC approximation are used to provide the relationship between $c^{(1)}$ and $h^{(1)}$([33]). In [38-41] these

two approximations are used to treat spherical particles in contact with a wall. Because these two approximations achieved limited success, other approximations came into being, such as those discussed in [42-45], which either gave better descriptions of non-uniform reference states or made improvements to the approximation to $c^{(2)}$.

A numerical method to directly solve the OZ equation (3.1) and (3.2), with PY and HNC approximation, by introducing the 3D lattice to evaluate the distribution function of solvents around solutes with a complicated shape was proposed in references [11-13]. They reported that their result agreed with the molecular dynamics simulation. But according to [33], (3.1) and (3.2) are not valid when the adsorption layer density is much higher than the background density. Therefore, it is not proper to apply (3.1) and (3.2) to gas adsorption case.

The density functional theory dealing with inhomogeneous systems can be divided into local density functional theory and non-local density functional theory. The local density functional theory expresses the free energy as a functional of local density distribution and works well when fluid inhomogeneity is weak. Since the local density functional theory does not take into account strong short-ranged correlation, it is unable to predict the strong short ranged structure. Non-local density functional theory (Refs. [34-37]) treats the free energy as a functional of both a local and non-local averaged density, usually a coarse grained or weighted average varying slowly and smoothly. Non-local density functional theory has been used widely in theoretical predictions (Ref. [34,35] and [37]) of adsorption isotherms related to nano materials. But usually these systems are one-dimensional.

BGY equation can also be applied to adsorption case [46, 47]. And the most successful one is [26], where the pair potential is divided into attractive and repulsive part and the repulsive part is replaced by hard sphere model and the pair correlation function is related locally to that of a homogeneous hard-sphere fluid at average density.

It is interesting to notice that the BGY equation when introduced with the coarse grain feature, can predict the adsorption phenomenon as well as in density functional theory. Therefore the coarse-grained average or weighted average is central to the correctness of the prediction in the adsorption study. In the following part we will establish an OZ like equation with weighted density average feedback from the density functional theory [31, 32] and [48].

III. 3. The Integral Equation Method

Here we take the standard form of the integral equation from [48] (page 319 Eq 7.49, or see [31,32])

$$\ln\left[\frac{\rho(\vec{r})}{\rho_0}\right] + \beta u(\vec{r}) = \int_0^1 \int c_{12}(\vec{r},\vec{r}';\xi)[\rho(\vec{r}') - \rho_0]d\xi d\vec{r}' \tag{3.3}$$

There are a few ways to remove the ξ dependence but none of them has a solid theoretical basis. For example, [16] assumed that

$$\int_0^1 d\xi \int_0^{\xi'} d\alpha' c_{12}(\vec{r},\vec{r}';\xi) = \frac{1}{2} c_{12}(\vec{r},\vec{r}';\overline{\rho}) \tag{3.4}$$

where

$$\overline{\rho} = \frac{1}{2}[\rho(\vec{r}) + \rho(\vec{r}')] \tag{3.5}$$

Here in order to connect (3.3) with (3.1) or (3.2) used in [11-13], so that the equation can be applied to the real three dimensional system, we assume that

$$\int_0^1 \int c_{12}(\vec{r},\vec{r}'\xi)[\rho(\vec{r}') - \rho_0]d\xi d\vec{r}' = \int c_{12}(<\rho(\vec{r})>, |\vec{r} - \vec{r}'|)[\rho(\vec{r}') - \rho_0]d\vec{r}' \tag{3.6}$$

where

$$<\rho(\vec{r})> = \int \rho(\vec{r}') A \exp(-|\vec{r}' - \vec{r}|^4 / L^4) d\vec{r}' \tag{3.7}$$

And $c_{12}(<\rho(\vec{r})>, |\vec{r} - \vec{r}'|)$ is the direct correlation function of the homogenous system at density $<\rho(\vec{r})>$. The weighted density average form was suggested by [23]. Here we take the average

density form of (3.7) because exponential function is a continuous function rather than the simple step function. Since we are doing the calculation on discrete three-dimensional grids, this functional form of density average will produce better result than the simple step function. Finally, we have our equation

$$\ln\left[\frac{\rho(\vec{r})}{\rho_0}\right] + \beta u(\vec{r}) = \int c_{12}(<\rho(\vec{r})>, |\vec{r}-\vec{r}'|)[\rho(\vec{r}') - \rho_0]d\vec{r}' \tag{3.8}$$

(3.8) looks like an OZ equation (3.1) and (3.2) but with a feedback of weighted density. And the only inputs needed are the direct correlation functions of homogeneous fluid at different densities. In the following we will show in detail how this equation can be used in the real three-dimensional adsorption problem.

We take argon adsorption onto the graphite and carbon dioxide plane substrates under $120K$ and $131.78K$ respectively as our example. The argon-argon interaction is defined as follows

$$\Phi(r) = 4\varepsilon\left[\left(\frac{\sigma}{r}\right)^{12} - \left(\frac{\sigma}{r}\right)^{6}\right] \tag{3.9}$$

where, $\varepsilon/k = 119.8K$ and $\sigma = 3.405\text{Å}$. An argon molecule interacting with a plane substrate takes the form

$$\Phi(r) = 4\pi\varepsilon_w n_w {\sigma_w}^3\left[\frac{1}{45}\left(\frac{\sigma_w}{z}\right)^{9} - \frac{1}{6}\left(\frac{\sigma_w}{z}\right)^{3}\right] \tag{3.10}$$

where z is the distance between an argon atom and the plane surface. For argon-graphite system used in [1], $4\pi\varepsilon_w n_w {\sigma_w}^3 = 1.260\times10^4 K$, $\sigma_w = 2.678\text{Å}$, and for argon-carbon dioxide used in [2], $4\pi\varepsilon_w n_w {\sigma_w}^3 = 1.908\times10^3 K$, $\sigma_w = 3.727\text{Å}$. In the weighted density expression (3.7), we take $L = \sigma$, from the normalization condition $A = 151.902$, because we found that outside the hardcore diameter σ , $c_{12}(\rho, |\vec{r}-\vec{r}'|)$ is nearly same for different densities. In other words, the

main difference lies inside the hardcore diameter, and therefore it is reasonable to find the weighted density inside the hardcore diameter.

The other factor left to be determined is the $c_{12}(<\rho(\vec{r})>,|\vec{r}-\vec{r}'|)$. In [32], the author suggested a method to treat this problem, but it must be evaluated at many points on the T^*-n^* plane (Fig. 1 in [32]), where gives the phase coexistence line and would require considerable computer time. In order to overcome this shortcoming, we use the linear combination of a high density and a low-density $c_{12}(<\rho(\vec{r})>,|\vec{r}-\vec{r}'|)$ value to evaluate all points on the T^*-n^* plane, as pointed out by [49] and [50]

$$c(\rho,|\vec{r}-\vec{r}'|)=\frac{f(\rho)}{\rho_H-\rho_L}c(\rho_L,|\vec{r}-\vec{r}'|)+(1-\frac{f(\rho)}{\rho_H-\rho_L})c(\rho_H,|\vec{r}-\vec{r}'|) \tag{3.11}$$

For the points inside the phase coexistence region, where uniform OZ equation fails to give the correct answer to the direct correlation function, interpolation is needed. As pointed out in [24] linear interpolation is not good enough, therefore we construct our interpolation schemes as follows:

We choose two points on the T^*-n^* plane, which are far from the coexistence region, and call them ρ_{high} and ρ_{low}, then evaluate the direct correlation function at these two points and get the $c_{\vec{k}=0}$ value at these two points and call them c_H and c_L.

For those points not inside the phase coexistence region, where the OZ equation can give the correct answer of the direct correlation function, we use the OZ equation to evaluate the $c_{\vec{k}=0}$, which we call it c_k. For these points

$$f(\rho)=\frac{c_k-c_H}{c_L-c_H}(\rho_H-\rho_L) \tag{3.12}$$

We found that in the vicinity of ρ_H and ρ_L, $f(\rho)$ are nearly linear. For the points inside the phase coexistence region, so far no one can give the correct form of the direct correlation function

and interpolation has to be done, also there is no evidence that the direct correlation function has a jump across the phase coexistence region.

Therefore it is reasonable to assume that $f(\rho)$ is smooth and can reflect the nearly linear property at both high and low-density ends. Under this assumption, we decide the interpolation in the phase coexistence region by constructing a line according to the nearly linear property at both high and low density and let them cross at one point and get the value of this point; then do cubic spline interpolation form in the whole region. At low density there may arise some problem, for example the $f(\rho)$ value may be negative, so we do the exponential interpolation at low density instead. In this chapter, we have calculated the $f(\rho)$ value under two different temperatures for argon to be used in carbon dioxide and graphite substrate respectively. Following is the explicit form of the $f(\rho)$ function and their plot. For $T = 120K$

$$f(\rho) = -0.0452 \times 10^{-4} + 0.217\rho + 62.372\rho^2 - 103952.729\rho^3,$$

if $\rho <= 5.066 \times 10^{-6}$.

$$f(\rho) = 0.577 \times 10^{-4} \exp(311.242\rho),$$

if $5.066 \times 10^{-6} \le \rho \le 0.012$.

$$f(\rho) = 0.0337 - 8.049\rho + 582.060\rho^2 - 10719.429\rho^3,$$

if $0.012 \le \rho \le 0.018$.

$$f(\rho) = -0.0365 + 3.486\rho - 50.424\rho^2 + 840.399\rho^3,$$

if $\rho \le 0.02$.

(3.13)

In this case $\rho_H = 0.02$ and $\rho_L = 2.0 \times 10^{-4}$

And for $T = 131.78K$

$$f(\rho) = -0.826\times10^{-4} + 0.411\rho + 14.105\rho^2 - 23507.588\rho^3,$$

if $\rho \le 1.26\times10^{-3}$.

$$f(\rho) = -0.146\times10^{-3} + 0.563\rho - 106.1279\rho^2 + 8299.692\rho^3,$$

if $1.26\times10^{-3} \le 0.011$.

$$f(\rho) = 0.0217 - 5.438\rho + 444.236\rho^2 - 8526.827\rho^3,$$

if $0.011 \le \rho \le 0.016$.

$$f(\rho) = 0.889\times10^{-2} - 3.072\rho + 298.228\rho^2 - 5522.740\rho^3,$$

if $0.016 \le \rho \le 0.018$.

(3.14)

In this case $\rho_H = 0.018$ and $\rho_L = 2.0\times10^{-4}$

From Fig. 1 and Fig. 2 we may notice that the plot is nearly linear at both high-density and low-density end. And in the phase coexistence region the slope of the plot changed quickly. The linear combination of the high-density and low-density direct correlation functions as well as the interpolation rules inside the phase coexistence region plus Eq (3.8) is our main point in this chapter. Finally the integral equation is turned into

$$\ln\left[\frac{\rho(\vec{r})}{\rho_0}\right] + \beta u(\vec{r}) = \int\left\{\frac{f(\langle\rho(\vec{r})\rangle)}{\rho_H-\rho_L}c(\rho_L,|\vec{r}-\vec{r}\,'|) + (1-\frac{f(\langle\rho(\vec{r})\rangle)}{\rho_H-\rho_L})c(\rho_H,|\vec{r}-\vec{r}\,'|)\right\}[\rho(\vec{r}\,')-\rho_0]d\vec{r}\,'$$

(3.15)

There appears to be no better way than the iteration method to solve this kind of equation, and usually we have to use the mixing technique ([15])

$$\rho^{new} = (1-\alpha)\rho^{new} + \alpha\rho^{old} \tag{3.16}$$

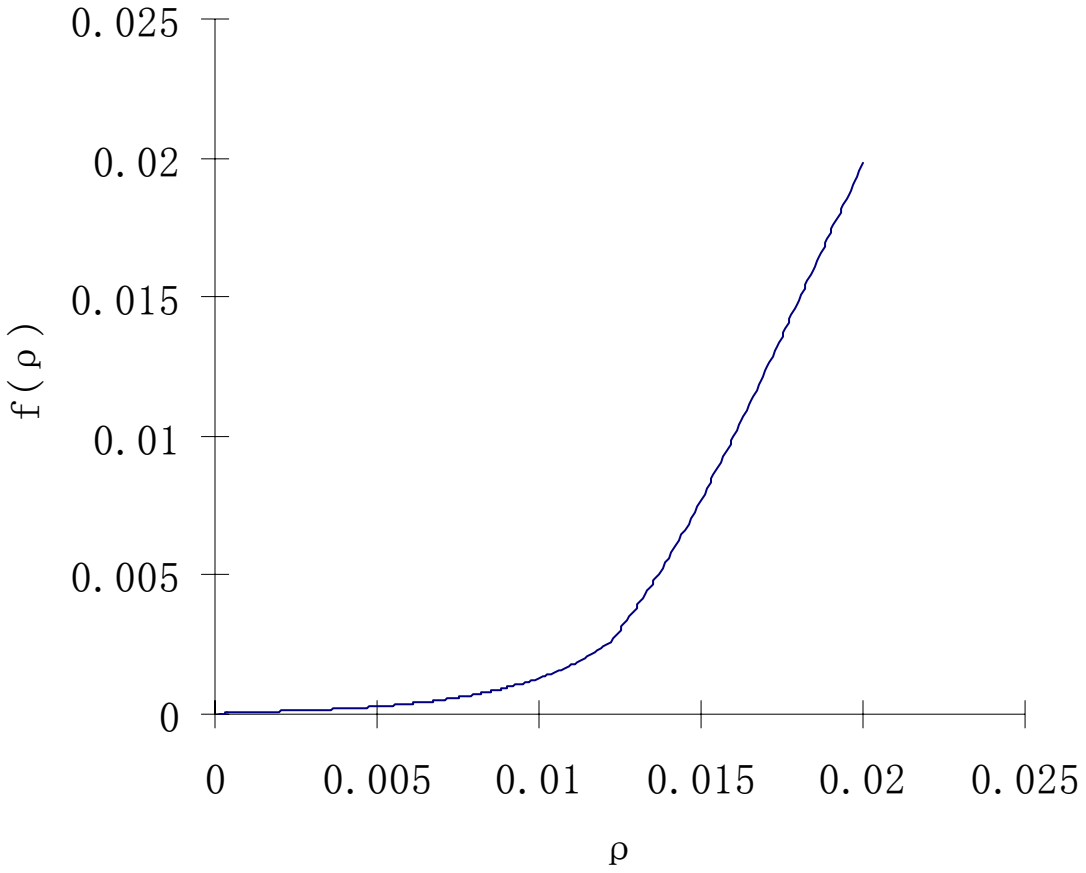

FIG. 1. $f(\rho)$ for $T = 120K$.

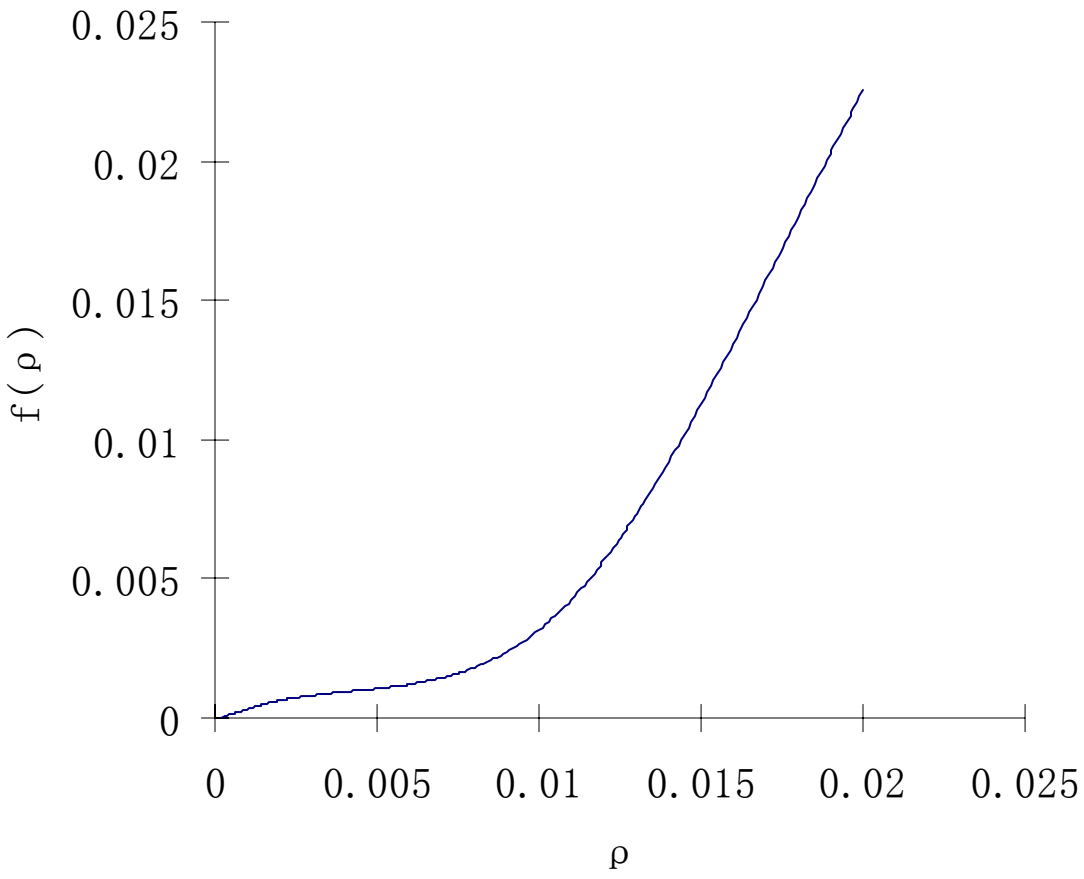

FIG. 2. $f(\rho)$ for $T = 131.78K$.

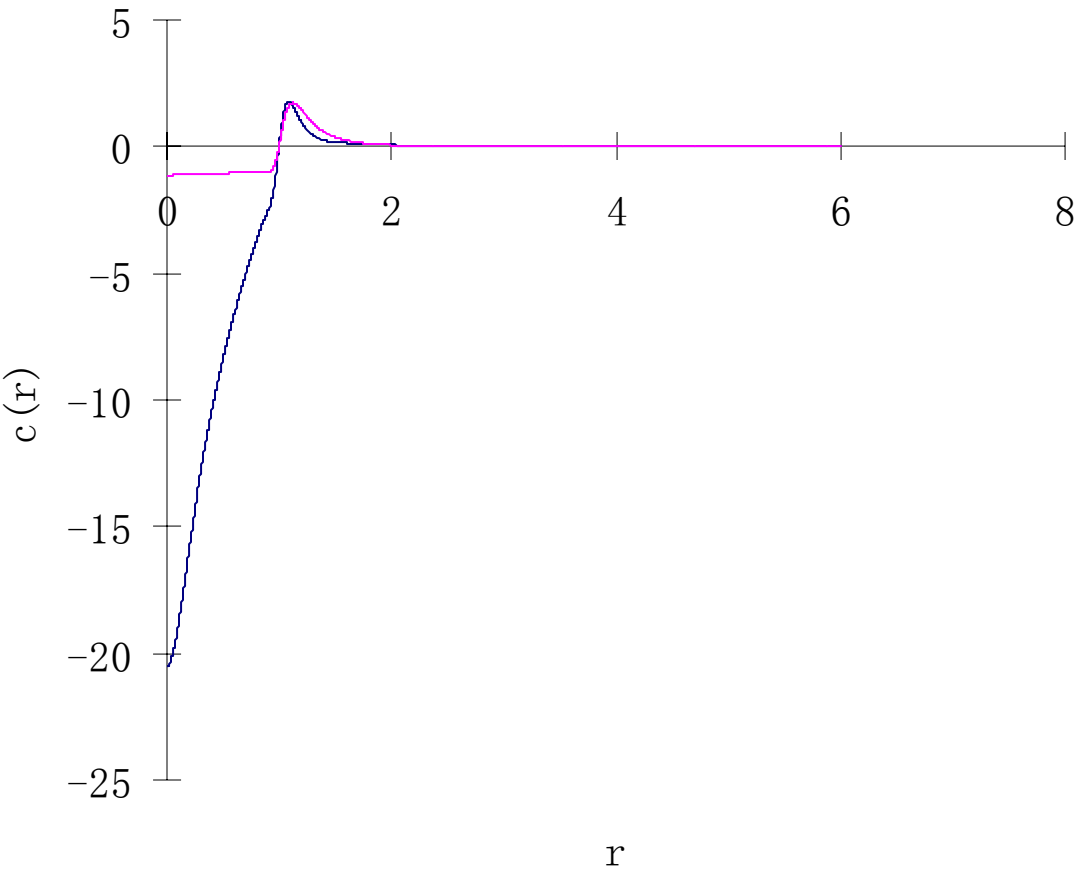

FIG. 3. $c_H(r)$ and $c_L(r)$ $T = 120K$.

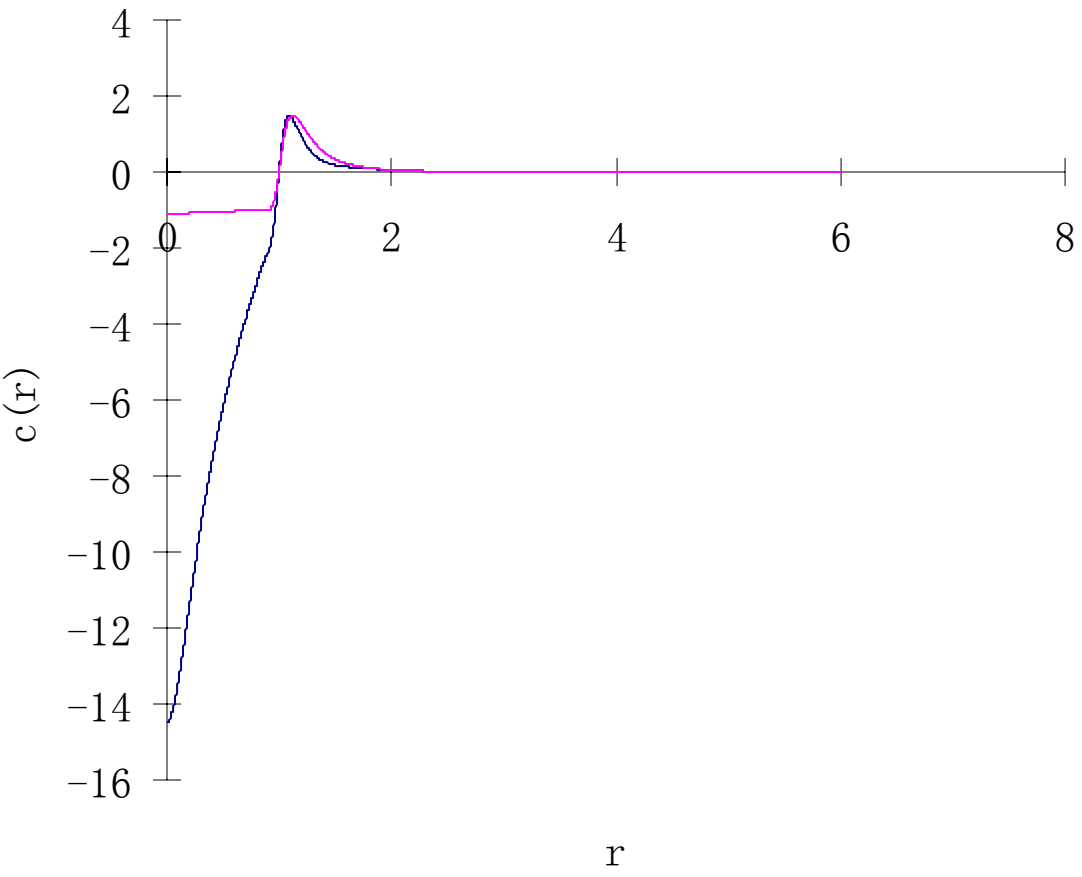

FIG. 4. $c_H(r)$ and $c_L(r)$ $T = 131.78K$.

The determination of α is not so strict and it depends on the convergence property of the integral equation. Commonly for the strong interaction between the molecule and substrate α should be high.

In our model, the three-dimensional FFT should be called only three times for each iteration, one is for the computing of the average density and the other two are for the direct correlation at low and high density.

The direct correlation function is determined via the homogeneous OZ equation [15,32], and Fig. 3 and Fig. 4 show the direct correlation functions used in our calculation.

In our calculation the three-dimensional grid size is $128 \times 128 \times 128$, and the cut-off distance is set to be 3.5σ.

III.4. Results and Discussion

We have calculate the argon adsorbed onto the plane substrate of carbon dioxide and graphite under 131.78K and 120K respectively using the method we suggested and compared them with the simulation result in [27] and [33] and found they correspond well with the simulation result.

The result shown in Fig. 5 is comparable with the simulation work Fig. 6 [27] and the BGY equation result Fig. 3 [26]. In Fig. 5 the height of the first peak is around 6.0 and the height of second peak is between 1.5 and 2.0, and we can see the development of the third peak. These three values are very close to the result in [27]. As shown in Fig. 6, when the density goes up, the height of the second peak is getting higher. The result shown in Fig. 6 is comparable with Fig. 3 [33]. It shows that our method works for the gas adsorption onto a plane.

Moreover, this method is to solve the adsorption problem on a three-dimensional grid and it can be easily extended to any substrate with a complex shape. In this paper we used the simplest molecule argon; as pointed by Refs. [23-25], this method can use even complex molecule like water [25]. In chapter IV we will use this method to compute argon adsorption onto

spherical substrates and the aggregates of the spherical substrates. In chapter V we will use this method to compute the water adsorption onto the spherical nano particles and the aggregates of spherical nano particles.

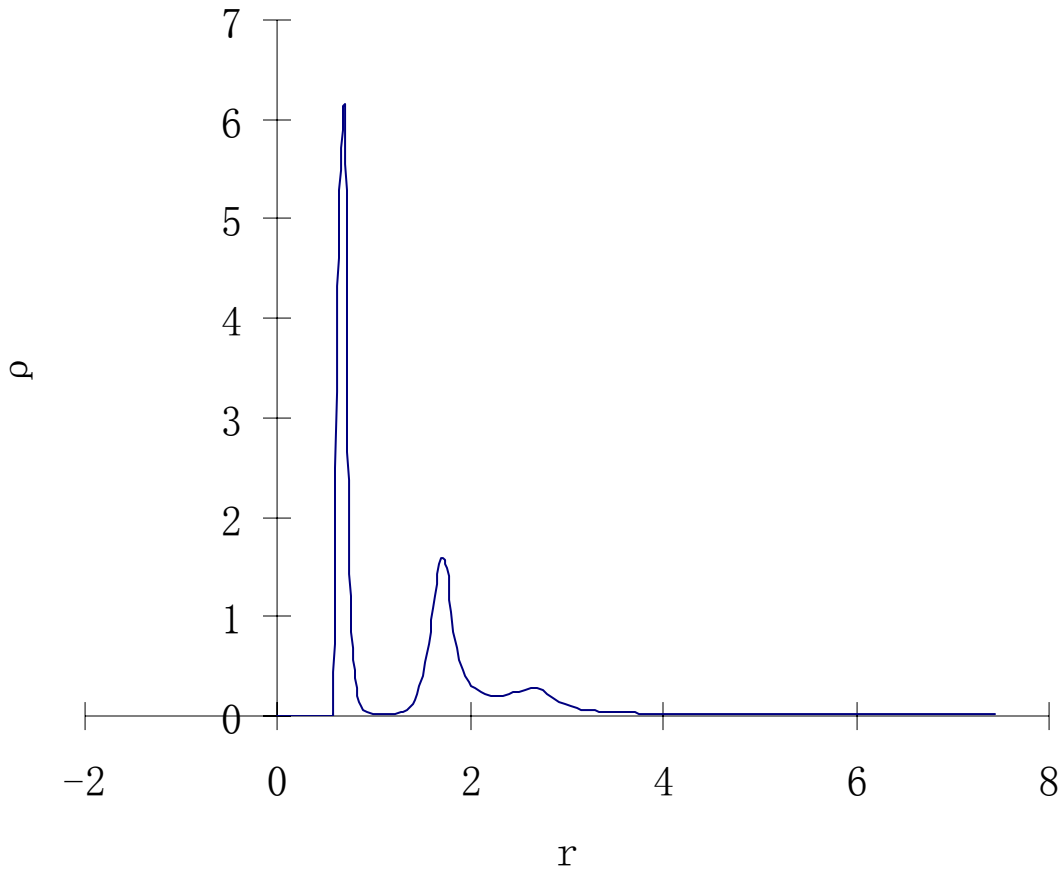

FIG. 5. Argon adsorbed on graphite plane substrate, $T = 120K$, $\rho^* = 0.02$.

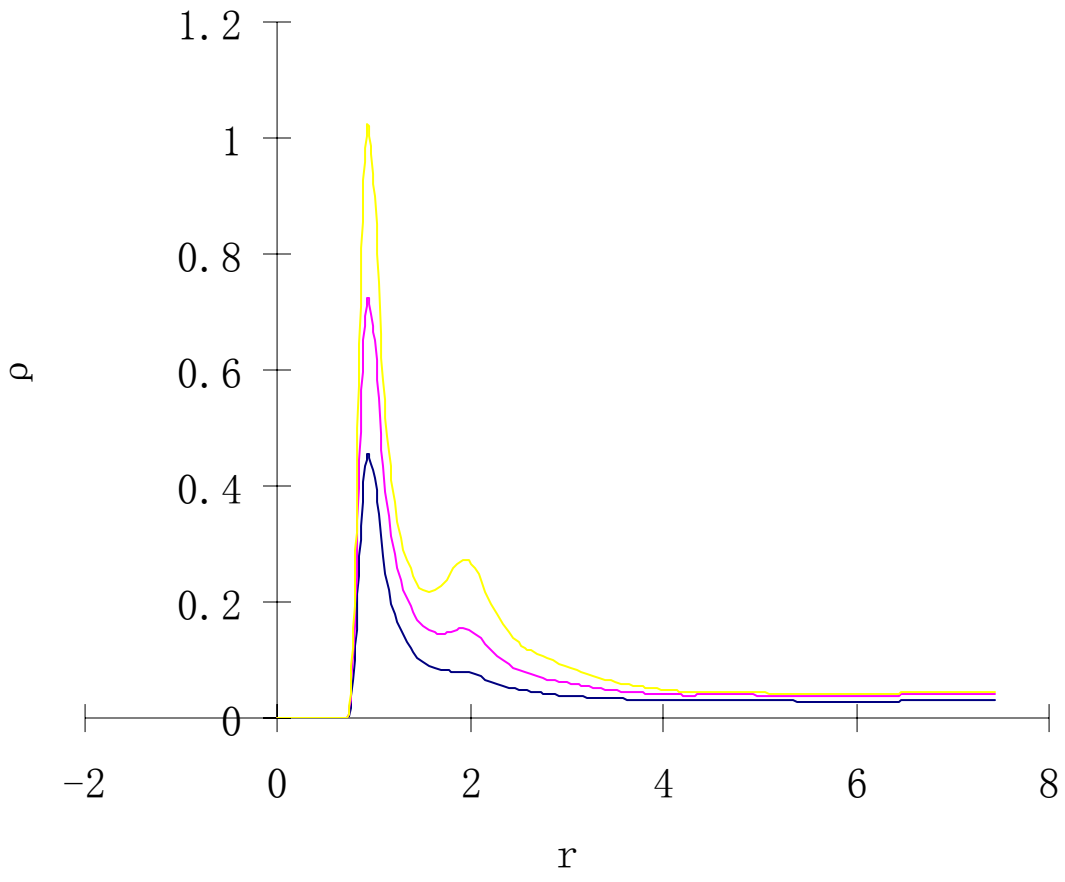

FIG. 6. Argon adsorbed on carbon dioxide plane substrate, $T = 131.78K$, $\rho^* = 0.03$, $\rho^* = 0.04$, $\rho^* = 0.0465$ respectively.

CHAPTER IV

ARGON ADSORPTION

IV.1. Overview

In this chapter, we compute: (1) the density distribution for argon adsorbed onto single, spherical graphite and carbon dioxide substrates with radii $r = 10\text{Å}$, 20Å, 50Å, 100Å; (2) the density distribution of argon adsorbed onto two identical carbon dioxide spheres in contact with radii $r = 10\text{Å}$, 20Å, 50Å, 100Å and (3) the density distribution for argon adsorbed onto the three identical carbon dioxide spheres with radii $r = 10\text{Å}$, with different angles subtended by the three spheres at $\theta = 85^\circ, 105^\circ, 125^\circ$ and 150°. Through the calculation we found that the aggregate structure of the two or three identical spheres can affect the adsorption of the argon molecules.

IV.2. Introduction

In the study of condensation on gas-borne particles, the particles are generally treated as a single isolated spheres. However, aerosols encountered in a variety of environments include particles consisting of contacting, spherical primary units. For large spherical particles, whose radii are greater than 50nm the, macroscopic picture is sufficient. The macroscopic treatment of the condensation is to connect the surface curvature with the Kelvin equation ([3]). Fletcher ([1]) solved the heterogeneous condensation onto a single spherical aerosol particle by adding an interfacial energy contribution due to the presence of the substrate to the Helmholtz energy. Crouzet and Marlow ([2]) applied a general solution for the meniscus between a sphere and plane ([51]) to compute the curvature of the pendular ring of condensation between two macroscopic aerosol spheres with radii greater than 10nm. Their results indicate that even somewhat hydrophobic adhering spheres may be capable of activating as cloud condensation nuclei at the moderate supersaturations encountered in the atmosphere.

However, in the microscopic range, both the theoretical and simulation works are rare; evidently the only seen one is given by Fang et al. [6]. They revealed that in the microscopic range, the adsorption structure and interaction between gas molecules and substrate are sensitive to the substrate size and shape.

In this chapter we will use the argon adsorption onto the aggregates of two or three identical nano spheres as an example to investigate what roles these structures play in gas condensation.

IV.3. Argon-Argon and Argon-Substrate Interaction Potential

The argon-argon interaction is represented here as [27, 33]

$$\Phi(r) = 4\varepsilon\left[\left(\frac{\sigma}{r}\right)^{12} - \left(\frac{\sigma}{r}\right)^{6}\right] \tag{4.1}$$

The simplest energy form between argon and a plane substrate is given by [27] or [33] and is written like

$$\Phi(r) = 4\pi\varepsilon_w n_w {\sigma_w}^3\left[\frac{1}{45}\left(\frac{\sigma_w}{z}\right)^{9} - \frac{1}{6}\left(\frac{\sigma_w}{z}\right)^{3}\right] \tag{4.2}$$

Lennard-Jones 6-12 potentials are assumed to be effective between the atoms of the adsorptive gas and wall. By integrating over the complete volume of the adsorbent, Eq (4.2) is derived.

According to the data provided by [27, 33], we found that for argon-graphite case, $4\pi\varepsilon_w n_w {\sigma_w}^3 = 1.260\times10^4 K$, $\sigma_w = 2.678\text{Å}$ and for Argon-carbon dioxide case, $4\pi\varepsilon_w n_w {\sigma_w}^3 = 1.908\times10^3 K$ and $\sigma_w = 3.727\text{Å}$. If we assume the substrate is spherical and repeat the integration process, we may reach the expression for an argon atom with a spherical substrate,

$$\Phi(r) = 8\pi\varepsilon_w n_w \sigma_w\left[\frac{2}{3}\frac{{\sigma_w}^6 R^3}{(z+R)^3(-z+R)^3} - \frac{2}{45}\frac{{\sigma_w}^{12} R^3(5R^6 + 45z^2R^4 + 63z^4R^2 + 15z^6)}{(z+R)^9(-z+R)^9}\right] \tag{4.3}$$

Fig. 7 is the interaction energy computed with (4.3) for an argon atom interacting with spherical and planar substrates. From the plot we can see that as the size increases, the interaction potential between argon and a substrate tends to that of the argon atom planar case and for large substrates the magnitude of the potential minimum does not change too much. This trend has been pointed out by [6]. We must point out that (4.3) is only a very crude approximation; it does not include the many-body effect. For the more accurate energy form, readers many go to [7], where a nonsingular van der Waals potential plus a Born type repulsive potential is used and give the binding energy accurately for many materials.

IV.4. Computational Details

The central task is to apply (3.8) plus the interpolation rules, (3.13) or (3.14) for high-density and low-density direct correlation function to the three-dimensional calculation. We will list the main procedure in the following.

For the one-sphere case, the grid size is $128\times128\times128$, and the grid spacing is 0.2Å, that is to say $dx = dy = dz = 0.2\text{Å}$, the cutoff distance used is 3.5σ. We assign the coordinate of the center of the spherical substrate to be $(0,0,-R)$. The three-dimensional grid is represented as (i,j,k), $i\in[1,128]$, $j\in[1,128]$, and $k\in[1,128]$. Each point inside the three-dimensional grid corresponds with a point in real space. Let $i_0 = 64$, $j_0 = 64$, $k_0 = 1$, the coordinate for each point in the three-dimensional grid is $x = (i - i_0)dx$, $y = (j - j_0)dy$, $z = ((k - k_0) - 0.2868)dz$. The shift of z is not a unique choice; we choose the value 0.2868 because we wish the grid to have a small intersection with the spherical substrate.

After arranging the spherical substrate and the three-dimensional grid, we use the iteration scheme to solve (3.8). First, we guess the density value for each grid point to be set as

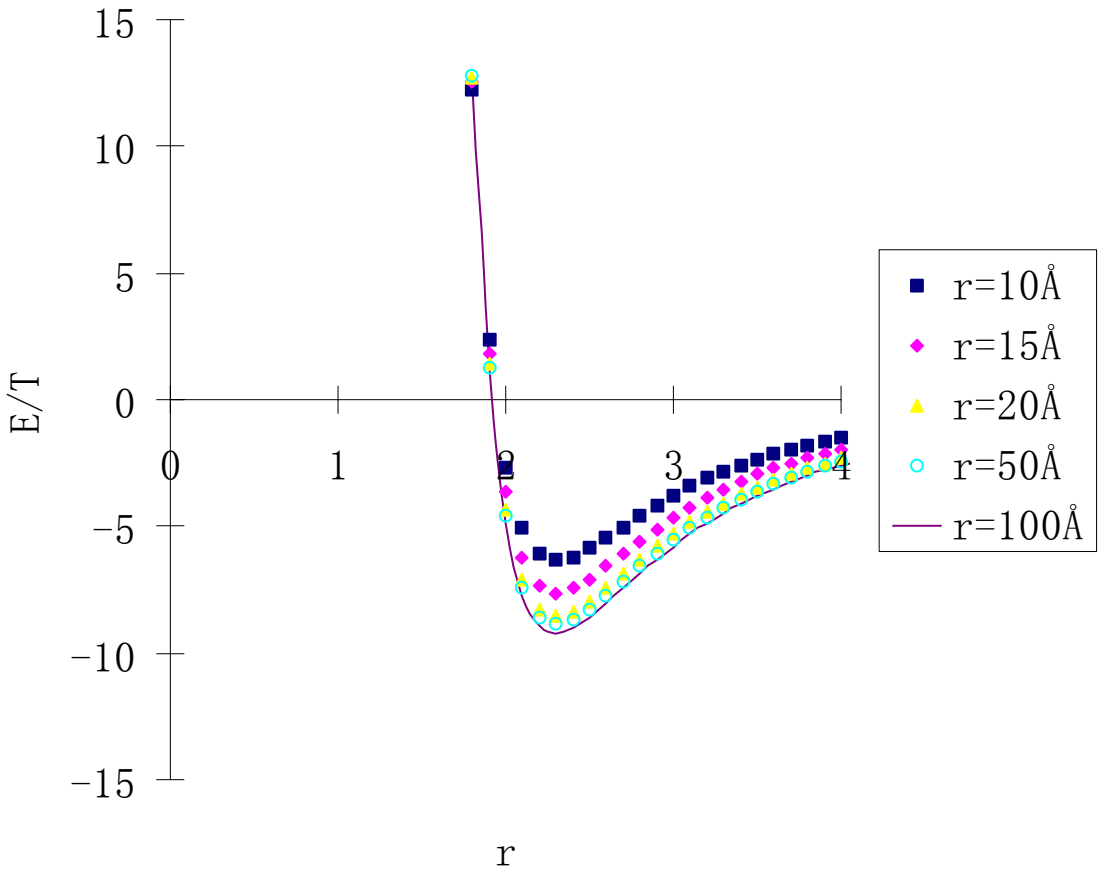

FIG. 7. The interaction energy between an argon atom and the spherical substrate with the radii $r = 10\text{Å}$, 20Å, 50Å, 100Å and plane case under 120K.

$$\rho(x, y, z) = \rho_0 \exp(-U_{sub} / T) \tag{4.4}$$

Where ρ_0 is the background density. The choice we made here is rather simple and explicit. Second, we compute the average density of each point in the three-dimensional grid using (3.7). From (3.7) we know that $<\rho(\vec{r})>$ is the convolution of $\rho(\vec{r})$ and $A\exp(-r^4/L^4)$. This convolution can be easily evaluated via the three-dimensional FFT. Third, we evaluate the other two convolutions related to the high-density direct correlation function $\int \{c(\rho_H, |\vec{r}-\vec{r}'|)\}[\rho(\vec{r}')-\rho_0]d\vec{r}'$ and low-density direct correlation function $\int \{c(\rho_L, |\vec{r}-\vec{r}'|)\}[\rho(\vec{r}')-\rho_0]d\vec{r}'$ respectively. So far we get the value of the right hand side of (3.8). Finally we evaluate the new density and compare the new value of the old value see if the iteration converges, if the iteration does not converge, repeat the above procedure until it converges. To permit the iteration process to converge quickly, the mixing technique is used as pointed out as (3.16).

In fact we may use the symmetry to facilitate our calculation. For the one-sphere case, we know that those points that have the same distance from the center of the spherical substrate should have the same values. Therefore we need only calculate the density on (i_0, j_0, k) grid and then interpolate on the remaining grids based on the symmetry rules.

For two identical spheres in contact, if we set the coordinates of the two spheres to be $(0,-R,0)$ and $(0,R,0)$, then the system, two planes $y=0$ and $z=0$ are the symmetry planes. Moreover, the system has rotational symmetry along the y-axis. Therefore we need only evaluate the density on grids in $x=0$ plane and then interpolate the others via the symmetry rules. The same happens in the three identical spheres case.

For the two or three-sphere case, $128 \times 128 \times 128$ is not large enough, and the larger size has to be used. However the direct evaluation FFT on the larger grid is a very time consuming job. We follow the idea proposed in [52], to do the convolution in blocks.

IV.5. Results and Discussion

First we have calculated the argon adsorbed onto single spherical graphite and carbon dioxide substrates at 120K and 131.78K respectively, and the results are shown in Fig. 8 and Fig. 9.

In Fig. 8 and Fig. 9 we may notice that for the smallest size spherical substrates, the first peak is low; as the size of the substrate increases, the first peak goes higher and when the substrate size goes to 10nm, the first peak value is nearly equal that of a plane.

This suggests that for the adsorption of a single spherical substrate, when the substrate size is over 10nm, we may treat it as a plane. Also we may notice the development of the second peak and the third peak as the substrate size goes larger. And for the plane case, both the density values we calculated correspond with reported simulation result [27, 33].

For two identical spherical substrates in contact, as we stated previously, the coordinates of the two spheres are $(0,-R,0)$ and $(0,R,0)$, and we plot the density from the contact point along $(0,0,l)$ direction in Fig.10.

From Fig. 10 we may notice that as the twin sphere size goes higher, both the first peak and the second peak grows more rapidly than the one sphere case. The value of the first peak is twice as large as the corresponding one sphere case. For r=10 nm, both the first peak and the second peak are far larger than the corresponding one sphere case, and we can draw the conclusion that this plot shows the starting of the condensation. The trend also corresponds to what [2] found in the macroscopic case.

In Fig. 11 to Fig. 15 we show more detailed view of the density value for the two-sphere case. This time the density is plotted in the vicinity of the central line and these plots can show

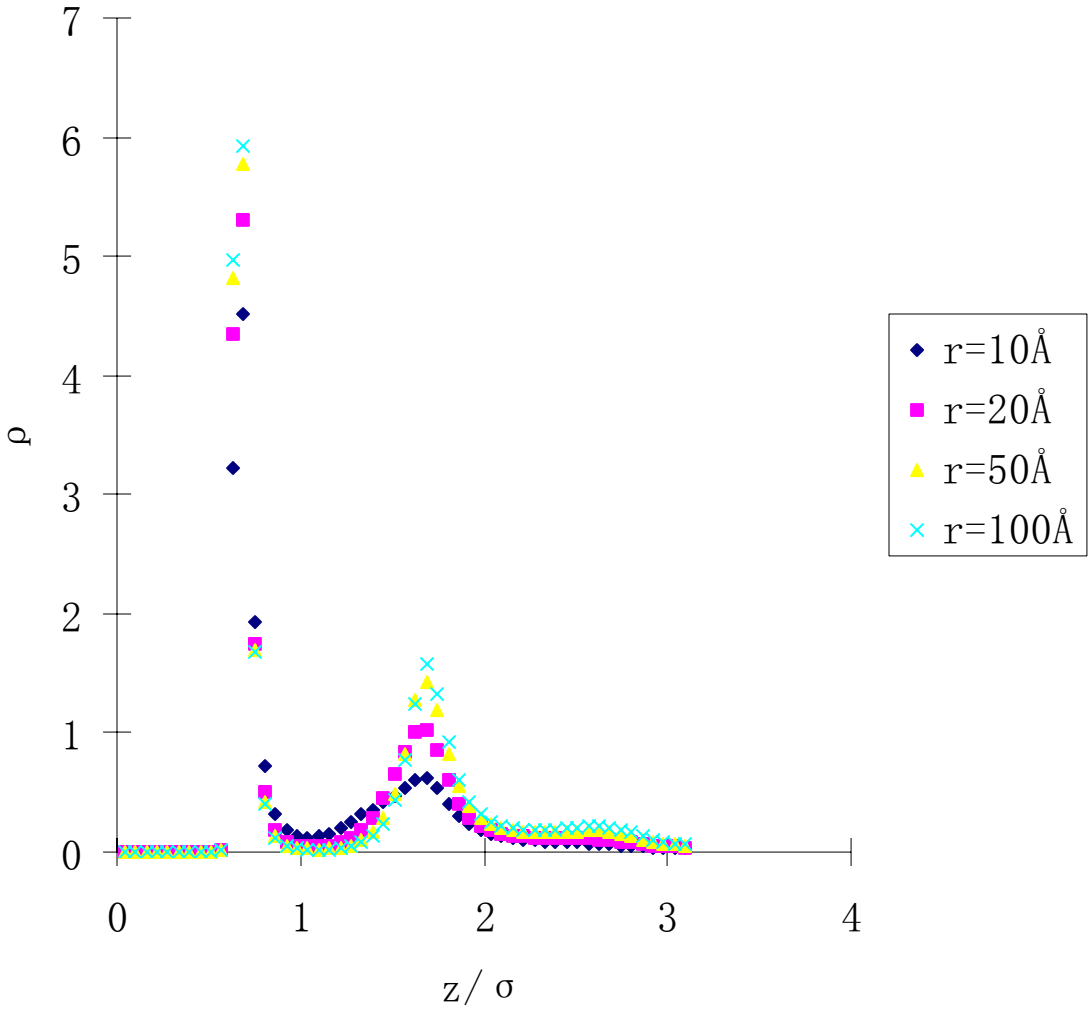

FIG. 8. Argon adsorbed onto the single spherical substrate with radii $r = 10\text{Å}$, 20Å, 50Å, 100Å and onto the plane case at 120K.

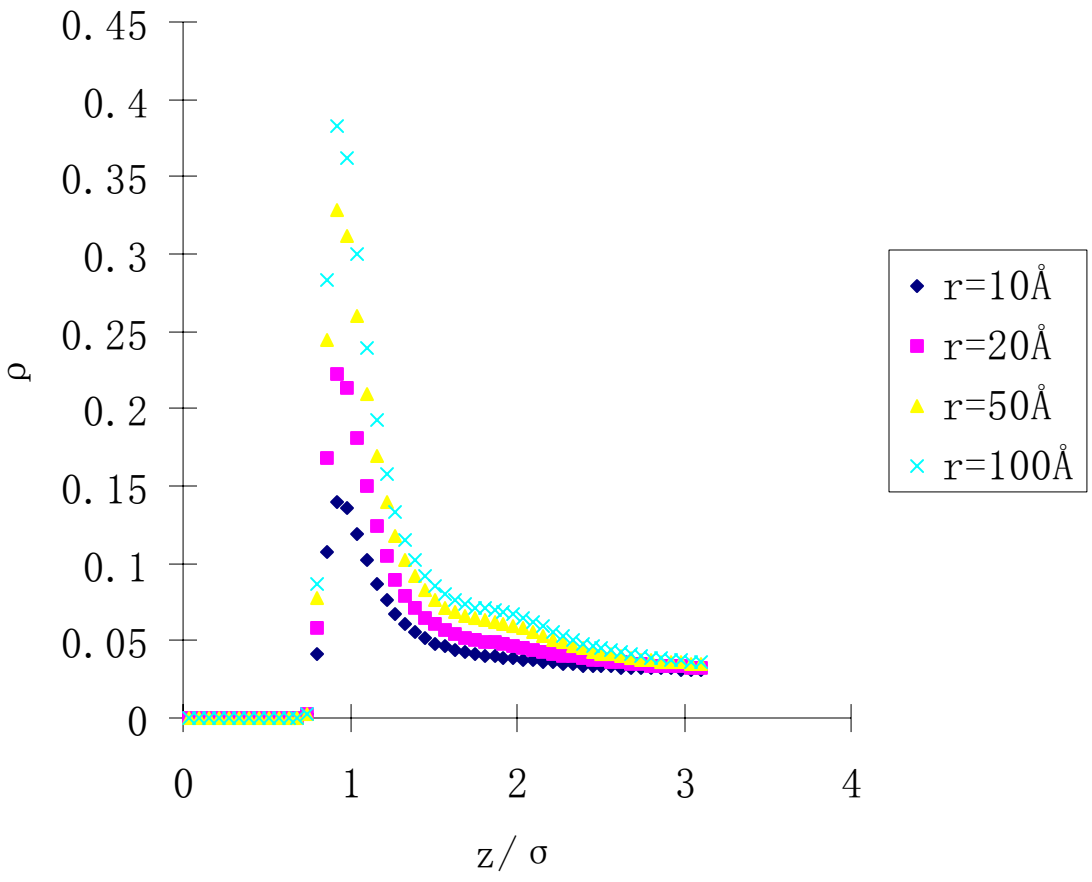

FIG. 9. Argon adsorbed onto the single spherical substrate with radii $r = 10\text{Å}$, 20Å, 50Å, 100Å, and plane case at 131.78K

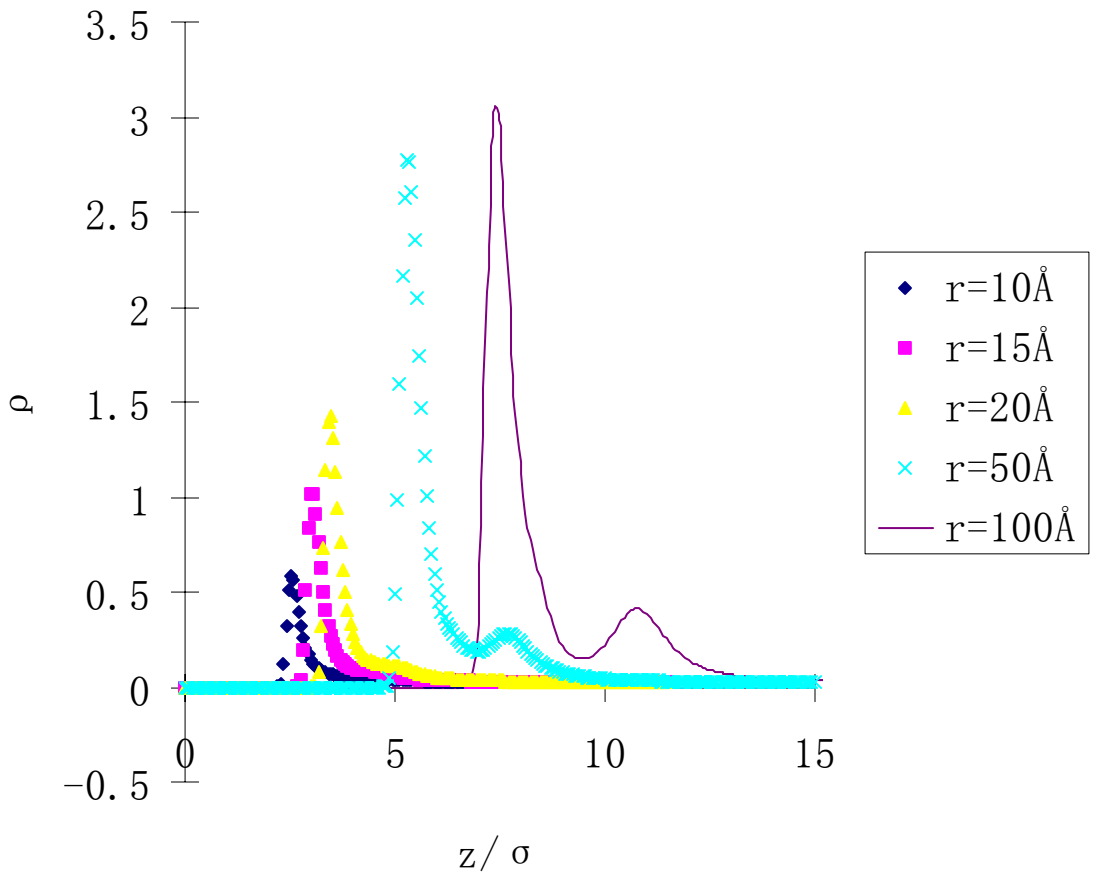

FIG. 10. Density along (0,0,1) direction from the contact point of the two identical spherical substrate with radii $r = 10\text{Å}$, 15Å, 20Å, 50Å, 100Å, the background density is 0.03 and T=131.78K.

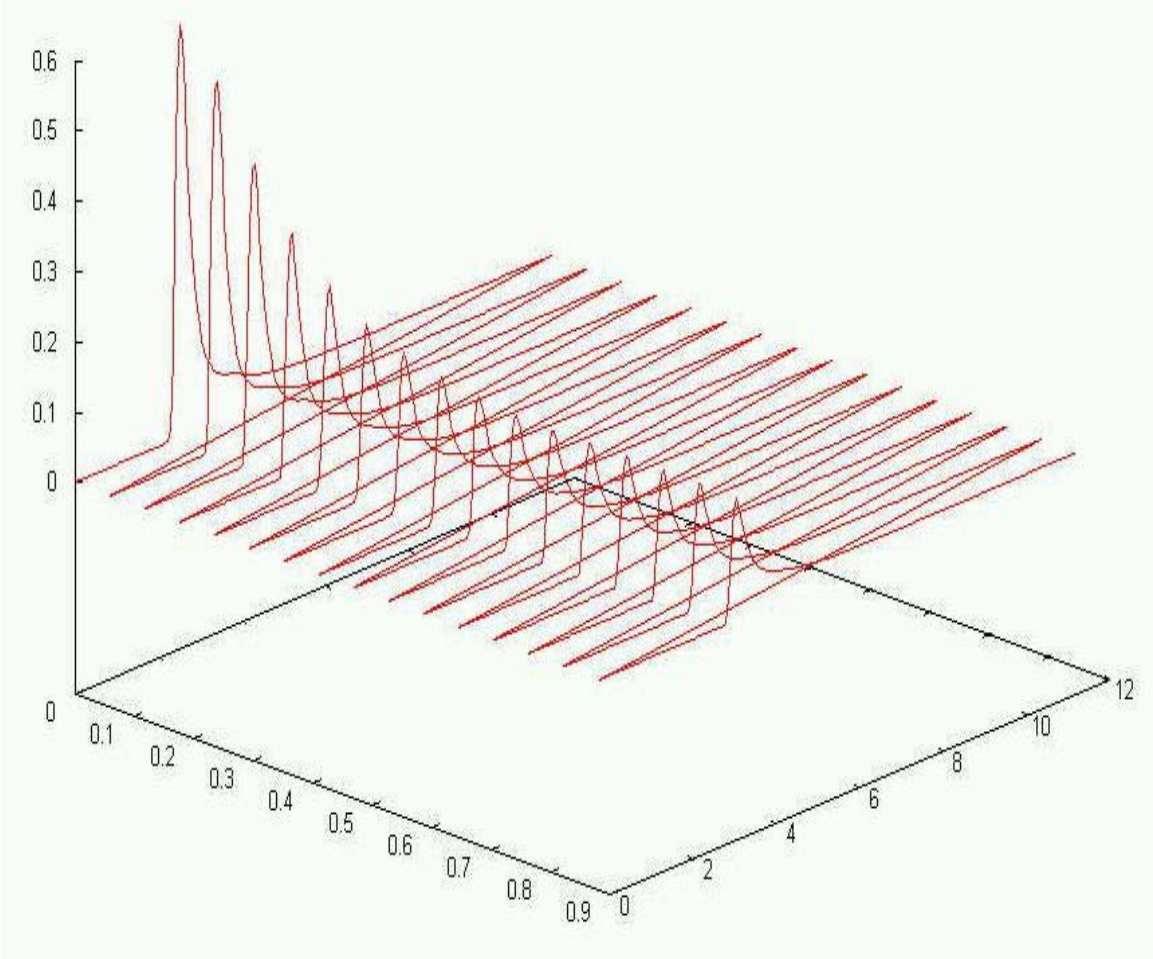

FIG. 11. Argon-uptake within the interstitial region for $r = 10\text{Å}$.

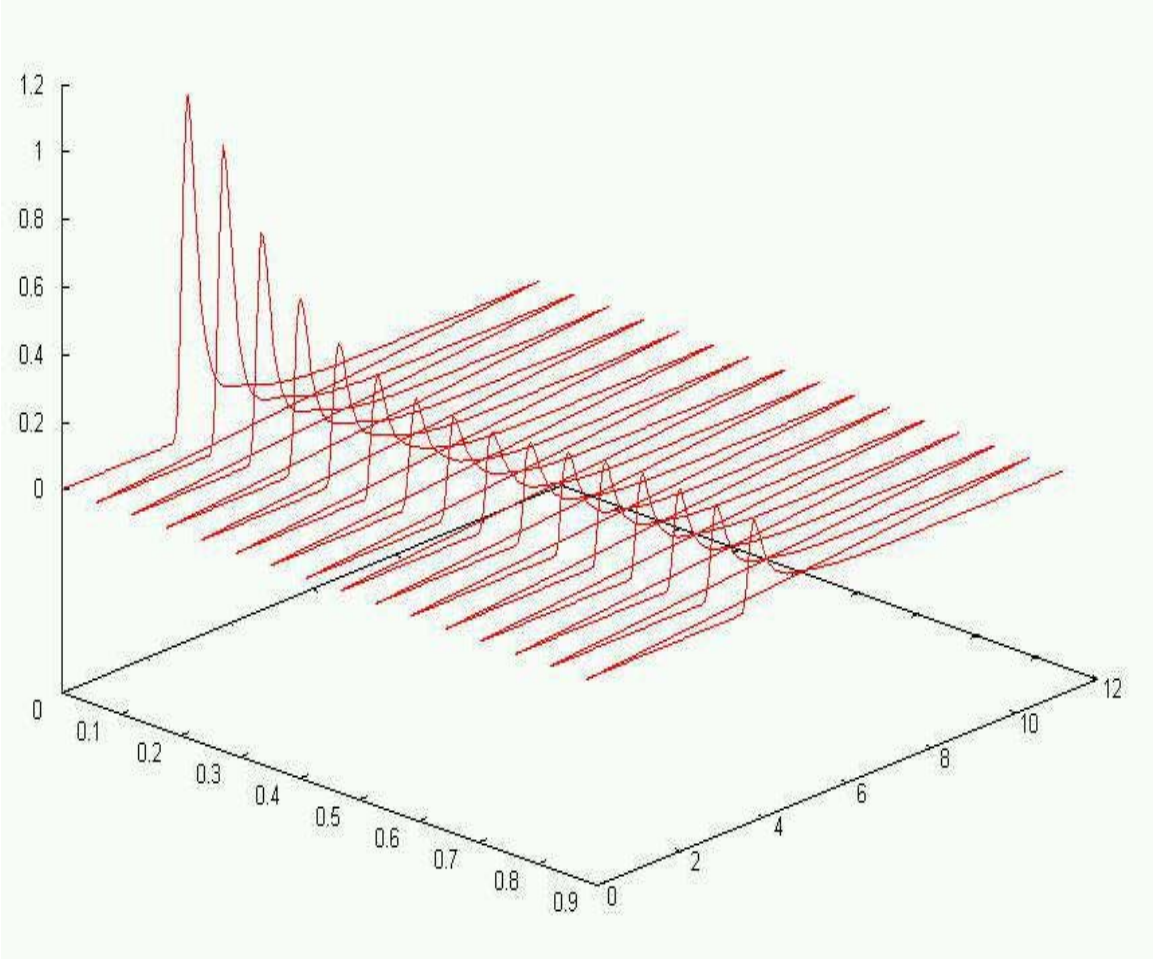

FIG. 12. Argon-uptake within the interstitial region for $r = 15\text{Å}$.

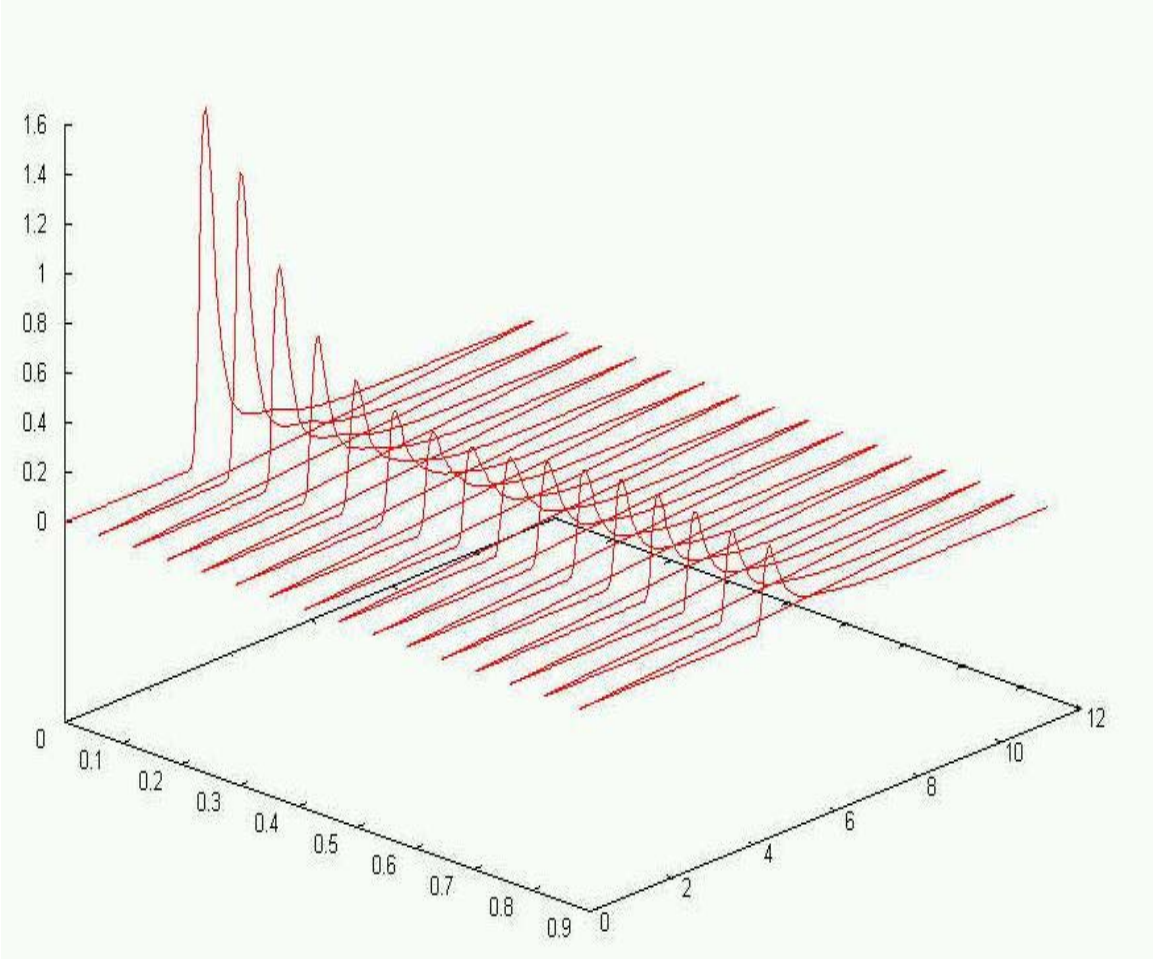

FIG. 13. Argon-uptake within the interstitial region for $r = 20\text{Å}$.

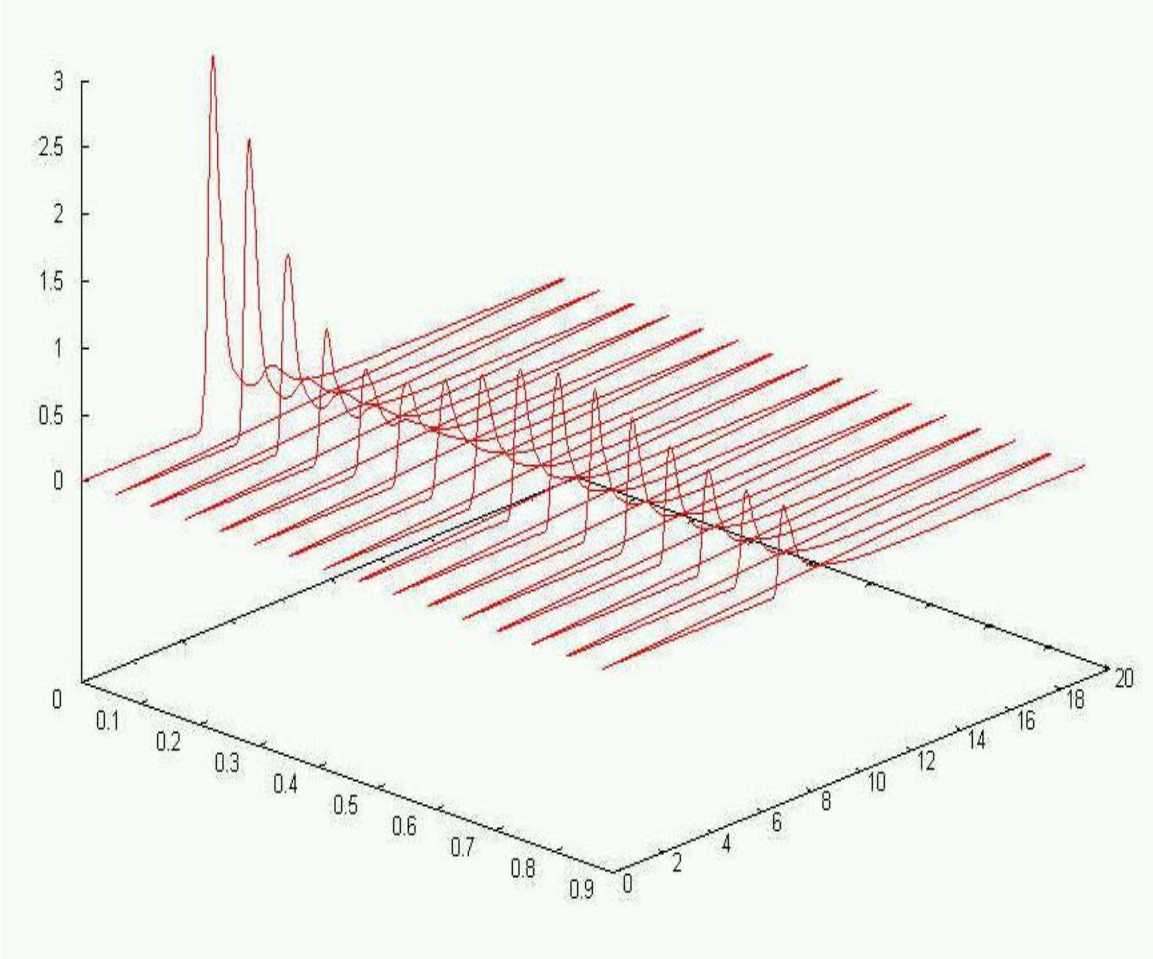

FIG. 14. Argon-uptake within the interstitial region for $r = 50\text{Å}$.

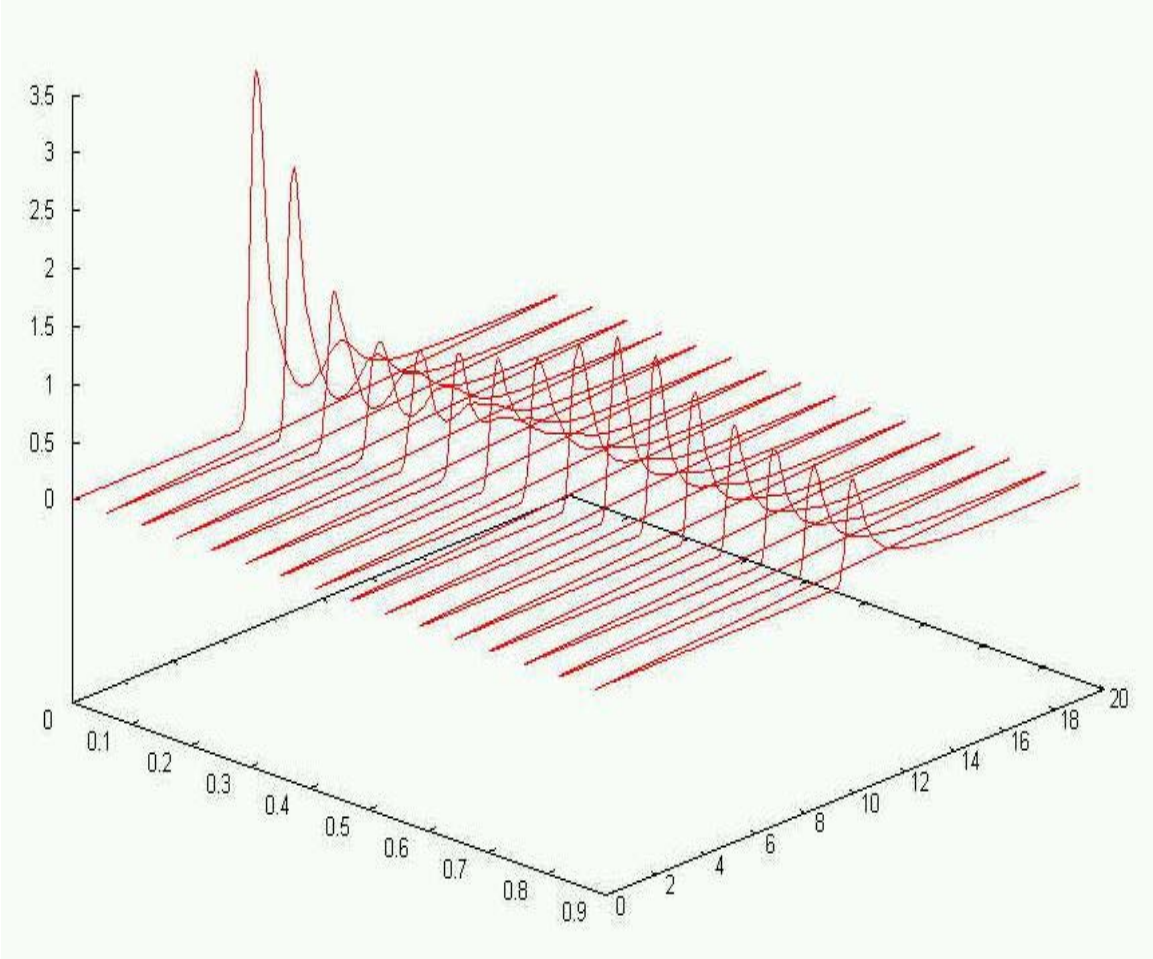

FIG. 15. Argon-uptake within the interstitial region for $r = 100\text{Å}$.

the detailed structure of the argon-uptake within the interstitial region. As pointed out previously the two-sphere structure has the rotational symmetry along y-axis, in these plots we only show the density on z=0 plane and due to the existence of the symmetry plane y=0, we only plot y>0 part.

From Fig. 11 to Fig. 15 we may notice that the ring structure is formed around the two spheres. This can be understood as for small size of the substrate, the argon atoms are piles on the central line and in the vicinity of the central line. As the substrate size increases, the density on the central line tends to go to saturation, and the argon cluster has to spread away from the central line. This trend is most remarkable for r=10nm case. This indicates that the two-sphere sphere structure really can help to accumulate more argon atoms within the interstitial region of the two spheres. And this phenomenon resembles the capillary condensation to some extent.

In Fig. 16 we show the density value for the three identical spherical substrate with radii 1nm, and the angle subtended by the three spheres are $\theta = 85^\circ, 105^\circ, 125^\circ$ and 150°. The axial line is taken from the surface of the central sphere. The purpose of this calculation is to see whether some cluster has formed with in the region that the three spheres form. Or in more detail, since the three-sphere structure contains two two-sphere structures, we will investigate whether the cluster formed within the pendular ring of the two two-sphere structures can be connected.

From this plot, it is clear that there exists a best angle for the three-sphere structure to take up the argon, and for $\theta = 85^\circ$ we have the highest adsorption. From 1.5σ to 2.0σ there is a pleatu formed, this is different from the corresponding one-sphere case, so we may imagine that a larger cluster formed here and the two clusters formed within the two pendular regions connected. As the angle increases, this trend is weak, and finally for $\theta = 150^\circ$, one sphere case. This also shows the similarity as the capillary condensation.

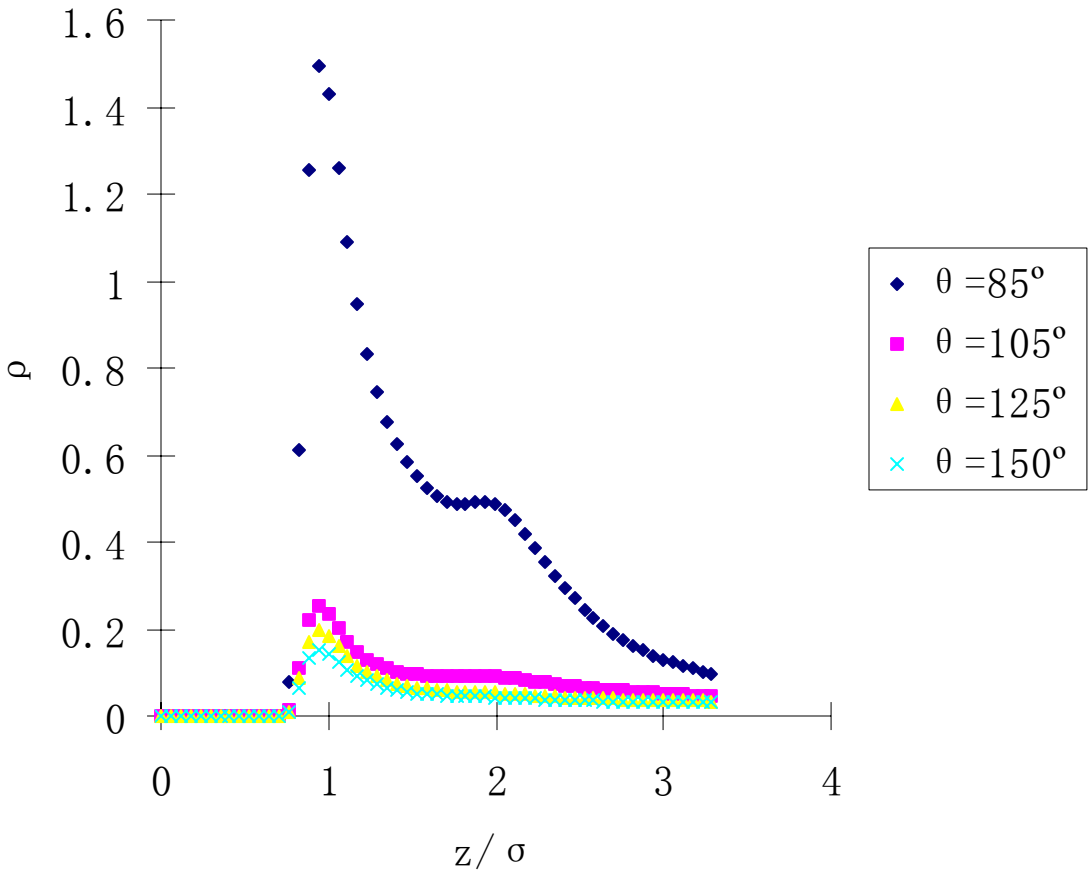

FIG. 16. The density value for the three identical spherical substrate with radii 1nm, and the angle subtended by the three spheres are $\theta = 85^\circ, 105^\circ, 125^\circ$ and 150°. The axial line is taken from the surface of the central sphere.

CHAPTER V

WATER ADSORPTION

V.1. Overview

In this chapter, we use the method developed in Chapter III and chapter IV to compute water adsorption onto nano spherical substrate and aggregates of the spherical substrates with the oxidized surfaces of different extents. From the calculation we find that the aggregation of identical nano spheres improves the water adsorption ability.

V.2. Introduction

Water uptake by aggregate aerosol particles is very important and poorly understood. In the macroscopic case, the equilibrium vapor pressure of water over a surface is a function of the thermodynamic free energies and entropies of the water in the vapor and condensed, or surface, phases. In the macroscopic or continuum treatment of substrate coverage by condensate, a widely used formalism of the equilibrium thermodynamics ([1, 2]) is to calculate the vapor pressure over a condensate droplet on the substrate surface. Then, condensation is thermodynamically favored when total interfacial energy loss due to growth of the droplet exceeds the heat gain resulting from entropy loss associated with condensation. No accounting is made for thin or thick films and, as in the Kelvin equation ([3]), the Laplace description of differential pressure across a curved condensate gas surface ([4]) is used. Provided the substrate particle is much larger than the condensate molecule, and other dimensions and conditions are suitable for use of experimentally determined, static contact angles, this approach can be useful for particles of radii on the order of or larger than 50 nm. For particulate substrates in the small nanometer range, a number of crucial differences from the macroscopic case can be identified. Substrate coverage by condensate is not adequately described as continuous in the same sense as for a macroscopic substrate where coverage can be averaged over areas that are significantly larger than the 0.5-1 nanometer domains where condensate clustering and discontinuity occur. When the substrate

size comes to the nanometer range, the word “density distribution” is a more precise terminology instead of vapor pressure because the macroscopic picture fails. In the earlier study ([6]), Monte Carlo simulations were made of the interaction energies of a nominal mono layer of water on a plane surface and on 1, 1.5 and 2nm radius spheres for which the substrate material interacted with the water via Van der Waals potential ([7]) expected of tetradecane. Those calculations showed the effect of substrate particle size on the interaction energy between condensate and substrate and the consequences of the resultant size dependence on the structuring of water on the substrate. But sufficient calculations were not conducted to show in useful detail the transition of water-substrate attraction energy from small sphere to plane. Therefore, no film information was derived to indicate when the macroscopic picture would be adequate, according to interaction energy and associated condensate structure criteria.

In this chapter, we will use the method developed in Chapter III and chapter IV to compute the water adsorption on one nano aerosol, two identical nano aerosol and three identical nano aerosol with different angles formed.

V.3. Water Model

The water model most widely used in computer simulation now days are TIP3P and TIP4P models ([53], [54]), SPC model ([55]) and SPC/E model ([56]). However, as pointed out by [18] and [19], these models are not applicable to the integral equation study of thermodynamic states of water. This is not because the models themselves are wrong, but because of the lack of the orientational dependence in the bridge function in the integral equation theory. Other models ([57-59]) do not have strong theoretical basis, but they can at least qualitatively show the main features of water and are applicable to the integral equation theory and we will adopt the models like these in our calculation of direct correlation functions of water at both high density and low density limit.

The water model we used here mainly follows [59]. The potential between two water molecules 1 and 2 with configurations X_1 and X_2 is in the form

$$V(X_1, X_2) = V_{sp}(X_1, X_2) + V_{dd}(X_1, X_2) + V_{qq}(X_1, X_2) + V_{hb}(X_1, X_2) \qquad (5.1)$$

Where sp means the spherical London type interaction, dd means electrostatic interaction, qq means the quadrupole-quadrupole interaction, and hh is the item that mimics the hydrogen bonds.

$$V_{sp}(X_1, X_2) = V_{sp}(r_{12}) = \frac{A_{sp}}{r_{12}} \exp(-z r_{12}) \qquad \text{If } r_{12} \geq \sigma$$

And

$$V_{sp} = \infty \qquad \text{If } r_{12} < \sigma \qquad (5.2)$$

$$V_{dd} = -\sqrt{\frac{10}{3}} \frac{\mu^2}{{r_{12}}^3} {\Phi_{00}}^{112} \qquad (5.3)$$

$$V_{qq} = 2\sqrt{\frac{14}{3}} \frac{Q^2}{{r_{12}}^5} \left[{\Phi_{-2-2}}^{224} + {\Phi_{-22}}^{224} + {\Phi_{2-2}}^{224} + {\Phi_{22}}^{224} \right] \qquad (5.4)$$

$$V_{hb} = A_{hb} z k_3(z r_{12}) [{\Phi_{0-2}}^{033} + {\Phi_{02}}^{033} - {\Phi_{-20}}^{303} - {\Phi_{20}}^{303}] \qquad (5.5)$$

Where

$$A_{sp} = -0.2925 \times 10^2 \, KJcm / mol$$

The value we used in this chapter is only one fourth of the value used in [59], for with the value used in [59], we cannot reproduce the structure of the liquid water.

$$A_{hb} = -0.19 \times 10^2 \, KJcm / mol$$

$$z = 6.8 \times 10^8 \, / cm$$

${\Phi_{\mu\nu}}^{mnl}$ are the generalized spherical harmonics. And

$$k_n(x) = \sqrt{\frac{\pi}{2x}} K_{n+\frac{1}{2}}(x)$$

With $K_{n+\frac{1}{2}}(x)$ the modified spherical Bessel function of the third kind.

$$k_3(x) = \frac{\pi}{2}\frac{e^{-x}}{x}\left(1 + \frac{6}{x} + \frac{15}{x^2} + \frac{15}{x^3}\right)$$

The closure relation for solving the OZ equation is

$$c = -\beta V(X_1, X_2) + W \tag{5.6}$$

$$\begin{aligned} W = {} & w^{110}(r_{12})\Phi^{110} + w^{112}(r_{12}) + \\ & w^{003}(r_{12})\left[\Phi_{0-2}{}^{033} + \Phi_{02}{}^{033} - \Phi_{-20}{}^{303} - \Phi_{20}{}^{303}\right] + \\ & w^{330}(r_{12})\left[\Phi_{-2-2}{}^{330} + \Phi_{-22}{}^{330} + \Phi_{2-2}{}^{330} + \Phi_{22}{}^{330}\right] + \\ & w^{332}(r_{12})\left[\Phi_{-2-2}{}^{332} + \Phi_{-22}{}^{332} + \Phi_{2-2}{}^{332} + \Phi_{22}{}^{332}\right] + \\ & w^{334}(r_{12})\left[\Phi_{-2-2}{}^{334} + \Phi_{-22}{}^{334} + \Phi_{2-2}{}^{334} + \Phi_{22}{}^{334}\right] + \\ & w^{336}(r_{12})\left[\Phi_{-2-2}{}^{336} + \Phi_{-22}{}^{336} + \Phi_{2-2}{}^{336} + \Phi_{22}{}^{336}\right] \end{aligned} \tag{5.7}$$

Where

$$w^{110}(r_{12}) = -\frac{\sqrt{3}}{\pi}k_0{}^{11}z_0{}^{11}k_0(z_0{}^{11}r_{12})$$

$$w^{112}(r_{12}) = \frac{1}{\pi}\sqrt{\frac{15}{2}}k_0{}^{11}z_0{}^{11}k_2(z_0{}^{11}r_{12})$$

$$w^{033}(r_{12}) = -\frac{2\sqrt{7}}{\pi}k_0{}^{03}z_0{}^{03}k_3(z_0{}^{03}r_{12})$$

$$w^{330}(r_{12}) = -\frac{2\sqrt{7}}{\pi}k_0{}^{33}z_0{}^{33}k_3(z_0{}^{33}r_{12})$$

$$w^{332}(r_{12}) = \frac{\sqrt{105}}{\pi}k_0{}^{33}z_0{}^{33}k_2(z_0{}^{33}r_{12})$$

$$w^{334}(r_{12}) = -\frac{2}{\pi}\sqrt{\frac{77}{2}}k_0{}^{33}z_0{}^{33}k_4(z_0{}^{33}r_{12})$$

$$w^{336}(r_{12}) = \frac{2}{\pi}\frac{\sqrt{3003}}{5}k_0{}^{33}z_0{}^{33}k_6(z_0{}^{33}r_{12}) \tag{5.8}$$

Where

$$k_0(x) = \frac{\pi}{2}\frac{e^{-x}}{x}$$

$$k_2(x) = \frac{\pi}{2}\frac{e^{-x}}{x}(1+\frac{3}{x}+\frac{3}{x^2})$$

$$k_3(x) = \frac{\pi}{2}\frac{e^{-x}}{x}(1+\frac{6}{x}+\frac{15}{x^2}+\frac{15}{x^3})$$

$$k_4(x) = \frac{\pi}{2}\frac{e^{-x}}{x}(1+\frac{10}{x}+\frac{45}{x^2}+\frac{105}{x^3}+\frac{105}{x^4})$$

$$k_6(x) = \frac{\pi}{2}\frac{e^{-x}}{x}(1+\frac{21}{x}+\frac{210}{x^2}+\frac{1260}{x^3}+\frac{4725}{x^4}+\frac{10395}{x^5}+\frac{10395}{x^6}) \tag{5.9}$$

And

$$\sigma = 2.7\text{Å}$$

$$\frac{k_0^{11}}{\sigma} = -3.79\times10^3$$

$$z_0^{11}\sigma = 10.0$$

$$\frac{k_0^{03}}{\sigma} = -4.8\times10^8$$

$$\frac{k_0^{33}}{\sigma} = -1.0\times10^7$$

In [59], the direct correlation function of water for high density (liquid density) was solved analytically, and here we solve the problem numerically with iteration method. The following is the procedure, which was suggested in [15].

The OZ equation for liquid theory looks like

$$h(12) - c(12) = \frac{\rho}{8\pi^2}\int c(13)h(32)d(3) \tag{5.10}$$

With the closure suggested by [59], Eq. (5.6)

Let $\eta(12) = h(12) - c(12)$

Eq. (5.10) turns into

$$\eta(12) = \frac{\rho}{8\pi^2}\int c(13)\left[c(32) + \eta(32)\right]d(3) \tag{5.11}$$

Next we expand the items used in OZ equation on the basis of generalized spherical harmonics ([15]). From (5.6) to (5.9) we find that the contributions needed are

$(m,n,l,\mu,\nu) = (0,0,0,0,0)\,,(1,1,0,0,0)\,,(1,1,2,0,0)\,,(2,2,4,\pm2,\pm2)\,,(0,3,3,0,\pm2)\,,(3,0,3,\pm2,0)\,,$

$(3,3,0,\pm2,\pm2)\,,(3,3,4,\pm2,\pm2)\,,(3,3,6,\pm2,\pm2)\,.$

$$c(\vec{r}_1,\vec{r}_2) = \sum_{mnl,\mu\nu} c_{\mu\nu}{}^{mnl}(R_{12})\Phi_{\mu\nu}{}^{mnl}(\Omega_1,\Omega_2,\hat{R}_{12}) \tag{5.12}$$

$$\eta(\vec{r}_1,\vec{r}_2) = \sum_{mnl,\mu\nu} \eta_{\mu\nu}{}^{mnl}(R_{12})\Phi_{\mu\nu}{}^{mnl}(\Omega_1,\Omega_2,\hat{R}_{12}) \tag{5.13}$$

Because (5.10) contains the convolution term, we have to do the Fourier transformation of (5.12) and (5.13). The Fourier transformation are done in two steps, first do the so called hat transformation, suggested by [12, 13]

$$\hat{c}_{\mu\nu}{}^{mnl}(r) = c_{\mu\nu}{}^{mnl}(r) - \int_r^\infty \frac{c_{\mu\nu}{}^{mnl}(s)}{s} P^e{}_l\left(\frac{r}{s}\right)ds \qquad \text{for } l \text{ even}$$

$$\hat{c}_{\mu\nu}{}^{mnl}(r) = c_{\mu\nu}{}^{mnl}(r) - \int_r^\infty \frac{c_{\mu\nu}{}^{mnl}(s)}{s}\left(\frac{r}{s}\right) P^o{}_l\left(\frac{r}{s}\right)ds \qquad \text{for } l \text{ odd} \tag{5.14}$$

Where

$$P^e{}_0(x) = P^o{}_1(x) = 0$$

$$P^e{}_{2q+2}(x) = \frac{2}{q!}\sum_{i=0}^{q} x^{2i}(-1)^{q-i}\binom{q}{i}\frac{(q+i+\frac{3}{2})!}{(i+\frac{1}{2})!}$$

$$P^o{}_{2q+3}(x) = \frac{2}{q!}\sum_{i=0}^{q} x^{2i}(-1)^{q-i}\binom{q}{i}\frac{(q+i+\frac{5}{2})!}{(i+\frac{3}{2})!} \tag{5.15}$$

Then do the Hankel transformation for the hat functions

$$c_{\mu\nu}{}^{mnl}(k) = 4\pi \int_0^\infty r^2 j_0(kr)\hat{c}_{\mu\nu}{}^{mnl}(r)dr \qquad \text{for } l \text{ even}$$

$$c_{\mu\nu}{}^{mnl}(k) = 4\pi i \int_0^\infty r^2 j_1(kr)\hat{c}_{\mu\nu}{}^{mnl}(r)dr \qquad \text{for } l \text{ odd} \tag{5.16}$$

Where $j_0(kr)$ and $j_1(kr)$ are the spherical Bessel functions of the zeroth and first order.

Then do the so-called χ transformation ([12, 13])

$$c_{\mu\nu,\chi}{}^{mn}(k) = \sum_{l=|m-n|}^{m+n} \begin{pmatrix} m,n,l \\ \chi,-\chi,0 \end{pmatrix} c_{\mu\nu}{}^{mnl}(k) \tag{5.17}$$

All the $c_{\mu\nu,\chi}{}^{mn}(k)$ forms a matrix under the following rules

$$i = m(m+1) + \mu + 1$$

$$j = n(n+1) + \nu + 1 \tag{5.18}$$

With (5.18), (5.11) can be rewritten as a matrix equation

$$\mathrm{N}_\chi = (-1)^\chi C_\chi P C_\chi \left[I + (-1)^{\chi+1} \rho P C_\chi \right]^{-1} \tag{5.19}$$

Where the capital letter denotes the corresponding matrix and

$$P_{ij} = (-1)^\mu$$

when $i = m(m+1) - \mu + 1$ and $j = m(m+1) + \mu + 1$, and

$P_{ij} = 0$ for the other case.

With the known $c_{\mu\nu,\chi}{}^{mn}(k)$, we can find the $\eta_{\mu\nu,\chi}{}^{mn}(k)$. Then do the inverse χ transformation

$$\eta_{\mu\nu}{}^{mnl}(k) = (2l+1) \sum_{\chi=-\min(m,n)}^{\min(m,n)} \begin{pmatrix} m,n,l \\ \chi,-\chi,0 \end{pmatrix} \eta_{\mu\nu,\chi}{}^{mn}(k) \tag{5.20}$$

Next do the inverse Hankel transformation

$$\hat{\eta}_{\mu\nu}{}^{mnl}(r) = \frac{1}{2\pi^2} \int_0^\infty k^2 j_0(kr)\eta_{\mu\nu}{}^{mnl}(k)dk \qquad \text{for } l \text{ even}$$

$$\hat{\eta}_{\mu\nu}{}^{mnl}(r) = \frac{1}{2\pi^2} \int_0^\infty k^2 j_1(kr)\eta_{\mu\nu}{}^{mnl}(k)dk \qquad \text{for } l \text{ odd} \tag{5.21}$$

Finally, the inverse hat transformation

$$\eta_{\mu\nu}{}^{mnl}(r) = \hat{\eta}_{\mu\nu}{}^{mnl}(r) - \frac{1}{r^3}\int_0^r \hat{\eta}_{\mu\nu}{}^{mnl}(s) P^e{}_l\left(\frac{s}{r}\right) s^2 ds \qquad \text{for } l \text{ even}$$

$$\eta_{\mu\nu}{}^{mnl}(r) = \hat{\eta}_{\mu\nu}{}^{mnl}(r) - \frac{1}{r^4}\int_0^r \hat{\eta}_{\mu\nu}{}^{mnl}(s) P^o{}_l\left(\frac{s}{r}\right) s^3 ds \qquad \text{for } l \text{ even} \qquad (5.22)$$

If we do (5.12) to (5.22) successively, we will finally get the numerical result of $\eta_{\mu\nu}{}^{mnl}(r)$. With the known $\eta_{\mu\nu}{}^{mnl}(r)$, $\hat{c}_{\mu\nu}{}^{mnl}(r)$ can be known easily. We used the above numerical scheme, with the water model presented here, computed the water-water direct correlation function of the (0,0,0) component and shown in Fig. 17, because with the (0,0,0) component, it is easy to compare with either the simulation work or the experimental work.

With the mass center direct correlation function, we can also get the radial density distribution function between oxygen atoms with the formula (95) in [58], which is shown in Fig. 18. Compared with the experimental and simulation result in [60, 61], this result of oxygen-oxygen radial density distribution function is qualitively correct.

For the low-density limit, only the dipole-dipole interaction plays the role. We assume the water is only a hard core with a dipole embedded, therefore the calculation is much simplified and in Fig. 19 we show the direct correlation of the water-water mass center at low density case. In fact the line shape of the direct correlation function at even low density nearly does not change

V.4. Interaction between Water and Substrate

In this chapter we use tetradecane as the substrate and the detailed information of the non-singular Van der Waals potential was discussed in [6] and [7], in Fig. 20 we show the

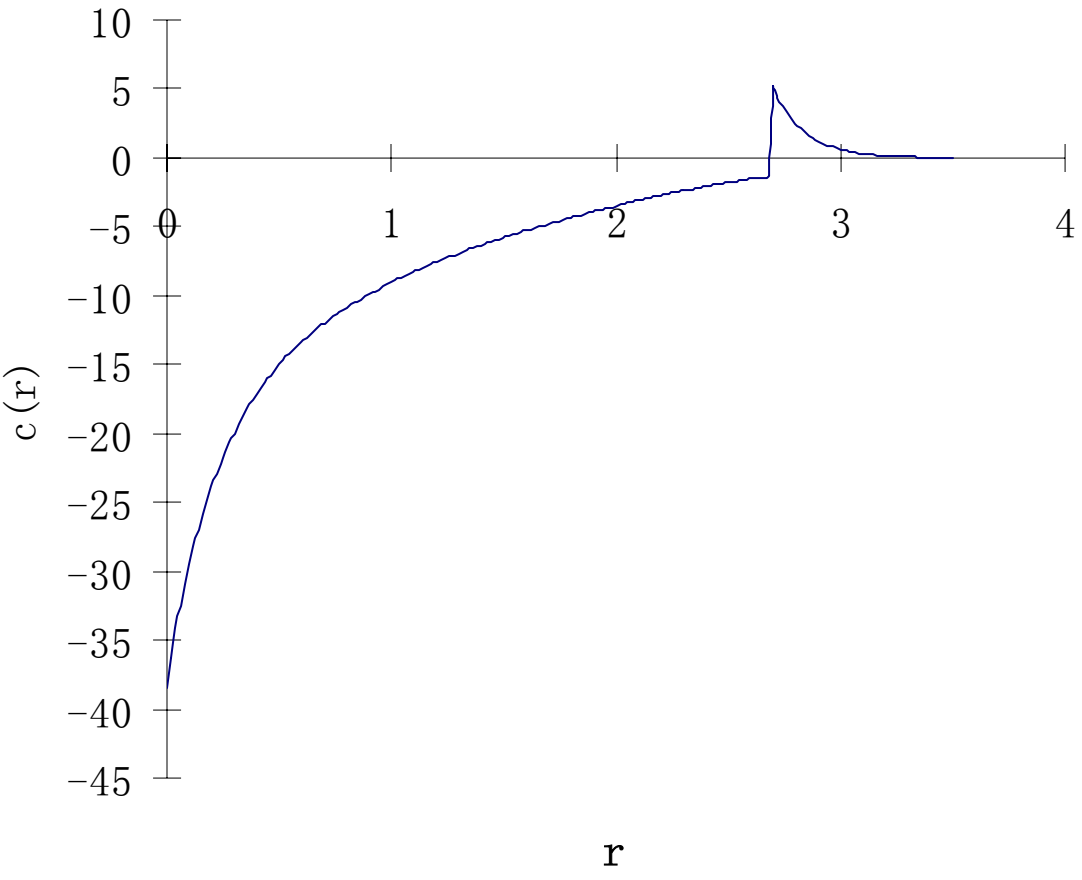

FIG. 17. (0,0,0) component of water-water mass center direct correlation function, under the density 3.3×10^{-2} / Å^3, temperature is 300K. The unit in plot is Å.

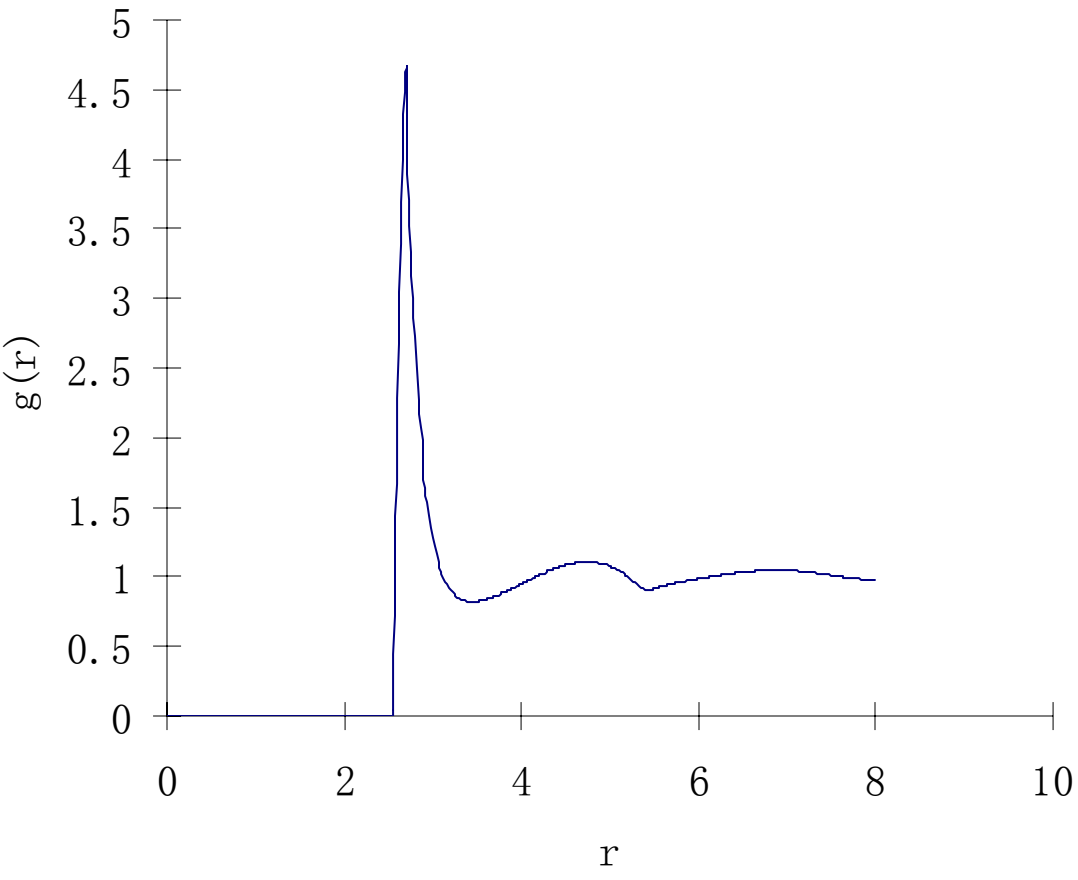

FIG. 18. Oxygen-oxygen radial density distribution for water under the density 3.3×10^{-2} / Å^3, temperature is 300K. The unit in plot is Å.

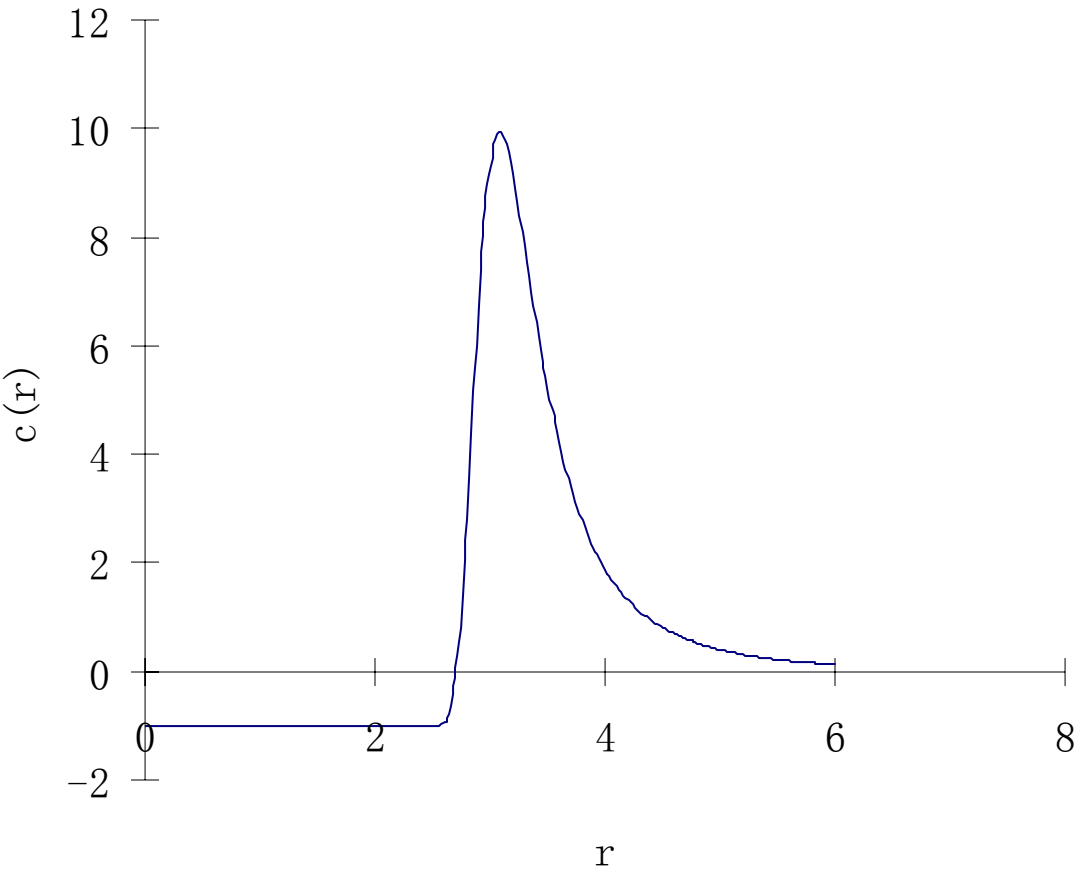

FIG. 19. (0,0,0) component of water-water mass center direct correlation function, under the density 2.45×10^{-6} / Å^3, temperature is 300K. The unit in plot is Å.

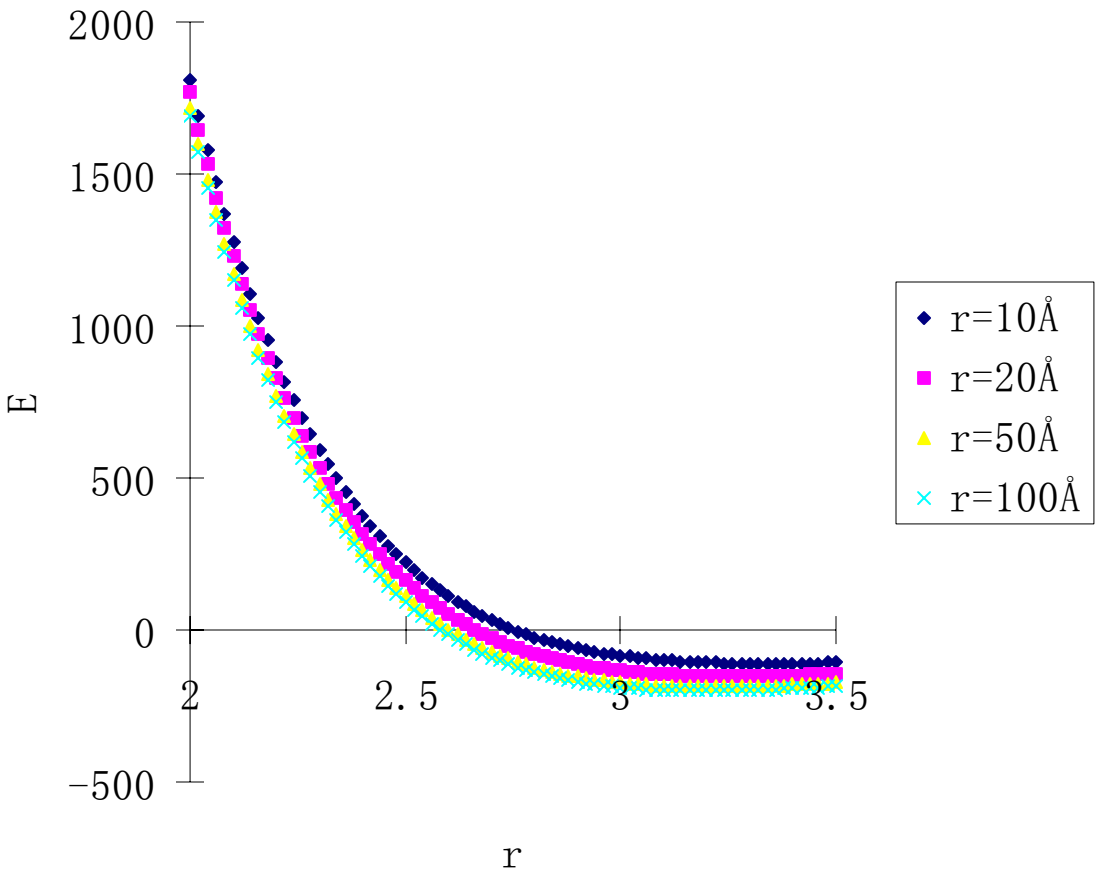

FIG. 20. Interaction energy between a single water molecule and a spherical substrate with different size. The unit of energy is in K.

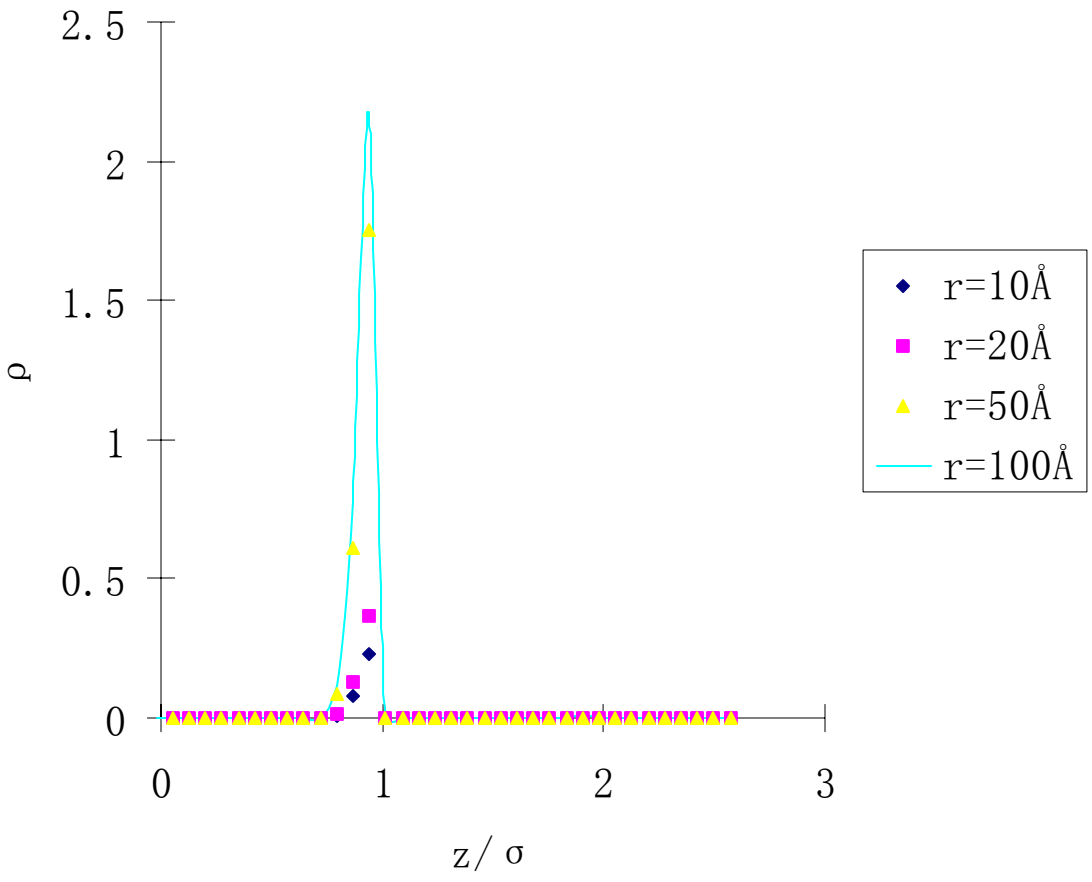

FIG. 21. Water adsorbed onto single nano spherical aerosol particle with radius $r = 10\text{Å}$, 20Å, 50Å, 100Å, at T=300K, and the background is $7.7 \times 10^{-7} / \text{Å}^3$, which is nearly the saturated vapor density at this temperature, and with $xp = 0.1$.

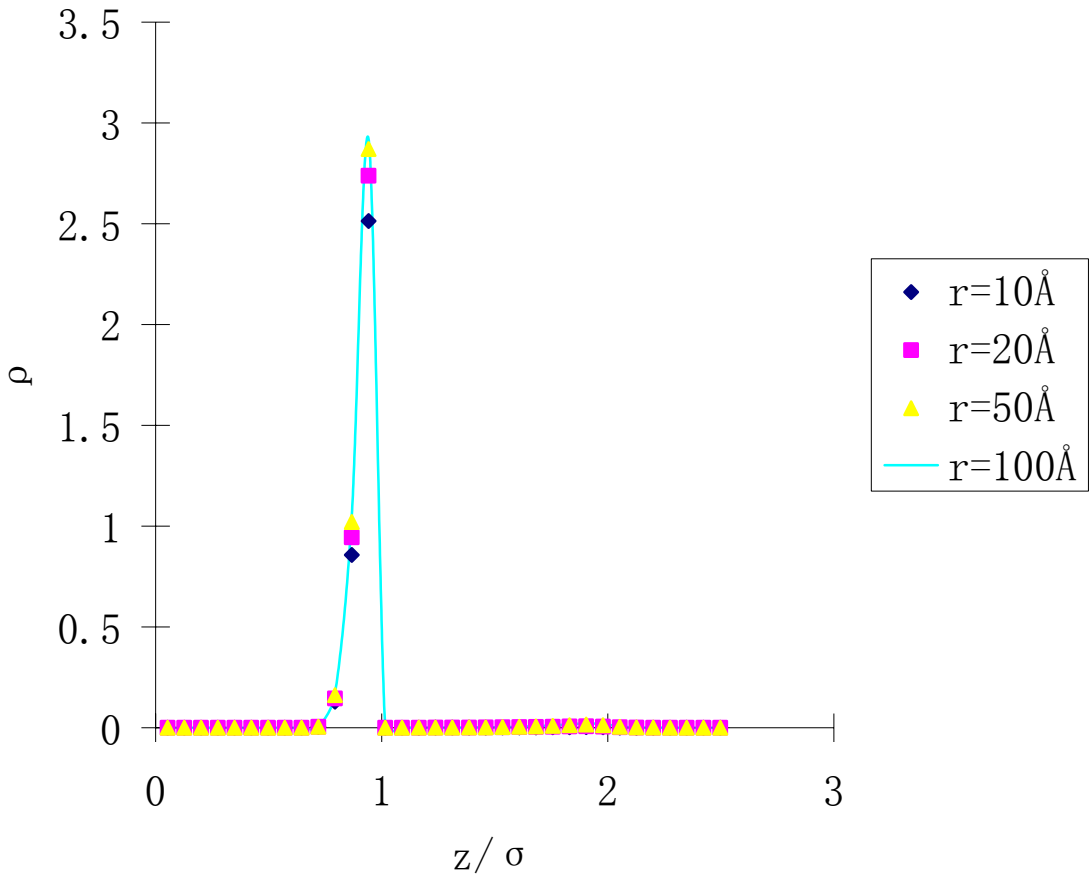

FIG. 22. Water adsorbed onto single nano spherical aerosol particle with radius $r = 10\text{Å}$, 20Å, 50Å, 100Å, at T=300K, and the background is $7.7 \times 10^{-7} / \text{Å}^3$, which is nearly the saturated vapor density at this temperature, and with $xp = 0.2$.

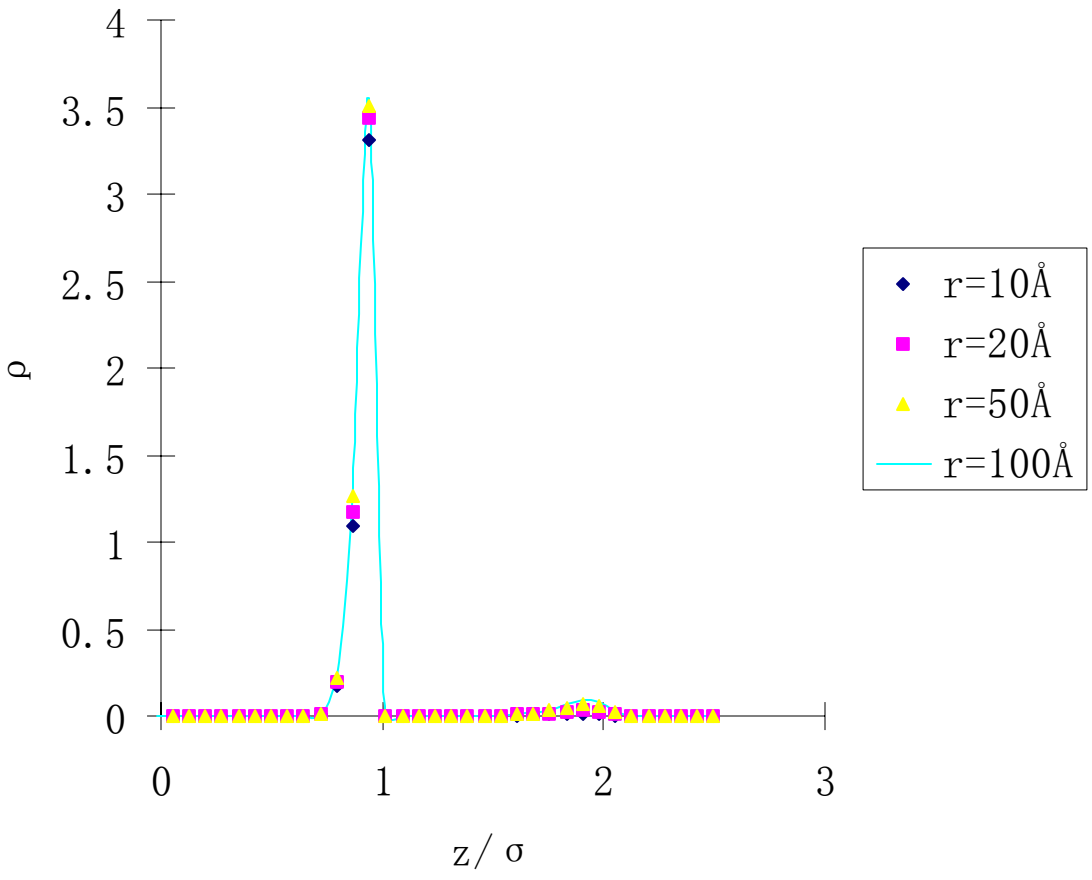

FIG. 23. Water adsorbed onto single nano spherical aerosol particle with radius $r = 10\text{Å}$, 20Å, 50Å, 100Å, at T=300K, and the background is $7.7 \times 10^{-7} / \text{Å}^3$, which is nearly the saturated vapor density at this temperature, and with $xp = 0.5$.

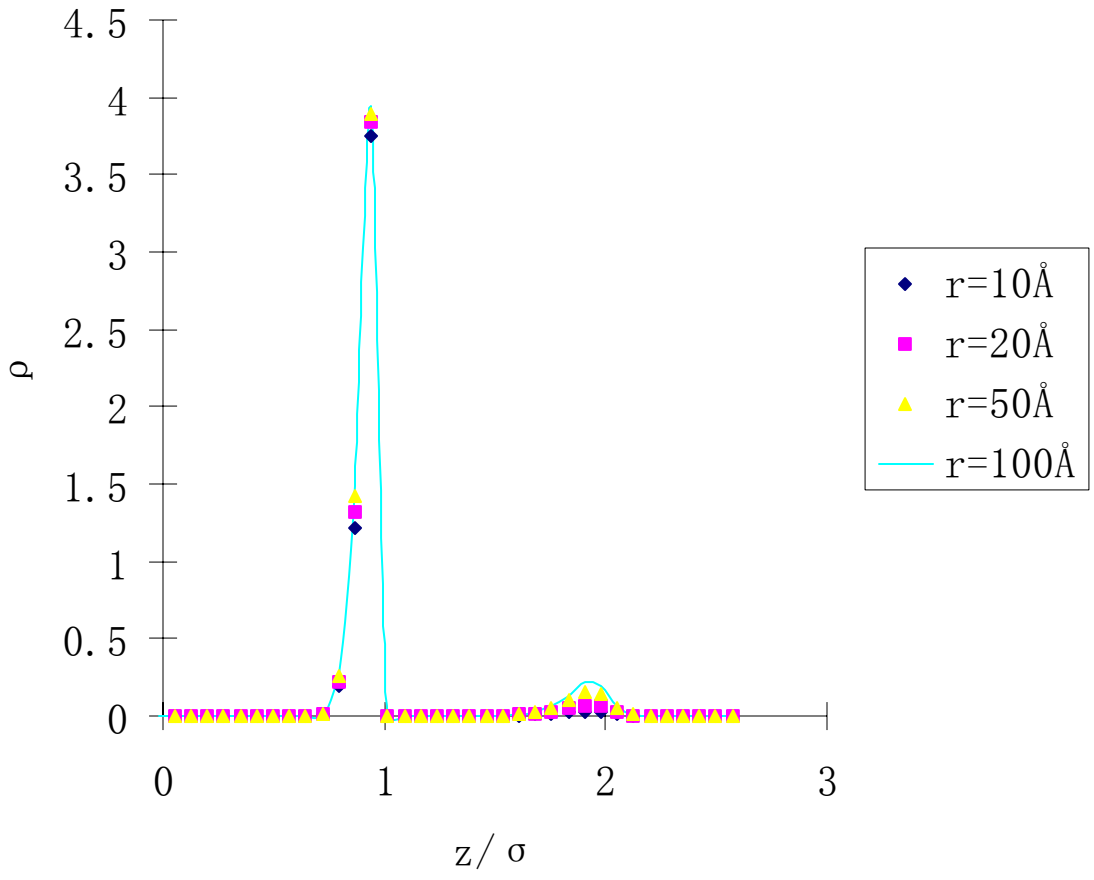

FIG. 24. Water adsorbed onto single nano spherical aerosol particle with radius $r = 10\text{Å}$, 20Å, 50Å, 100Å, at T=300K, and the background is $7.7 \times 10^{-7} / \text{Å}^3$, which is nearly the saturated vapor density at this temperature, and with $xp = 1.0$.

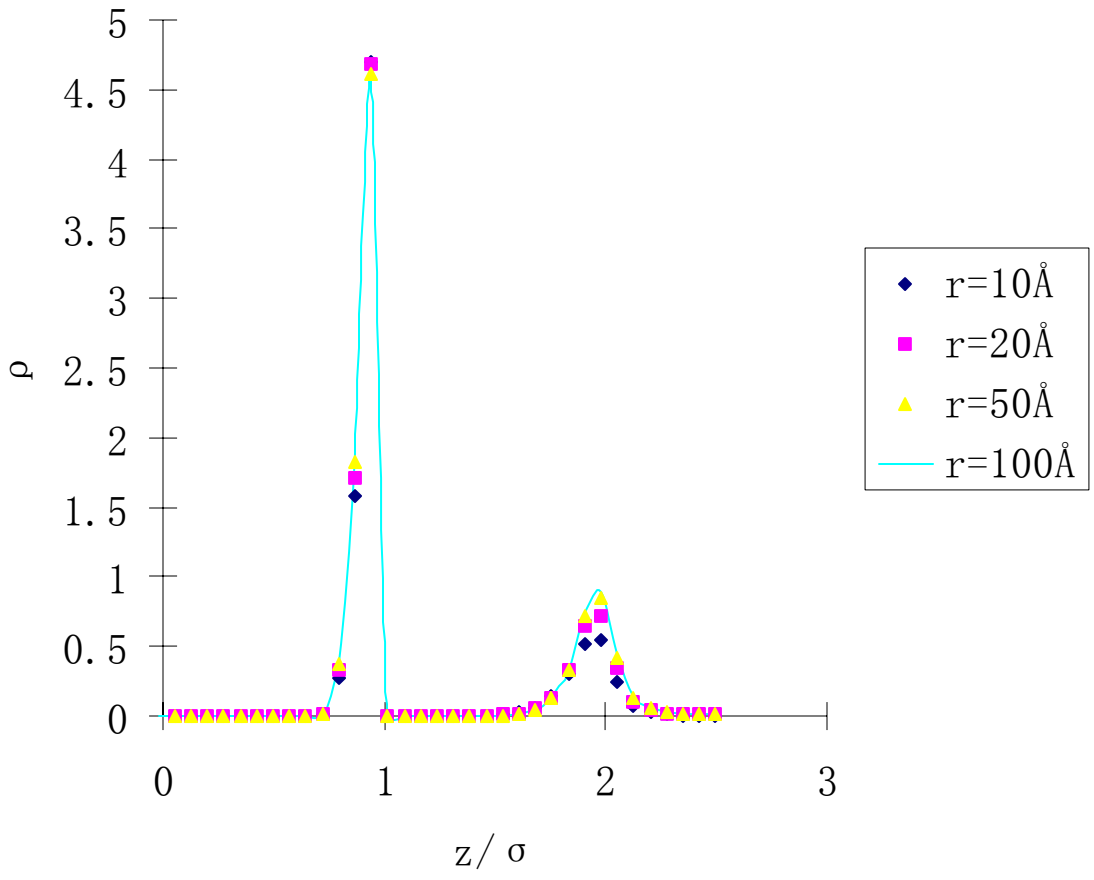

FIG. 25. Water adsorbed onto single nano spherical aerosol particle with radius $r = 10\text{Å}$, 20Å, 50Å, 100Å, at T=300K, and the background is $38.5 \times 10^{-7} / \text{Å}^3$, which is nearly five times the saturated vapor density at this temperature, and with $xp = 1.0$.

interaction energy between a single water molecule a spherical substrate with different size. It is clear shown in the plot that the interaction energy increases as the substrate size goes up.

In order to consider the real case of aerosol particles released into the air, we have to put some oxidized sites onto the surface of the spherical substrates. This is because in the real case, some part of the surface of the spherical substrate may be oxidized or there are other atoms or molecules that have strong ability to adsorb water molecules. In order to mimic this situation, we follow [62], by assuming that once the water molecule enters a thin layer in the vicinity of the surface there is a possibility that a hydrogen bond will be formed, and we call the possibility variable xp, which varies from 0 to 1. With the high possibility means that the surface is highly oxidized or the surface density of the other kind atoms or molecules is high.

$$U = -3600K \quad \text{if} \quad r < R + \sigma \tag{5.23}$$

Though (5.23) may not be very accurate, we think it may reflect the nature of the problem qualitively.

The non-singular Van der Waals potential plus short-ranged potential (5.23) forms the complete interaction potential between the nano spherical substrate and a single water molecule.

V.5. Computational Details

The central task is to apply the (3.8) plus the interpolation rules, (3.13) or (3.14) for high-density and low-density direct correlation function to the three-dimensional calculation. And we will list the main procedure in the following part.

For the interpolation function between the high density and low density we take the following form

$f(\rho) = 0.0$,

if $\rho \le 2.45 \times 10^{-6}$.

$f(\rho) = -0.033 \times 10^{-5} + 1.345\rho + 0.235 \times 10^{-2}\rho^2 - 320.140\rho^3$,

if $2.45 \times 10^{-6} \le \rho \le 3.0 \times 10^{-2}$.

$$f(\rho) = -0.095 + 10.853\rho - 316.912\rho^2 + 3201.134\rho^3$$

$$\text{if } \rho > 3.0 \times 10^{-2}. \qquad (5.24)$$

The (0,0,0) component of the direct correlation function at high density and low density was used as listed in Fig. 17 and Fig. 19. The reason why only (0,0,0) component is needed is because the interaction between the substrate and the water molecule in orientation independent, the integral of the other component over the angular variables would be zero (see [23-25]).

For the geometry configurations, of the one, two and three cases, are the same as mentioned in chapter IV. All the calculation were done at T=300K, which is the room temperature.

V.6. Results and Discussion

First, we have computed water adsorbed onto single spherical substrate with different size, different oxidized surface coverage and different background densities.

From Fig. 21-Fig. 24, we may see that both the substrate size and the surface oxidized sites density have influence on the water adsorption. When the surface oxidized site's density is low, as plotted in Fig. 24, we may only see the development of the first peak, and in fact the formation of this peak is only because the existence of the surface oxidized sites. The growth of the first peak is easily understood; this is because the surface oxidized sites may attract the water molecules in the air, the larger the substrate size, the larger the number of oxidized sites it may offer. As the surface oxidized sites density increase, we may perceive the development of the second peak. The formation of the second peak is due to the water molecules absorbed onto the surface. If the absorbed water number is large enough and the background density of water vapor is high enough, we may imagine the onset of condensation. In Fig. 24 we may see such a good example. In Fig. 25 we may see the strong development of the second peak. However, according to Kelvin equation, if $P_H / P_0 = 5.0$, which is nearly what we used in Fig. 25, $r^* = 6.46\text{Å}$. The result from Kelvin equation seems contradictory with what we get in Fig. 25. The discrepancy

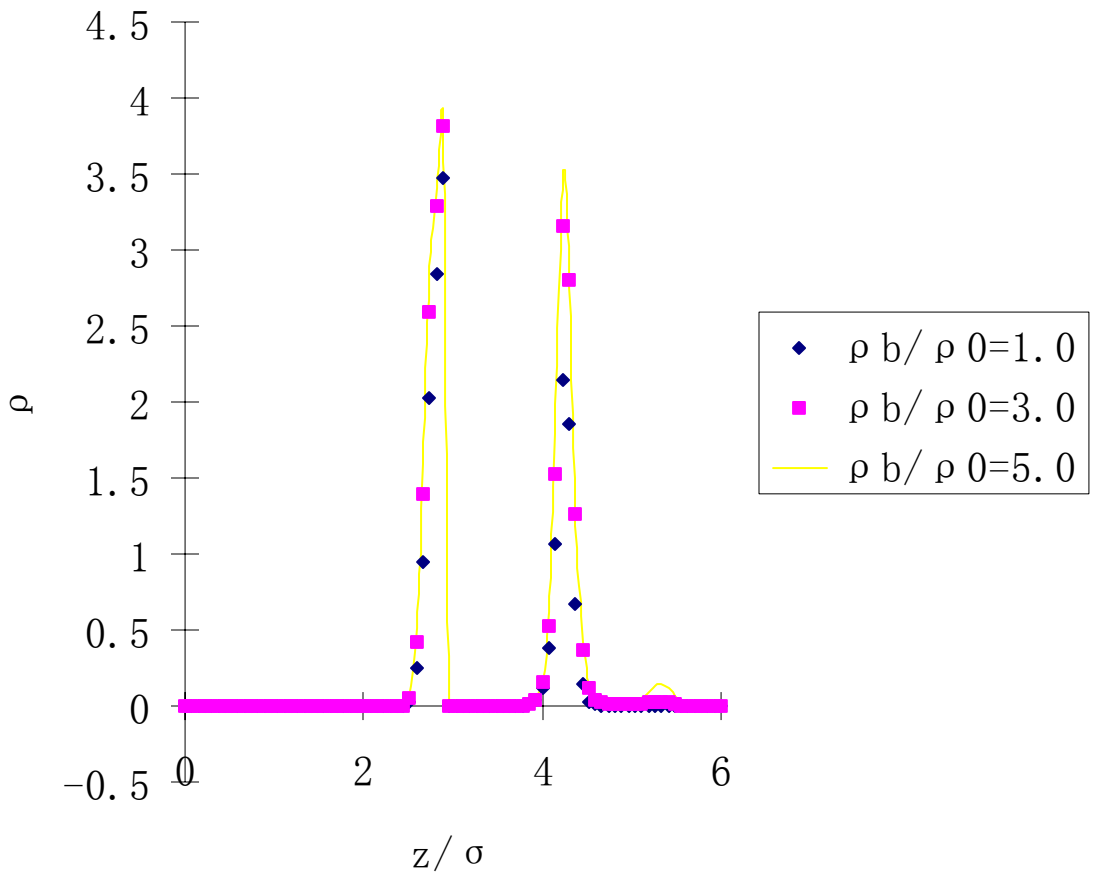

FIG. 26. Water adsorbed onto two identical nano spherical aerosol particles with radius $r = 10\text{Å}$, at T=300K, and the background is, $7.7\times10^{-7}/\text{Å}^3$, $23.1\times10^{-7}/\text{Å}^3$, $38.5\times10^{-7}/\text{Å}^3$, and with $xp = 1.0$. The density is plotted along the symmetry line of the two identical spheres.

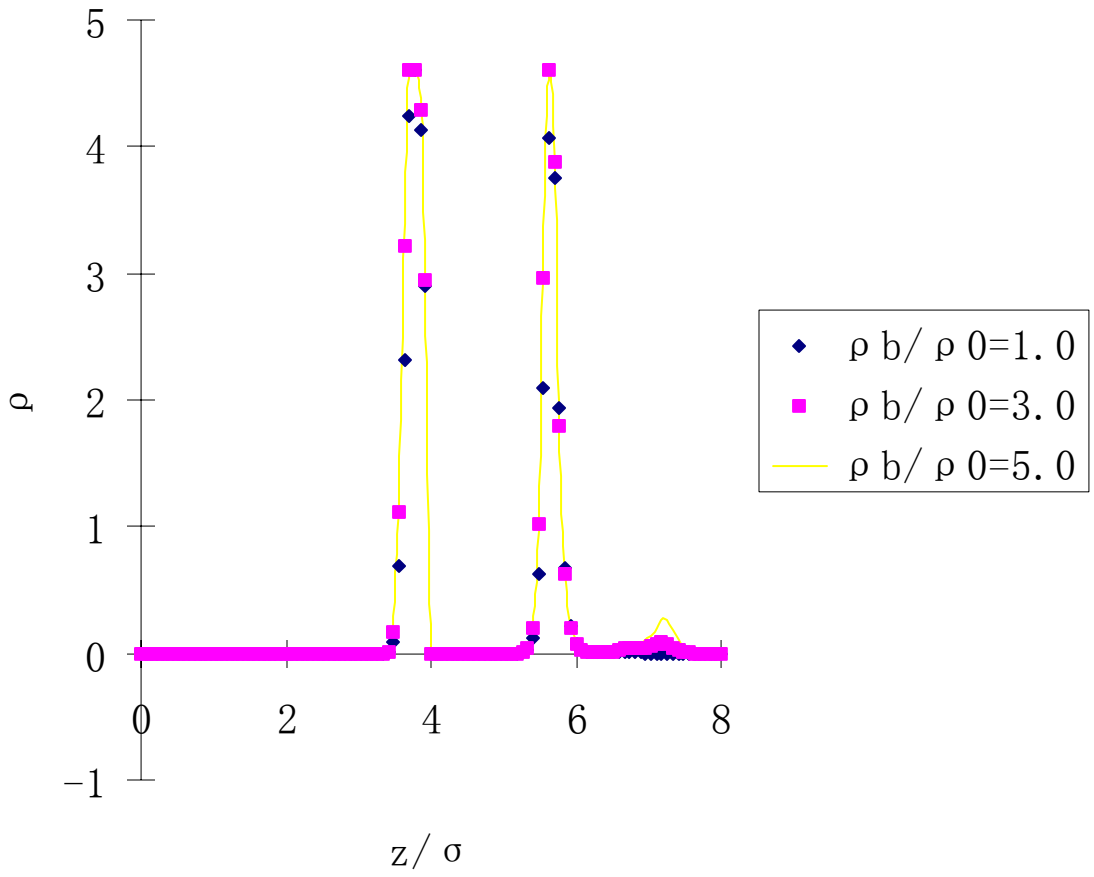

FIG. 27. Water adsorbed onto two identical nano spherical aerosol particles with radius $r = 20\text{Å}$, at T=300K, and the background is, $7.7\times10^{-7}/\text{Å}^3$, $23.1\times10^{-7}/\text{Å}^3$, $38.5\times10^{-7}/\text{Å}^3$, and with $xp = 1.0$. The density is plotted along the symmetry line of the two identical spheres.

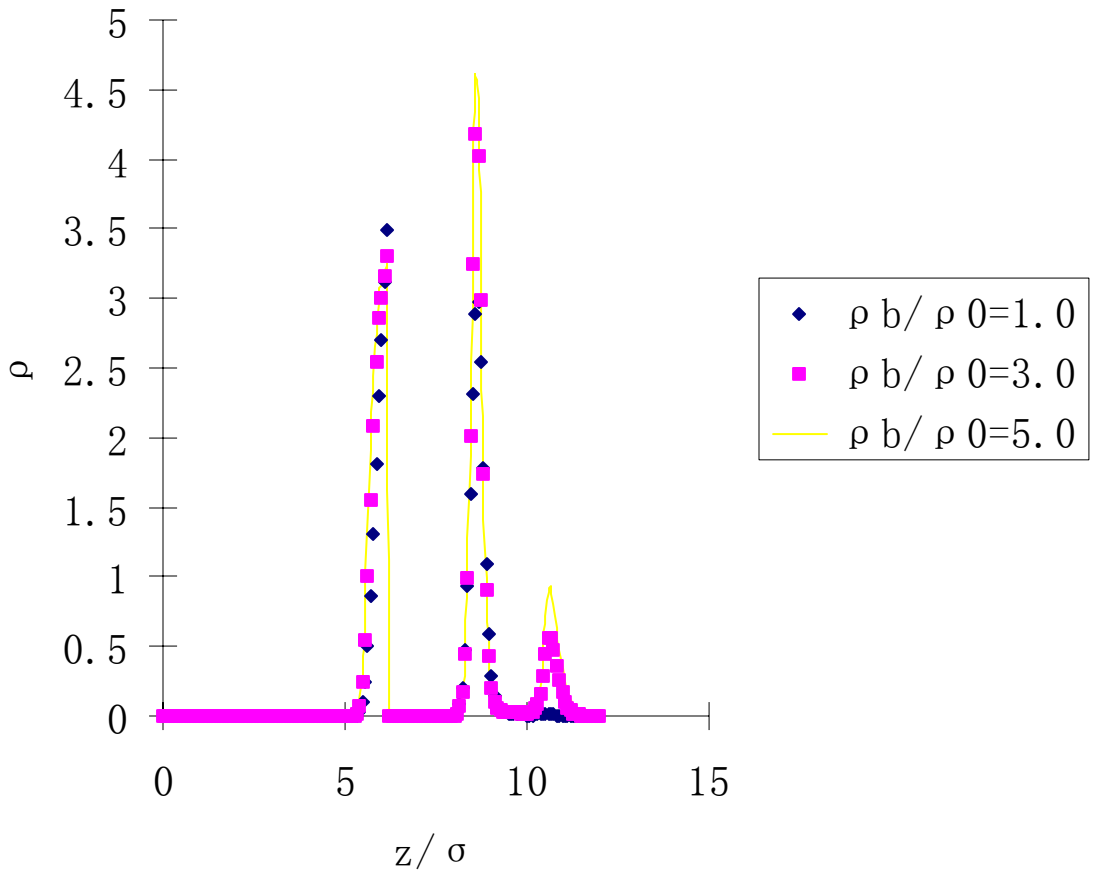

FIG. 28. Water adsorbed onto two identical nano spherical aerosol particles with radius $r = 50\text{Å}$, at T=300K, and the background is, $7.7\times10^{-7}/\text{Å}^3$, $23.1\times10^{-7}/\text{Å}^3$, $38.5\times10^{-7}/\text{Å}^3$, and with $xp = 1.0$. The density is plotted along the symmetry line of the two identical spheres.

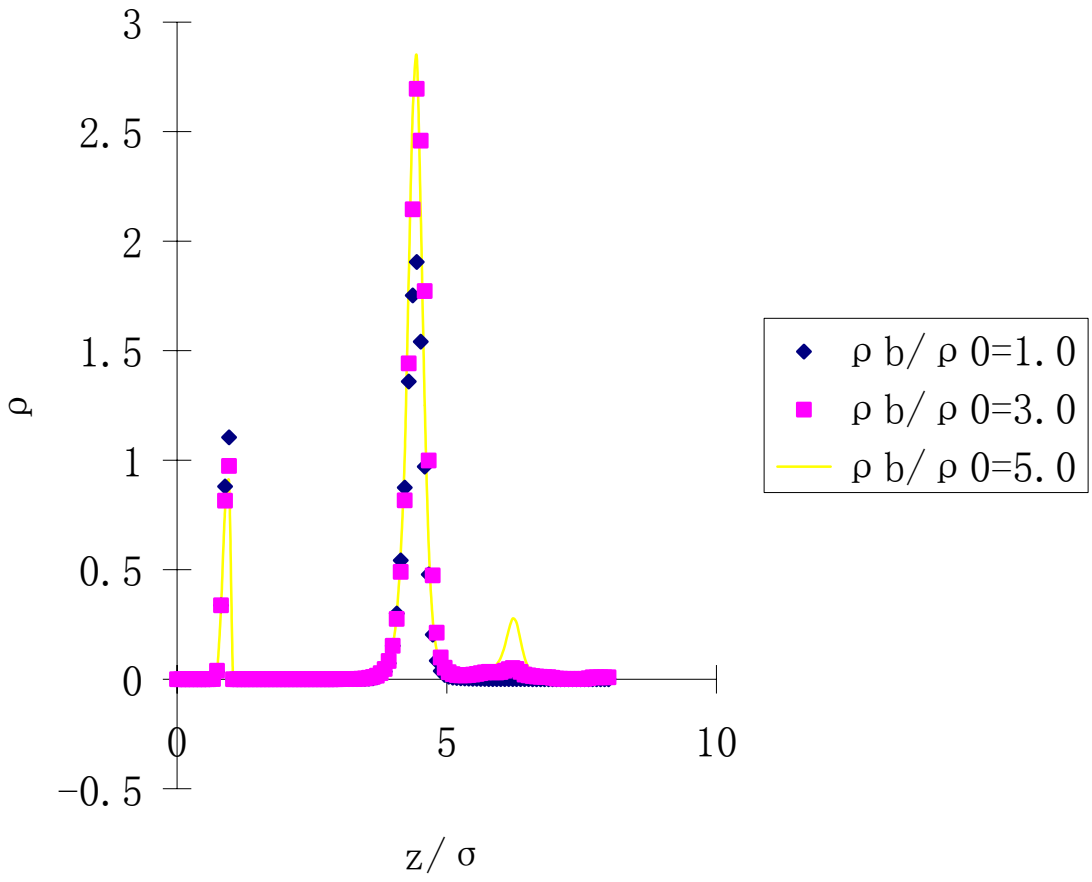

FIG. 29. Water adsorbed onto three identical nano spherical aerosol particles with radius $r = 10\text{Å}$, at T=300K, and the background is, $7.7\times10^{-7}/\text{Å}^3$, $23.1\times10^{-7}/\text{Å}^3$, $38.5\times10^{-7}/\text{Å}^3$, and with $xp = 1.0$. The density is plotted along the symmetry line of the two identical spheres. The angle formed by the three particles is $\theta = 85^\circ$.

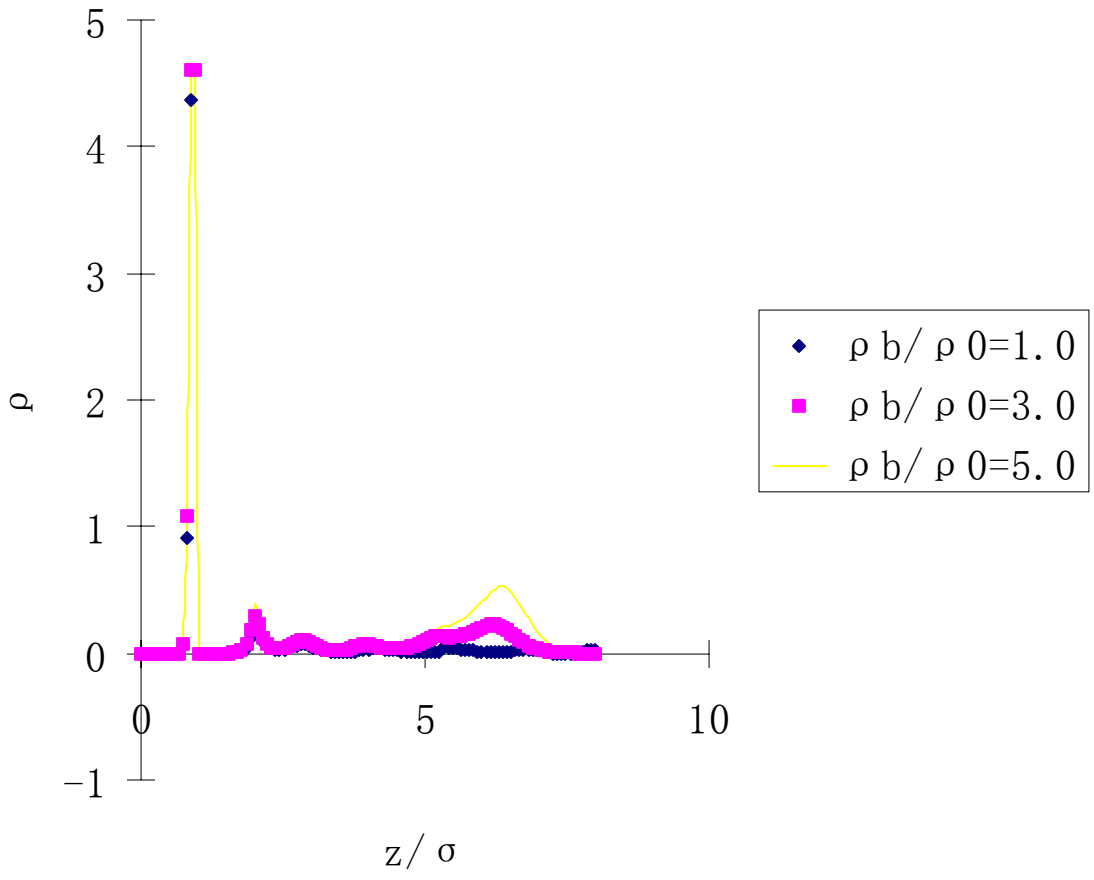

FIG. 30. Water adsorbed onto three identical nano spherical aerosol particles with radius $r = 20\text{Å}$, at T=300K, and the background is, $7.7\times10^{-7}/\text{Å}^3$, $23.1\times10^{-7}/\text{Å}^3$, $38.5\times10^{-7}/\text{Å}^3$, and with $xp = 1.0$. The density is plotted along the symmetry line of the two identical spheres. The angle formed by the three particles is $\theta = 85^\circ$.

can be understood in this way, in Kelvin equation, the surface tension is used, which is a macroscopic quantity, and in our case, only less than three water layers are formed; there is not a surface, therefore the concept of surface tension cannot be used in our case. Only many layers of water are formed, we may use the concept of surface tension safely. Through Fig. 21-Fig. 24 we may also notice that the adsorption profiles for $r = 50\text{Å}$ and $r = 100\text{Å}$ are very close, and totally different from those of $r = 10\text{Å}$ and $r = 20\text{Å}$. This very interesting phenomenon was stressed in [6] and [7], where it was called the size effect and this clearly tells us that the transition of the adsorption profiles occurs in the nano range. As concluded in [6] and [7] when the substrate size is over 10nm, it may be treated as a plane and we may easily reach this conclusion here.

Fig. 26-Fig. 28 show the density profiles of water adsorbed onto two identical nano spherical aerosol particles with radius $r = 10\text{Å}$, $r = 20\text{Å}$, $r = 50\text{Å}$ at T=300K, and the background is, $7.7 \times 10^{-7} / \text{Å}^3, 23.1 \times 10^{-7} / \text{Å}^3$, $38.5 \times 10^{-7} / \text{Å}^3$, and with $xp = 1.0$. The density is plotted along the symmetry line of the two identical spheres. It is clearly seen that the adsorption onto the two spheres are much stronger than the corresponding one sphere case. From these plots we may conclude clusters of water form in the interstitial regions formed by the two spheres. This result agrees with the results in [2], where they treat the macroscopic case. Because the proximity of the adjacent spheres exposes interstitial water to more oxidized sites than at a single sphere, it is easy to understand why the adsorption is stronger here. This result show clearly that when treating the adsorption of water onto an aerosol released into the air, the one sphere model is not sufficient, because we already show in Fig. 26 to Fig. 28 that the two identical spheres structure can have much stronger adsorption than one sphere case.

From Fig. 29 and Fig. 30 we may find that the adsorption of water within the region formed by three identical aerosol particles are more complicated. And from the plot we may find that the water molecules are beginning to fill in the region formed by the three identical aerosol

particles. Yet the change is not so surprising from two to three sphere cases as that of from one to two sphere case.

CHAPTER VI

CONCLUSION

In this dissertation we computed the argon adsorbed onto the one, two and three spherical substrates. For one-sphere case, we found that as the substrate size increases, the adsorption will approach that of a planar case. For the two-sphere case, the ring structure will be formed around the two-sphere rotational axis; as the substrate size increases some the ring structure will be more clearly shown. For the three-sphere case, when the angle formed by the three spheres smaller than a certain, the clusters formed within the interstitial regions of the two two-sphere may be connected. The results of two and three-sphere cases indicate that aggregates of the identical spherical substrates has a much stronger ability to take up the argon atoms than the single sphere case. This trend was also found by the previous paper that works with macroscopic case ([2]).

We explore water adsorption onto aerosol particles; we find that the oxidized surface sites play an important role during the adsorption process. Those sites may be used to bond a certain number of water molecules onto the surface. With the bonded water, if other conditions are met, condensation may take place. Also, the substrate size is also important, with the larger substrate, it may render more sites to bound water. But when the substrate size is larger than 10nm, we may treat it as a plane

The aggregates of aerosol particles have much stronger ability to adsorb water than single spheres. If we would like to treat the water vapor problem dealing with aerosol particles, we must first consider the aggregates rather than single sphere or we may reach misleading results.

The results found in this dissertation agree with that of [2], but it is only a qualitive result, because so far we can only assume the very rough potential between the water and the oxidized sites. Moreover, the water model we used in this chapter is only an empirical one. The future improvement may towards these two directions.

REFERENCES

[1] N. H. Fletcher, J. Chem. Phys. **29**, 572 (1958)

[2] Y. Crouzet and W. H. Marlow, Aerosol. Sci. Techn. **22**, 43 (1995)

[3] P. J. McElory, Journal Colloid Interface Sci. **72**, 147 (1979)

[4] L. Dufour and R. Defay, *Thermodynamics of Clouds* (Academic Press, New York, 1963)

[5] M. Schmeits and A. A. Lucas, J. Chem. Phys. **65**, 2901 (1976)

[6] J. X. Fang, W. H. Marlow, J. X. Lu, and R. R. Lucchese, J. Chem. Phys. **107**, 5212 (1997)

[7] J. X. Lu, W. H. Marlow and V. Arunachalam, J. Colloid Interface Sci. **181**, 429 (1996)

[8] J. Y. Xie and W. H. Marlow, Aerosol. Sci. Techn. **27**, 591 (1997)

[9] M. S. Werthiem, Journal of Mathematical Physics **5**, 643 (1964)

[10] M. S. Werthiem, J. Chem. Phys. **55**, 4291-4298 (1971)

[11] L. Blum and A. J. Torruella, J. Chem. Phys. **56**, 303 (1972)

[12] L. Blum, J. Chem. Phys. **57**, 1862 (1972)

[13] L. Blum, J. Chem. Phys. **58**, 3295 (1973)

[14] S. L. Carnie, D. Y. C. Chan and G. R. Walker, Mol. Phys. **43,** 1115 (1980)

[15] P. H. Fries and G. N. Patey, J. Chem. Phys. **82**, 429 (1985)

[16] J. M. Caillol, Chem. Phys. Lett. **121**, 347 (1985)

[17] F. Lado, E. Lomba and M. Lombardero, J. Chem. Phys. **103**, 481 (1995)

[18] M. Lombardero, C. Martín, S. Jorge, F. Lado and E. Lomba, J. Chem. Phys. **110**, 1148 (1999)

[19] J. Richardi, C. Millot and P. H. Fries, J. Chem. Phys. **110**, 1138 (1999)

[20] D. Chandler and H. Andersen, J. Chem. Phys. **57,** 1930 (1972)

[21] Y. Liu and T. Ichiye, Chem. Phys. Lett. **231**, 380 (1994)

[22] J. K. Percus, J. Stat. Phys. **15**, 423 (1976)

[23] D. Beglov and B. Roux, J. Chem. Phys. **103**, 360 (1995)

[24] D. Beglov and B. Roux, J. Chem. Phys. **104**, 8678 (1996)

[25] M. Lkeguchi and J. Doi, J. Chem. Phys. **103**, 5011 (1995)

[26] J. Fischer and M. Methfessel, Phys. Rev. A **22**,2836 (1980)

[27] L. A. Rowley, D. Nicholson and N. G. Parsonage, Mol. Phys. **31**, 365 (1976)

[28] R. Lovett, C. Y. Mou and F. P. Buff, J. Chem. Phys. **65**, 570 (1976)

[29] M. Kasch and F. Forstmann, J. Chem. Phys. **99**, 3037 (1993)

[30] S. Iatsevitch and F. Forstmann, Mol. Phys. **98**, 1309 (2000)

[31] W. F. Saam and C. Ebner, Phys. Rev. A **15**, 2566 (1977)

[32] C. Ebner, W. F. Saam and D. Stroud, Phys. Rev. A **14**,2264 (1976)

[33] J. E. Lane, T. H. Spurling, J. W. Perram and E. R. Smith, Phys. Rev. A **20**, 2147-2153 (1979)

[34] P. Tarazona, Phys. Rev. A **31**, 2672 (1985)

[35] Z. X. Tang, L. E. Scriven and H. T. Davis, J. Chem. Phys. **95**, 2659 (1991)

[36] Y. Rosenfeld, Phys. Rev. E **50**, 3318 (1994)

[37] P. I. Ravikovitch, A. Vishnyakov and A. V. Neimark, Phys. Rev. E **64**, 11602 (2001)

[38] D. E. Sullivan and G. Stell, J. Chem. Phys. **67**, 2567 (1977)

[39] D. E. Sullivan and G. Stell, J. Chem. Phys. **69**, 5450 (1978)

[40] W. F. Saam and C. Ebner, Phys. Rev. A. **17**, 1768 (1978)

[41] L. S. Smith and L. L. Lee, J. Chem. Phys. **71**, 4085 (1979)

[42] H. C. Andersen and D. Chandler, J. Chem. Phys. **57**, 1918 (1972)

[43] D. E. Sullivan, D. Levesque and J. J. Weis, J. Chem. Phys. **72**, 1170 (1980)

[44] F. F. Abraham. and Y. Singh, J. Chem. Phys. **67**, 2384 (1977)

[45] L. L. Lee, J. Chem. Phys. **62**, 4436 (1975)

[46] B. Borstnik and A. Azman, Mol. Phys. **30**, 1565 (1975)

[47] J. Fischer, Mol. Phys. **33**, 75 (1977)

[48] D. Nicholson and N. G. Parsonage, *Computer Simulation and the Statistical Mechanics of Adsorption*. (Academic Press. New York, 1982)

[49] M. Kasch and F. Frank, J. Chem. Phys. **99**, 3037 (1993)

[50] S. Iatsevitch and F. Frank, Mol. Phys. **98**, 1309 (2000)

[51] F. M. Orr, L. E. Scriven, and A. P. Rivas, J. Fluid. Mech. **67**, 723 (1975)

[52] W. H. Press, B. P. Flannery, S. A. Teukolsky and W. T. Vetterling, *Numerical Recipes* (Cambridge University, Cambridge, 1990)

[53] W. L. Jorgensen, J. Chandrasekhar, J. D. Madura, R. W. Impey, and M. L. Klein, J. Chem. Phys. **79**, 926 (1983)

[54] W. L. Jorgensen, and J. D. Madura, Mol. Phys. **56**, 1381 (1985)

[55] H. J. C. Berendsen, J. P. M. Postma, W. F. van. Gunsteren, and J. Hermans, *In Intermolecular Forces*, edited by B. Pullmann (Reidel, Dordrecht, 1981), p. 331

[56] H. J. C. Berendsen, J. R. Grigera, and T. P. Straatsma, J. Phys. Chem. **91**, 6269 (1987)

[57] D. Bratko, L. Blum and A. Luzar, J. Phys. Chem. **83**, 15 (1985)

[58] L. Blum, F. Vericat and L. Degrève, Physica A 265, 396 (1999)

[59] C. M. Carlevaro, L. Blum and F. Vericat, J. Phys. Chem. **119**, 5198 (2003)

[60] P. Jedlovszky and J. Richardi, J. Chem. Phys. **110**, 8019 (1999)

[61] A. K. Scoper, F. Bruni and M. A. Ricci, J. Chem. Phys. **106**, 247 (1997)

[62] E. A. Muller, L. F. Rull, L. F. Vega and K. E. Gubbins, J. Chem. Phys. **100**, 1189 (1996)

VITA

NAME: Chu Nie

Address: Nuclear Engineering Department
Texas A&M University
3133 TAMU
College Station, TX 77843-3133

Email Address: niechu@hotmail.com

Education: B.S., Physics, Nanjing University, 1998
Ph.D, Nuclear Engineering, Texas A&M University, 2005